BOND CHARACTERISTICS OF PRESTRESSING STRAND IN GROUT

THESIS SUBMITTED FOR A DEGREE OF MASTER OF PHILOSOPHY AT THE UNIVERSITY OF LEICESTER

BY S. LALDJI

MEMORANDUM

The accompanying thesis entitled "Bond Characteristics of Prestressing Strand in Grout" is submitted in support of an application for the degree of Master of Philosophy in the University of Leicester.

The work recorded in this thesis is original unless otherwise acknowledged by references. It has not been submitted for another degree in this University, or for an award of a degree or diploma of any other institution. This thesis is the result of work done mainly during the period of the registration.

I hereby declare that the statements in this memorandum are true in all particulars.

S. LALDJI
Department of Engineering,
University of Leicester,
October 1987.

AKNOWLEDGEMENTS

This work has been carried out under the supervision of Dr. A.G.YOUNG to whom I owe the greatest aknowledgement and without whose continual encouragement, advice and helpful criticism this thesis would not have been possible.

I also would like to extend my deep gratitude to the following who helped me throughout the investigation.

The Bridon Wire Limited, Doncaster, for supplying me with strands.

Mr. C.J.Morrison whose experimental skills made it possible to run the tests and recording of experimental data.

Mr. G.R.O'Connor for his considerable help in carrying out the experimental work in the concrete and structure laboratory.

Mr.D.Pratt; Mrs.N.Berridge, and Mrs J.Meredith for their considerable help in reproducing the diagrams in this thesis.

The workshop staff for the manufacture of test apparatus.

BOND CHARACTERISTICS OF PRESTRESSING STRAND IN GROUT

by SAID LALDJI

SUMMARY

Pull-out tests were conducted using a specially constructed rig on 100x100x100mm prism specimens with short embedment length. All tests show a sharp increase in pull-out load with negligible slip until a "maximum bond force" is developed and the adhesion fails. After this point slip occurs at load levels which depend upon the test variables. For the case of zero lateral pressure and long embedment length a maximum bond stress of 1.9N/mm² is obtained for normal strand embedded in a grout of 57N/mm² compressive strength. This value is less than that recommended by DD81 but is based upon the true contact area.

The effect of biaxial lateral pressure up to 0.26 times the compressive strength is to linearly increase the maximum bond stress as follows for 1N/mm² increase in lateral pressure.

Normal strand 0.26N/mm² ± 0.04
Dyform strand 0.24N/mm² ± 0.04
Indented strand 0.47N/mm² ± 0.22

The maximum bond stress for the case of zero lateral pressure and 25.4mm embedment are in the ratio 1.00:0.90:1.20 for normal strand, dyform, and indented strand respectively.

The increase in bond due to added length of embedment is not linear. The maximum bond stress tends towards a constant value beyond an embedment length of 50mm.

The maximum bond force increases at an average rate of 0.07KN for 1N/mm² increase in grout strength for up to lateral pressures of 0.26 compressive strength.

An equation is developed which predicts the maximum bond force well, provided values of shrinkage and material constants are known. Comparison with the results obtained by other investigators shows good correlation for the case of zero lateral pressure. Differences with others using lateral pressure are due primarily to differences in the loading system.

It is shown both experimentally and theoretically that the torsional stiffness of the strand has little effect on bond.

CONTENTS

CHAPTER 1 INTRODUCTION

1.1 BACKGROUND

In recent years there has been a dramatic increase in the use of ground anchorages. Although ground anchorage technology is still in an active stage of development the use of anchorages is widespread for both temporary and permanent applications. There is a wide range of applications, ranging from dam stressing of underground excavations in rock to tying back earth retaining structures and holding down tower and bridge foundations. For these applications the geometry of a ground anchorage and its mode of operation requires a detailed knowledge of ground conditions local to the fixed anchor, and a good understanding of the bond mobilized at ground/matrix and at matrix/prestressing tendon interface. There are still gaps in understanding with respect to anchor behaviour[1], particularly of the bond at the matrix/prestressing tendon interface.

The guidelines of the British Standard Draft for Development[2] (DD81) "Recommendations for Ground anchorages" state that grout and prestressing tendon are suitable materials for a ground anchor. Since seven-wire strand has become established as the most popular tendon for prestressing it has been chosen in this test programme.Grout is studied as its use is strongly recommended. Grout is a cementitious slurry which has desirable physical properties of fluidity and cohesion. It can contain other materials in addition to cement and water. Sand has always been used when a considerable volume of void surface with a relatively open structure is to be filled. In the early years of its use, grout was injected into cracks, ducting, and other voids and fissures in concrete or adjacent to concrete structures to provide an impermeable barrier to movement of water with the principal advantage of preventing corrosion of steel. The injection procedure was such to ensure proper filling of the total void surface. In recent applications, however, in addition to the advantage of preventing corrosion of the steel, grout has an important structural role of ensuring transfer of stress between steel and its surroundings.

The transfer of stress between steel and its surrounding matrix has been found to be dependent upon adhesion, friction due to the naturally occuring phenomenon of shrinkage, and mechanical interlock developed within the matrix during curing. An idealized representation of major components of bond as illustrated in DD81[2] is given in figure 1.1.

The adhesion is defined as the physical interlocking between the microscopically rough steel surface and the surrounding cementitious material. It characterizes the bond resistance developed before any movement of the steel with respect to the surrounding matrix. This resistance to motion is given by the shear strength of the weaker material i.e the cement which is keyed into the steel surface. According to Martin[3] the adhesion is not only of physical but also of strong chemical nature. He reported that water together with dissolved substances of the fresh cement penetrated the complete oxide layer which covers every steel surface after being exposed to air for a short time. The oxide layer is so porous and coarse in its structure that penetration is very easy. After failure of the adhesion the bond developed from then on is due to the frictional forces between the plain surface of the steel and the matrix, and/or the mechanical interlocking between the deformed surface of the steel and the matrix.

According to Abrams[4], after failure of adhesion of a plain bar the frictional force is provided by the shrinkage of the matrix about the bar. This follows from the basic quantitative law of friction given by the expression:

$$F = \mu . N$$

where F is the frictional force between the plain steel and the surrounding matrix, N is the normal force acting normal to the direction of sliding due to shrinkage, and μ is the coefficient of friction. The friction was found by Alexander[5] to decrease with increasing movement between steel and concrete and after a very large motion the surface of the softer material (i.e the concrete) becomes polished and the friction falls to a lower limit where it remains practically constant.

Although the bond of plain bars depends primarily upon adhesion and friction, the bond of deformed bars depends primarily on mechanical interlocking. This does not mean that friction and adhesion are negligeable in case of deformed bars but that they are secondary. Deformed bars are characterized by a bar surface with indentations or projections (ribs) at regular intervals which ensure a definite interlocking action between the embedded bar and the surrounding matrix. The quality of the bond developed by deformed bars depends upon the type of deformations protruding from their surface. Many experimental investigations which have been conducted into the effect of the surface condition upon the bond of bars showed that there was a better performance in the bond of deformed when compared to that of plain bars[6,7,8]. This was attributed to the bearing action of the deformations on the surface of deformed bars against the surrounding matrix. However the stresses that are generated by the bearing action can cause splitting of the concrete matrix if the cover of the steel is not sufficient[9].

The bond characteristics of prestressing strand are different from either plain or deformed bars. Although strand consists only of plain wires, the arrangement of the exterior wires results in an overall surface geometry which makes the strand belong neither to the above categories. Strand, with its long-pitched, helical arrangement of the exterior wires, untwists or unscrews itself when forced to slip through the rigid matrix embedment. This may affect the contact stress. The helical shape can differ from one lot of strand to another eg: Dyform, Normal (or plain). Strand has been produced with indentations on its surface and these indentations can have considerable effect on bond.

Stocker;M.F, and Sozen;M.A[10] studied the effect of the shape of strand by carrying out several pull-out tests on straight (nontwisted) strand, normal (twisted) strand, and single plain wire. Since strand is usually manufactured with standard pitch for each size and because it was desired to vary the pitch, they also tested solid square bars which were twisted by different amounts. It was shown that the wires tested in a group (straight and normal) developed a higher pull-out load than the single plain wire. The initial pull-out load (pull-out load before any slip occurs) of normal strand, which was found to be almost equal to that of straight strand, was about 4 times greater than that of single plain wire. Grouping of the wires was also found to affect the nature of the whole pull-out load/slip relation. The different rate at which the pull-out load of all the strands increased is shown in figure 1.2. After the adhesion was exceeded, the pull-out load of plain wire decayed rapidly and continued to decrease until at a slip of about 1.27mm it remained practically constant. The characteristics of the pull-out load/slip relationship of normal and straight strand were different. The pull-out load of straight strand, after a slight decrease following the failure of the adhesion, started increasing slightly. The pull-out load of normal strand, however, depending of its surface condition behaved differently. The pull-out load of normal strand of clean and shiny surface (coil II) decreased rapidly after reaching the bond force and after a slip of about 0.3mm it started peaking up whereas the pull-out load of normal strand with dull and dry appearance (coil I) does not exhibit any decrease. It is apparent from figure 1.2 that the rate of increase in pull-out load with slip is higher for the twisted strand. The increase in pull-out load with slip has been explained in terms of the lack of fit which results from the imperfect shape of the strand i.e the angle of twist, the pitch or the diameter varies along the bonded length of the strand.

While the helical shape of the strand has only a small effect on the initial pull-out load, the twisting of the bars was found to increase appreciably the contact pressure between the bar and the concrete which, consequently,

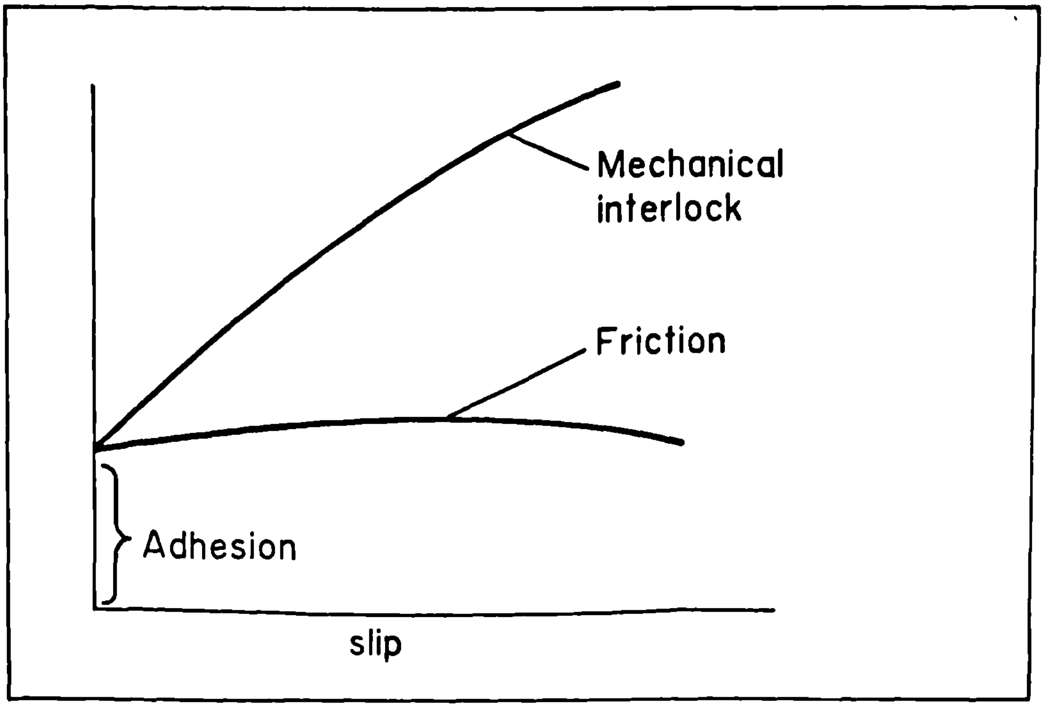

Fig. 1.1 Idealized representation of major components of bond

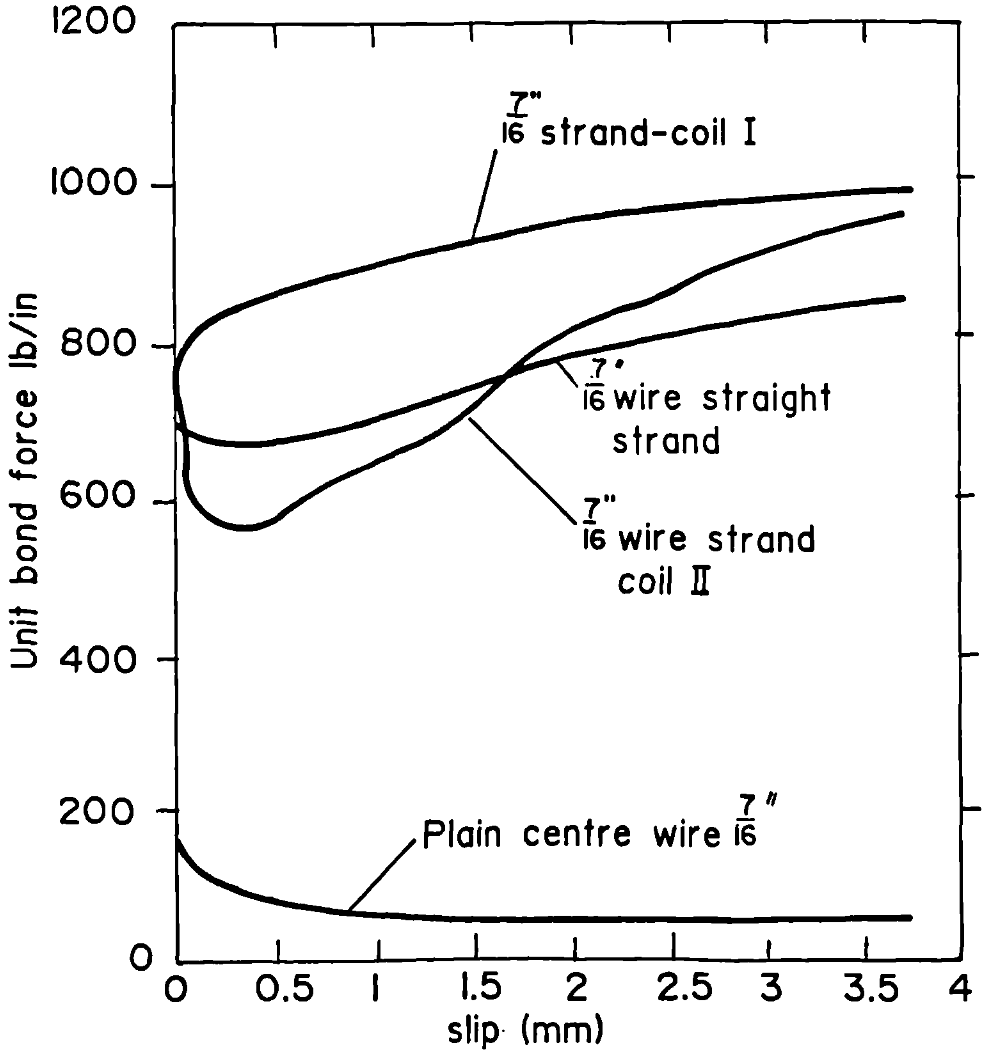

Fig. 1.2 Comparison of unit bond force. Slip relationship of straight (nontwisted) strand, plain $\frac{7}{16}$" strand of shiny surface (coil II) and dry and dull surface (coil I), and plain wire.
(From the investigation of Stocker and Sozen)

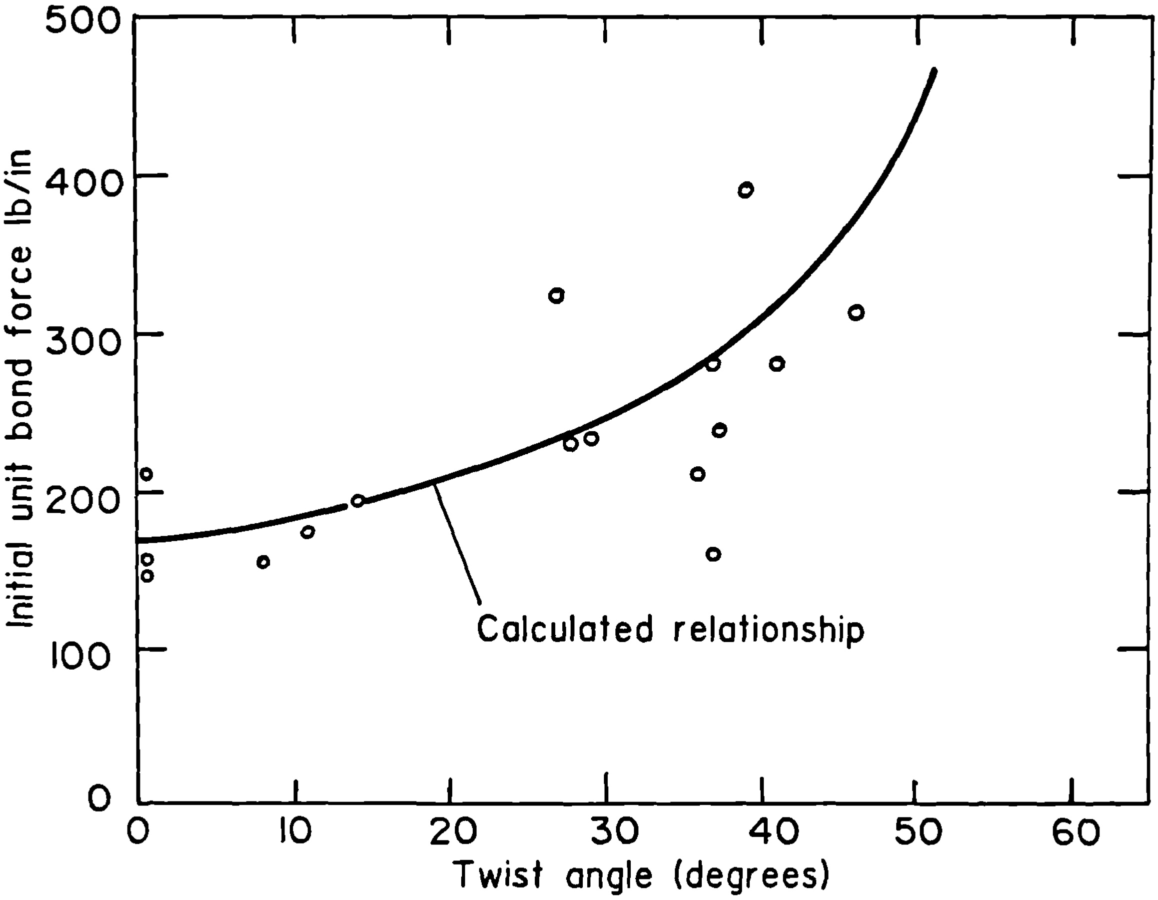

Fig 1.3 Initial unit bond force vs twist angle for square bar.
(From the Investigation of Stocker and Sozen)

improved the bond. The effect of the twist angle on the initial pull-out load is shown in figure 1.3. The reason for the discrepancies between the bar and the strand was attributed to the fact that the torsional stiffness of the strand was very small when compared to that of a square bar.

Shaffu[11] found that normal strand, on average, developed slightly more bond than the smoother (dyform) of a similar size but no concrete value was given).

The results obtained from the above investigations cannot be projected to the bond mobilized at the grout/prestressing strand interface because of the difference in the properties of grout when compared to concrete. Table 25,26,27 of DD81[2] present some recommended bond values for tendons embedded in cement grout. It has been suggested that the ultimate bond stress (i.e ultimate pull-out load per bonded unit area) for cement grout which is assumed to be uniform over the tendon bond length, should not exceed the following (bearing in mind that the strength of the grout is $30 N/mm^2$).

a) $1.0\ N/mm^2$ for clean plain wire or plain bar

b) $1.5\ N/mm^2$ for clean crimped wire

c) $2.0\ N/mm^2$ for clean strand or deformed bar

The above information is scanty and no convincing explanation for this variation has been found.

1.2 LATERAL PRESSURE

In addition to shrinkage, lateral pressure on the steel can be produced by the following:

- Stress at column-beam junctions exerted by the support reactions.

- Confining pressure around a ground anchorage due to earth pressure.

Lateral stresses perpendicular to the prestressing tendon occur in practically all ground anchorages because of the presence of the earth pressure surrounding the anchors. These pressures can have considerable influence on bond and cannot be neglected.

Untrauer and Henry[12] investigated the effect on bond of lateral pressure using concrete cylinders reinforced with deformed bars. The specimens were cast with the bar held horizontally. The lateral pressure, which ranged from 0 to 0.35 times the compressive strength of the concrete, was applied on two parallel faces of the specimens. The bond force was found to increase roughly in proportion to the square root of the lateral pressure.

Navaratnarajah and Speare[13] studied the effect of lateral pressure on bond using a double tension concrete pull-out test. The specimen consisted of a large concrete block reinforced with deformed bars simulated to the case of a pilecap. The lateral pressure which varied from 0 to 0.25 of the compressive strength of the concrete was applied to the specimen by means of a hydraulic jack, to one face of the specimen. The bond force was found to increase in proportion to the square root of the applied pressure.

Robins and Standish[14] performed pull-out tests on concrete blocks, using both plain and deformed bars, to study the effect of lateral pressure on bond. The pressure was applied by means of bearing plates on two parallel faces of the concrete specimen. The bond force of plain bars was found to increase linearly with laterally applied pressure of a magnitude ranging from 0 to 28N/mm^2. A theoretical approach was advanced to estimate the load in the bar at pull-out. The bond force of deformed bars exhibited a similar trend of increase as shown by Untrauer and Henry[12], however, above a lateral pressure of about 10N/mm^2 there was a levelling off in bond force.

Stocker and Sozen[10] were the first to investigate the effect of a hydrostatic pressure on bond in concrete cylinders, in which a seven-wire strand was embedded. The specimens were inserted in a pressure chamber where they were subjected to a uniform pressure which varied from 0 to 0.36 of the compressive strength of the concrete. The conclusion drawn was that the maximum bond force increased in proportion to the lateral confining pressure.

1.3 EMBEDMENT LENGTH

The question here is the effect of the length of embedment on bond stress (bond resistance per unit area).

Gilkey et al[15] found that up to a length of embedment-diameter ratio (L/D) of 24, the bond force for plain bars embedded in concrete increased, but not in proportion to the added length of embedment. Beyond this point the rate at which the bond force increased became negligible.

Stocker and Sozen[10] stated that at small slip the pull-out load per unit length of a seven-wire strand decreased when increasing the length of embedment. The trend of the decrease has not been evaluated since the relative magnitude was not consistent.

1.4 CONCRETE STRENGTH

The concrete strength is also a factor which can appreciably influence the bond.

Untrauer and Henry[12] reported that the bond force of deformed bars increases approximately in proportion to the square root of the compressive strength of the concrete, ranging from 25 N/mm^2 to 48 N/mm^2 (see chapter 4)

Neville[16] found that the bond force of deformed and plain bars was approximately proportional to the compressive strength of the concrete up to $21N/mm^2$. However at higher compressive strength the effect became negligible.

Stocker and Sozen[10] investigated the effect of concrete strength, ranging from $16N/mm^2$ to $52N/mm^2$, on bond of strand and plain wire. The concrete strength was found to have a small but a distinct effect on pull-out load throughout the whole range of slip. The mean pull-out load of plain wire at given slip was expressed as a percentage of the pull-out load developed at a concrete strength of approximately $34N/mm^2$. They found that the pull-out load of plain wire increased by roughly 4 percent for every $7N/mm^2$ increase of concrete strength. The pull-out load of seven-wire strands measured at various concrete strength was expressed as a percentage of that pull-out load that was found for a concrete strength of approximately $38N/mm^2$. It was observed that the bond resistance increased at a rate of 8 percent per $7N/mm^2$ of concrete strength for a slip of 0.0025mm and at rate of 11 percent per $7N/mm^2$ for a slip of 2.4mm.

Summarizing all the above discussion, it must be concluded that although there has been extensive investigations on bond in reinforced and prestressing concrete there are still disagreements between the findings of various investigations. The effectiveness of the lateral confining pressure, the surface condition of steel, the embedment length, and the matrix strength on bond requires further work to resolve these points of disagreements. Furthermore, there is little published information on the bond mobilized at the grout/prestressing strand interface. The present work is carried out to provide a basic data of the bond characteristics of prestressing strand in grout. The scope of the investigation can be divided into two parts.

1) A theoretical investigation as described in chapter 2 with the objective of deriving a means of predicting the load in the steel at pull-out, as affected by the mechanical properties of the materials in contact and the externally applied pressure.

2) The experimental study, dealt with in chapter 3, included a great number of simple pull-out specimens with short embedment lengths. The tests provided the necessary information on the relationship between pull-out load and slip. The major variables investigated were: lateral confining pressure, strand type, embedment length, and grout strength.

CHAPTER 2 ANALYSIS OF BOND FORCES

2.1 FIBRE REINFORCEMENT

Takaku,A and Arridge,R.G.C[17] studied the pull-out of a steel fibre from an epoxy matrix (see figure 2-1) and developed a theoretical model with which to predict the bond stress to produce slip between the fibre and the matrix. They based their predictions on the argument that the bond force is a result of the frictional resistance to movement at the interface of the fibre and the surrounding matrix due to forces acting normal to the fibre surface. The normal forces are result of shrinkage and dependent upon the relative stiffness of the materials in contact. They derived a relation for the stress in the fibre at pull-out as:

$$\sigma_f = \frac{\varepsilon_0 . E_f}{\nu_f} \left[1-\exp(- \frac{2.E_m . \nu_f . \mu . X}{E_f . r_f . (1+\nu_m)}) \right] \qquad (2.1)$$

where σ_f is the stress in the wire at pull-out, ε_0 is original lateral strain in the matrix (due to shrinkage), E_m and E_f are Young's moduli of matrix and fibre, ν_m and ν_f are Poisson's ratio of matrix and fibre, μ is the coefficient of friction between fibre and matrix, X is the embedment length, and r_f is the radius of the wire.

Pinchin,D.J[18] applied similar arguments to steel fibres embedded in concrete but included the effect on pull-out of the compression of the fibre by the matrix, which resulted in lowering of the effective interfacial stress, giving:

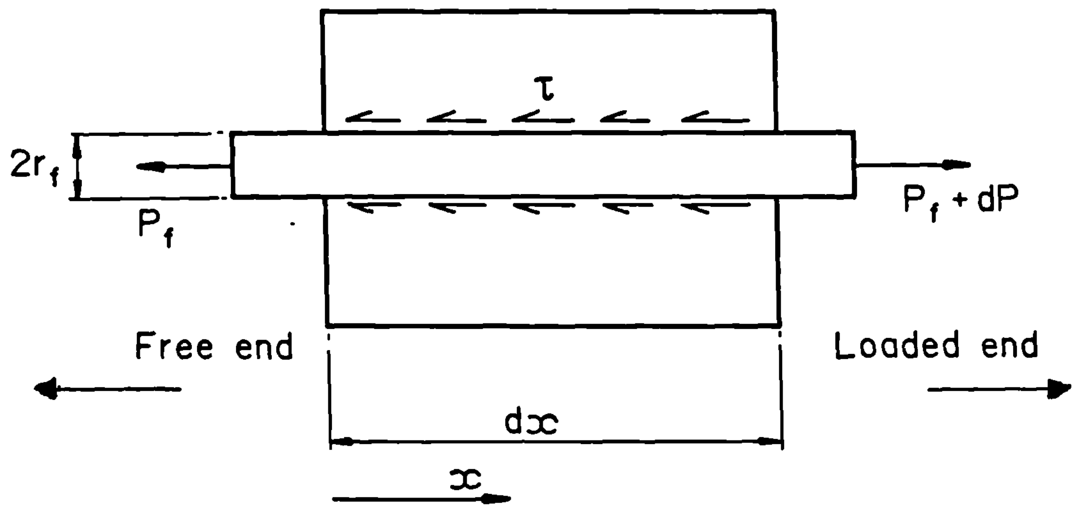

Fig. 2.1 Pull-out of an embedded continuous fibre from a matrix prism

$$\sigma_f = \frac{\varepsilon_0 . E_f}{\nu_f} \left[1-\exp-\left(\frac{2.\nu_f.\mu.X}{E_f.r_f\left(\frac{1+\nu_m}{E_m} + \frac{1-\nu_f}{E_f}\right)} \right) \right] \quad (2.2)$$

Pinchin's equation reduces to that derived by Takaku & Arridge[17] in the case where $E_f >> E_m$.

2.2 PLAIN BARS

Robins & Standish[14] studied the pull-out of a plain round bar from a concrete prism subjected to a lateral pressure applied on two parallel faces of the specimens. They reported that the result of applying a lateral pressure to the concrete matrix was to increase the interfacial pressure, or effectively the value of ε_0 and therefore the bond stress that can be mobilized. Using a similar arguments as Pinchin[18] they derived a new expression of the stress in the bar at pull-out as affected by the lateral pressure given by:

$$\sigma_f = \left(\frac{\varepsilon_0 + \varepsilon_0'}{\nu_f}\right) \left[1-\exp- \frac{2.\mu.\nu_f.X}{E_f.r_f\left(\frac{1+\nu_m}{E_m} + \frac{1-\nu_f}{E_f}\right)} \right] \quad (2.3a)$$

where ε_0' is the increase in strain resulting from the externally applied pressure which following Timoshenko[19] is equal to:

$$\varepsilon_0' = \sigma_{av} \left[\frac{1}{E_m}\left(\frac{r_f^2+(r_f+c)^2}{(r_f+c)^2-r_f^2} + \nu_m\right) + \frac{1-\nu_f}{E_f} \right] \quad (2.3b)$$

where σ_{av} is the average interfacial pressure acting on the bar perimeter due to the externally applied pressure.

c is cover to the reinforcement.

2.3 STRAND

Strand is a group of plain wires spun in helical form around a common longitudinal axis formed by a straight center wire. The analysis of the bond forces between strand and its surrounding matrix is made difficult by the complicated surface geometry of the strand. Following Stocker and Sozen[10] the problem may be simplified by considering the strand as a round bar with several lugs protruding from its surface. These lugs, representing the exterior wires of the strand, run helically around the bar forming an angle α with the axis of the bar (see figure 2.2a). It is assumed that only the lug is bonded to the grout (see figure 2.2a′).

Consider an elemental length, dl, of the strand model, similarly as that considered by Stocker and Sozen[10], which is subjected to a vertical pull P shown in figure 2.2a and redrawn in figure 2.2b. Neglecting the torsional stiffness of the strand, the following forces act on each lug.

1) A variation in pull-out force dP/n where n is the number of lugs, number of exterior wires in case of strand, and dP is the load transferred from the strand into the grout over the length dl.

2) A normal force N/n due to P acting on the inclined plane of the lug.

3) A friction force $N.\mu/n$ where μ is the coefficient of friction between strand and grout.

4) A lateral force F/n where F is due to shrinkage, externally applied pressure, and the relative contraction of

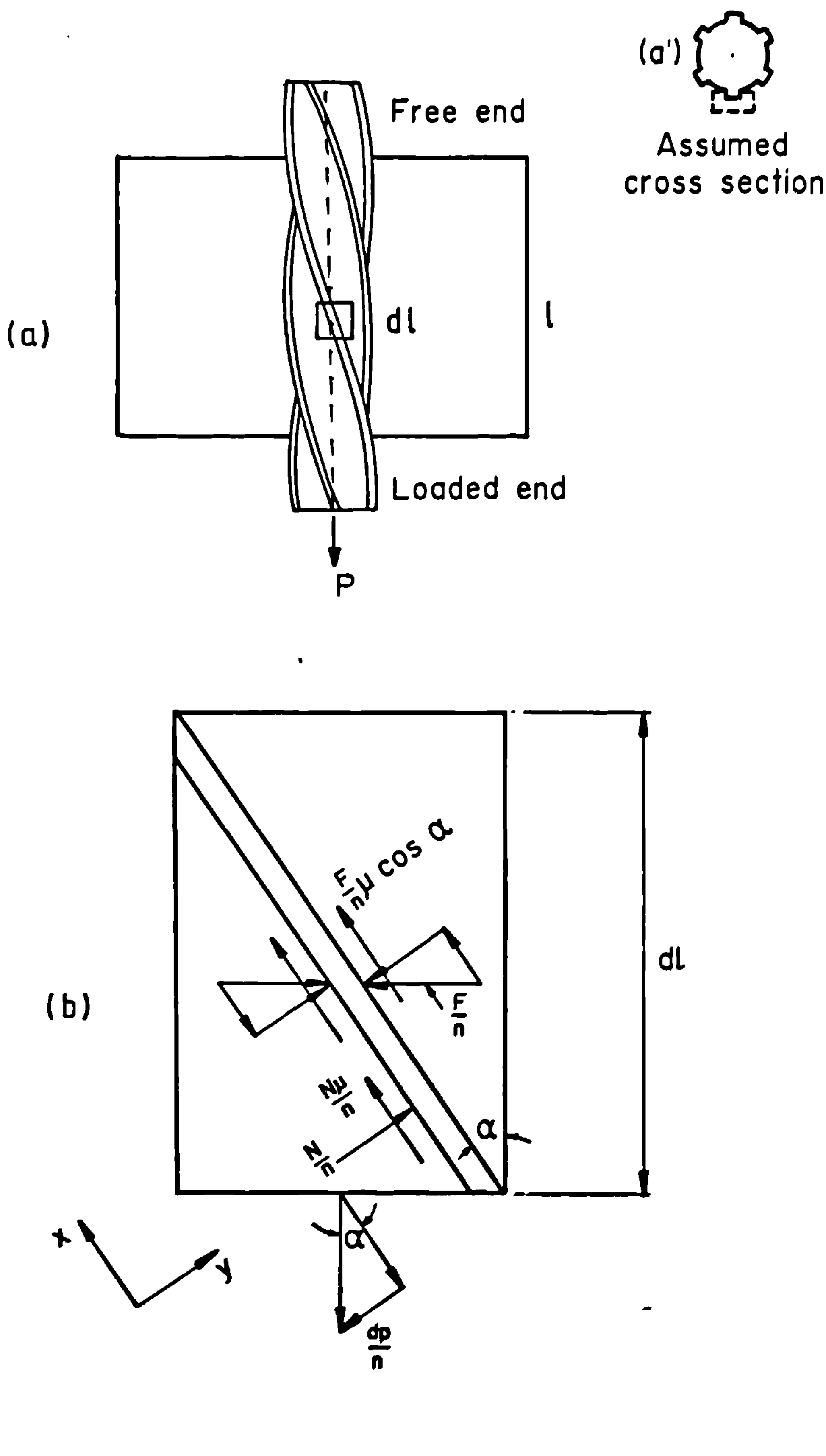

Fig. 2.2 A conceptual model for friction bond of strand

the steel due to its Poison's ratio.

5) A friction force $F.\mu.\cos\alpha/n$ parallel to the lug.

Summing the forces in the X- and Y- direction the following two equilibrium equations are obtained:

$$dP.\cos\alpha/n - N.\mu/n - F.\mu.\cos\alpha/n = 0$$

$$dP.\sin\alpha/n - N/n = 0$$

These two equations lead to the following expression for dP:

$$dP= \frac{F.\mu}{1-\mu\tan\alpha} \qquad (2.4)$$

F may be expressed in terms of two components.

$$F = F_1 + F_2 \qquad (2.5)$$

F_1 is lateral force due to the externally applied pressure.

F_2 is lateral force due to the shrinkage reduced by the relative contraction of the steel.

To determine the contact stresses caused by externally applied pressure and the shrinkage a similar assumption made by the above investigators has to be made i.e the grout and the strand are homogeneous linearly elastic materials. The grout prism is considered to be circular cross section. The problem is that of a thick-walled hollow cylinder subjected to uniform pressure on the inner and outer surface. The pressure on the outer surface is equal to the externally applied pressure.The pressure on the inner face is generated when the deformation of the grout cylinder directed inward is restrained by the steel which forms the core of the cylinder. Using Timoshenko[19] elastic theory, the stresses in a thick walled cylinder are given by the expressions:

$$\sigma_r = \frac{P_1 . a^2 - P_0 . b^2}{b^2 - a^2} + \frac{a^2 . b^2 \ (P_0 + P_1)}{r^2 \ (b^2 - a^2)} \quad (2.6)$$

$$\sigma_t = \frac{P_1 . a^2 - P_0 . b^2}{b^2 - a^2} - \frac{a^2 . b^2 \ (P_0 - P_1)}{r^2 \ (b^2 - a^2)} \quad (2.7)$$

where σ_r is the normal stress in the radial direction, σ_t is the normal stress in the circumferential direction, r is a radial coordinate, a is the radius of steel core or inner radius of the grout cylinder, b is the outer radius of the grout cylinder, P_0 is the external pressure and P_1 is the internal pressure caused the external pressure.

Under the influence of the inner presure P_1, the radius of the steel core, a, shortens by:

$$e_1 = \frac{- a . P_1}{E_s}(1-v_s) \quad (2.8)$$

where E_s is the modulus of elasticity of steel and v_s its Poisson´s ratio.

Any radius of the grout cylinder, which is subjected to an externally applied uniform pressure P_0 and an internal pressure P_1 deforms by:

$$e_2 = \frac{a}{E_m (b^2 - a^2)} \left[P_1 [b^2 (1+v_m) + a^2 (1-v_m)] - 2b^2 P_0 \right] \quad (2.9)$$

The displacements of the steel, e_1, and the displacement of the grout e_2 should match at their common boundary. Thus, the unknown contact pressure P_1 is:

$$P_1 = \frac{2.m.b^2.P_0}{(b^2-a^2)(1-v_s) + m[b^2(1+v_m)+a^2(1-v_m)]} \qquad (2.10)$$

where m is the modular ratio=E_s/E_m

The contact pressure caused by shrinkage can be determined in a similar fashion. The grout cylinder in this case is subjected only to uniform pressure P_2 on the inner surface. This inner pressure is generated when the grout tends to shrink and is restrained by the steel forming the core of the cylinder. If longitudinal shrinkage is neglected, any element of the cross section may be considered as being in a state of plane stress. The stresses in the grout cylinder which are set up when the grout surrounding the steel tends to shrink are determined by equations 6 & 7 with external pressure P_0 is equal to zero. Following equation 2.9 the radial displacement of the inner radius of the grout cylinder due to the restraining pressure p_2 becomes:

$$d_1 = \frac{a.P_2}{E_m(b^2-a^2)}\left[(1+v_m)b^2 + (1-v_m)a^2\right] \qquad (2.11)$$

Subjected to shrinkage P_2, the radius of the steel decreases by:

$$d_2 = \frac{-\ a.P_2}{E_s}(1-v_s) \qquad (2.12)$$

During pull-out, the steel radius contracts elastically by an amount depending on the axial stress in the steel and Poisson's ratio of the steel. This amount is given by:

$$d_3 = \frac{-a.v_s.P}{E_s.A_s} \qquad (2.13)$$

where P is the pull-out load, and A_s is the cross sectional area of the steel.

If the steel had been replaced by grout, the radius of the circular area taken by the steel would shrink by an amount:

$$d_4 = -a.\varepsilon_0 \qquad (2.14)$$

where ε_0 is the linear shrinkage strain of the grout.
In order to satisfy compatibility, the total deformation of the grout at radius a must equal the deformation of the steel i.e that:

$$d_2 + d_3 = d_1 + d_4 \qquad (2.15)$$

Solving this equation lead to the shrinkage pressure P_2 given as:

$$P_2 = \frac{(b^2-a^2)(\varepsilon_0 - \frac{v_s.P}{A_s.E_s})}{\frac{b^2-a^2}{E_s}(1-v_s) + \frac{1}{E_m}\left[(1+v_m)b^2+a^2(1-v_m)\right]} \qquad (2.16)$$

Neglecting $a^2 \ll b^2$ we get:

$$P_2 = \frac{(\varepsilon_0 - \frac{v_s.P}{A_s.E_s})}{\frac{1+v_m}{E_m} + \frac{1-v_s}{E_s}} \qquad (2.17)$$

From equation 2.10 we have:

P_1 is the inner pressure due to the externally applied

$$P_1 = \frac{\dfrac{2.P_0}{E_m}}{\dfrac{1+v_m}{E_m} + \dfrac{1-v_s}{E_s}} \qquad (2.18)$$

pressure.

If the contact area between the steel and the grout is A then the lateral forces F_1 and F_2 corresonding respectively to the ex ternally applied pressure and shrinkage reduced by the relative contraction of the steel are as follows:

$$F_1 = A.\frac{\dfrac{2.P_0}{E_m}}{\dfrac{1+v_m}{E_m} + \dfrac{1-v_s}{E_s}} \qquad (2.19a)$$

$$F_2 = A.\frac{\varepsilon_0 - \dfrac{v_s.P}{A_s.E_s}}{\dfrac{1+v_m}{E_m} + \dfrac{1-v_s}{E_s}} \qquad (2.19b)$$

By substituting F_1 and F_2 into equation 5 we obtain:

$$F = A.\frac{\dfrac{2.P_0}{E_m} + \varepsilon_0 - \dfrac{v_s.P}{A_s.E_s}}{\dfrac{1+v_m}{E_m} + \dfrac{1-v_s}{\varepsilon_s}} \qquad (2.19c)$$

Hence equation 2.4 becomes:

$$dP = \frac{A.\mu}{K(1-\mu\tan_a)}\left[\frac{2.P_0}{E_m} + \varepsilon_0 - \frac{v_s.P}{A_s.E_s}\right] \qquad (2.20)$$

where $K = \dfrac{1+v_m}{E_m} + \dfrac{1-v_s}{E_s}$

A is the contact area of the small element of length dx and perimeter C, where $dx=dl/\cos\alpha$ (see figure 2.2b). Rearranging A and subtituting into equation 2.20 we get (an expression for C is given in the Appendix) :

$$dP = \frac{C.\mu}{\cos\alpha.K(1-\mu\tan\alpha)}\left[\frac{2.P_0}{E_m} + \varepsilon_0 - \frac{\nu_s.P}{A_s.E_s}\right] dl \quad (2.21a)$$

Rearranging 2.21a we obtain:

$$dl = \frac{dP}{\dfrac{C.\mu}{K.\cos\alpha(1-\mu\tan\alpha)}\left[\dfrac{2.P_0}{E_m} + \varepsilon_0 - \dfrac{\nu_s.P}{A_s.E_s}\right]} \quad (2.21b)$$

Integrating this equation from zero load at the free end of the specimen to P_1 at the loaded end situated at a distance L from the free end, putting the result into exponential form and rearranging we get the load in the strand at pull-out as:

$$P_1 = \frac{A_s.E_s}{\nu_s}\left(\frac{2.P_0}{E_m} + \varepsilon_0\right)\left[1-\exp - \frac{L.C.\mu.\nu_s}{A_s.E_s.K.\cos\alpha(1-\mu\tan\alpha)}\right] \quad 2.22$$

where A_s is the cross sectional area of the steel

E_s is the modulus of elasticity of the steel

E_m is the modulus of elasticity of the grout

ν_m, ν_s are Poisson'ratio of grout and steel

ε_0 is the lateral strain due to shrinkage

L is the actual bonded length

C is the perimeter of the steel

μ is coefficient of friction between the two materials

α is the angle of twist of the wires around the axis of the strand.

2.4 EFFECT OF TORSIONAL STIFFNESS OF STRAND

This section contains a study of the effect of torsional stiffness of the strand on bond strength. Strand with its torsional stiffness can generate a torsional moment when sliding through the grout specimen. This is because the strand starts rotating about its own axis when it moves axially with respect to the grout in which it is embedded. The increase in pull-out load due the torsional stiffness can be derived by considering an elemental length as before similarly as made by Stocker and Sozen. In figure 2.3 the forces acting on the element as a result of torsional stiffness only are shown.

i) The spring force $k.s/n$ acting on each exterior wire of the strand represents a grout reaction that is equal in magnitude to the force necessary to untwist the strand.The constant k is a spring factor that corresponds to the torsional stiffness of the strand, s is the vertical slip of the strand over the elemental length dl.

ii) The force $k.s.\mu.\cos\alpha/n$ is the friction force acting on a plane parallel to the wire.

iii) dP/n load transferred from the strand over a length considered.

iv) N/n is the normal force due to P.

v) $N.\mu/n$ is the friction force.

Similarly as in the previous section the equilibrium of the element gives:

$$dP.\cos\alpha/n - k.s.\mu.\cos\alpha/n - k.s.\sin\alpha/n - N.\mu/n = 0$$

$$dP.\sin\alpha/n + k.s.\cos\alpha/n - N/n = 0$$

Solving these equation lead to:

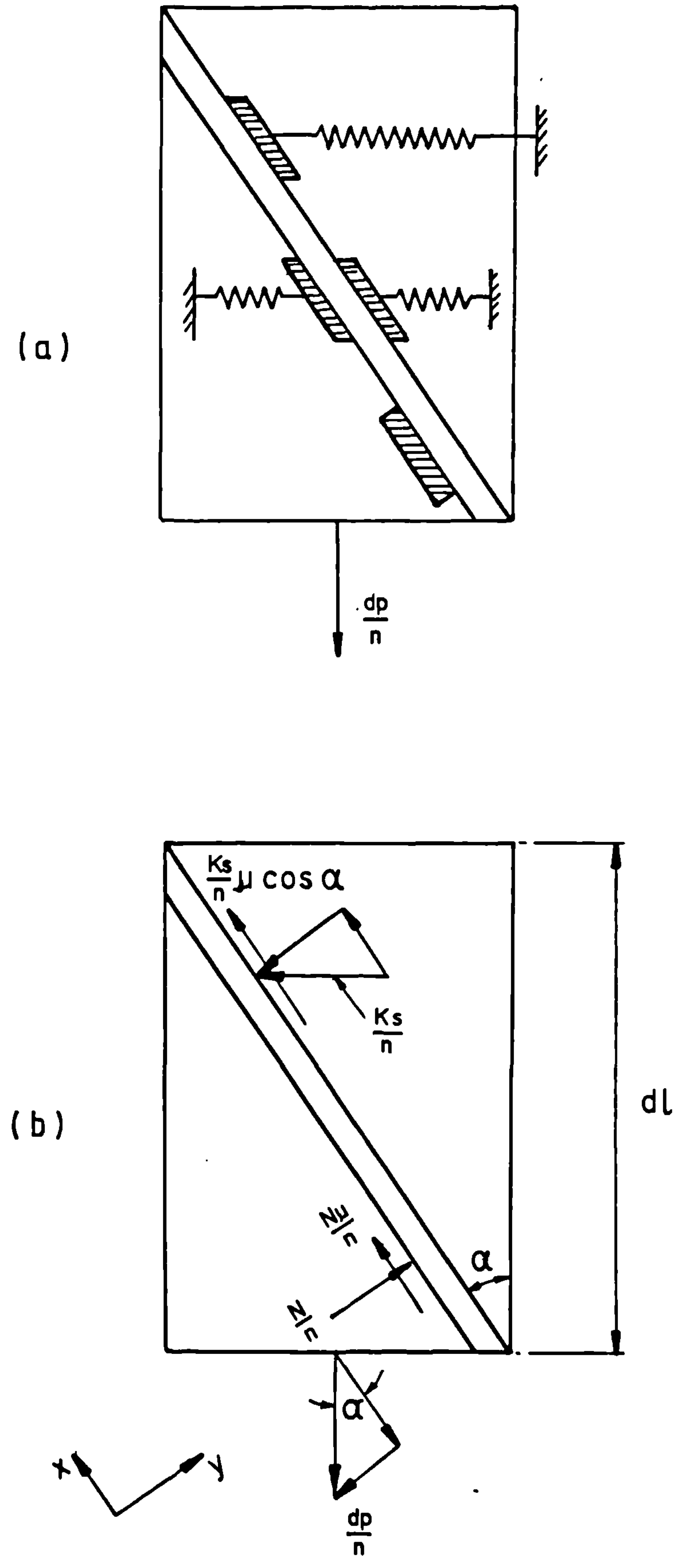

Fig 2.3. A conceptual model for torsional stiffness of strand

$$dP = \frac{k.s(2.\mu + \tan\alpha)}{1 - \mu.\tan\alpha} \qquad 2.23)$$

Because of the composite cross section of the strand it is very difficult to determine k theoretically. Therefore the torsional stiffness of the strand was measured experimentally using the apparatus shown in Plate 1. A gauge length of about 187mm (shorter than the actual twist length of the test specimens shown in figure 2.4) of plain strand and dyform was rotated by small weights acting over a lever arm. The weights needed to rotate the strand and the amount of rotation in degrees were measured. Figure 2.5 shows the measured relationship between the applied load and the rotation of the strands.

In order to determine the spring constant k a resultant force distribution representing the contact stress between the strand and the grout due to the untwisting of the strand is assumed to be as shown in figure 2.6.

The resulting force couples Q.t, where Q is the spring force k.s/n acting on each exterior wire perpendicular to the main diameter of the strand and its point of application is situated within the gap existing between two exterior wires, t is the moment arm as shown in fig.2.6. Since for seven-wire strand there are three couples then:

$$T = 3.Q.t \quad (2.24a) \qquad \text{with } Q = k.s/n \quad (2.24b)$$

$$k = \frac{n.T}{3.t.s} = \frac{6.T}{3.t.s} = \frac{2.T}{t.s} \qquad (2.25)$$

With the slip s and the angle of rotation, θ, being inter-related by the equation $\theta = 2.\pi.s/p$ the spring constant

Plate 1 Torsion apparatus

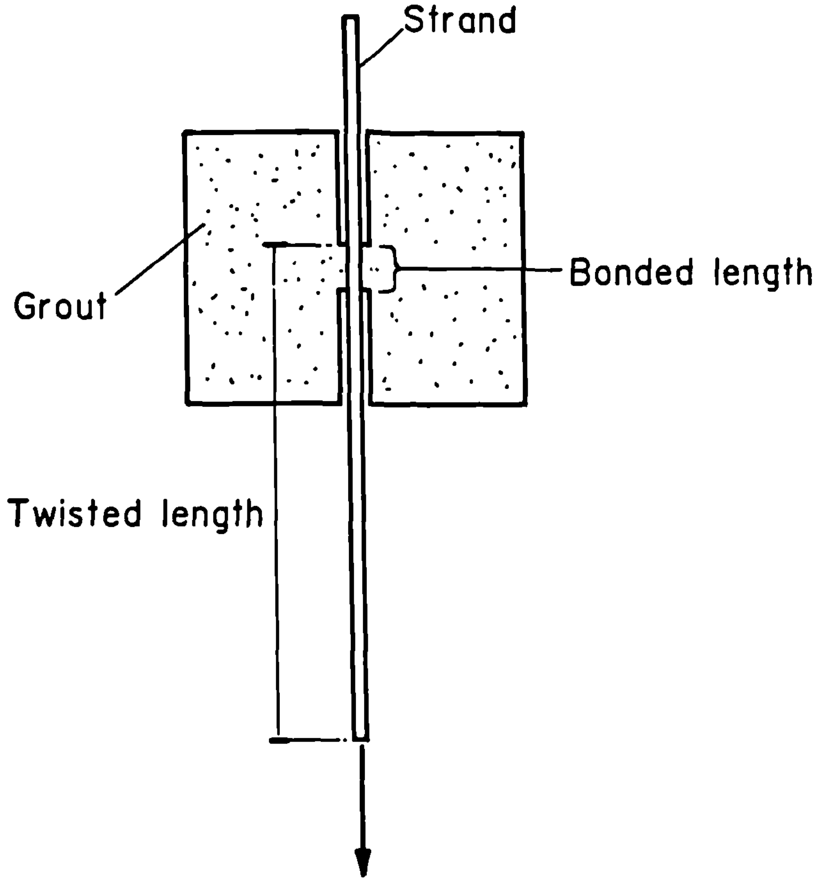

Fig 2.4 Typical specimens split into halves

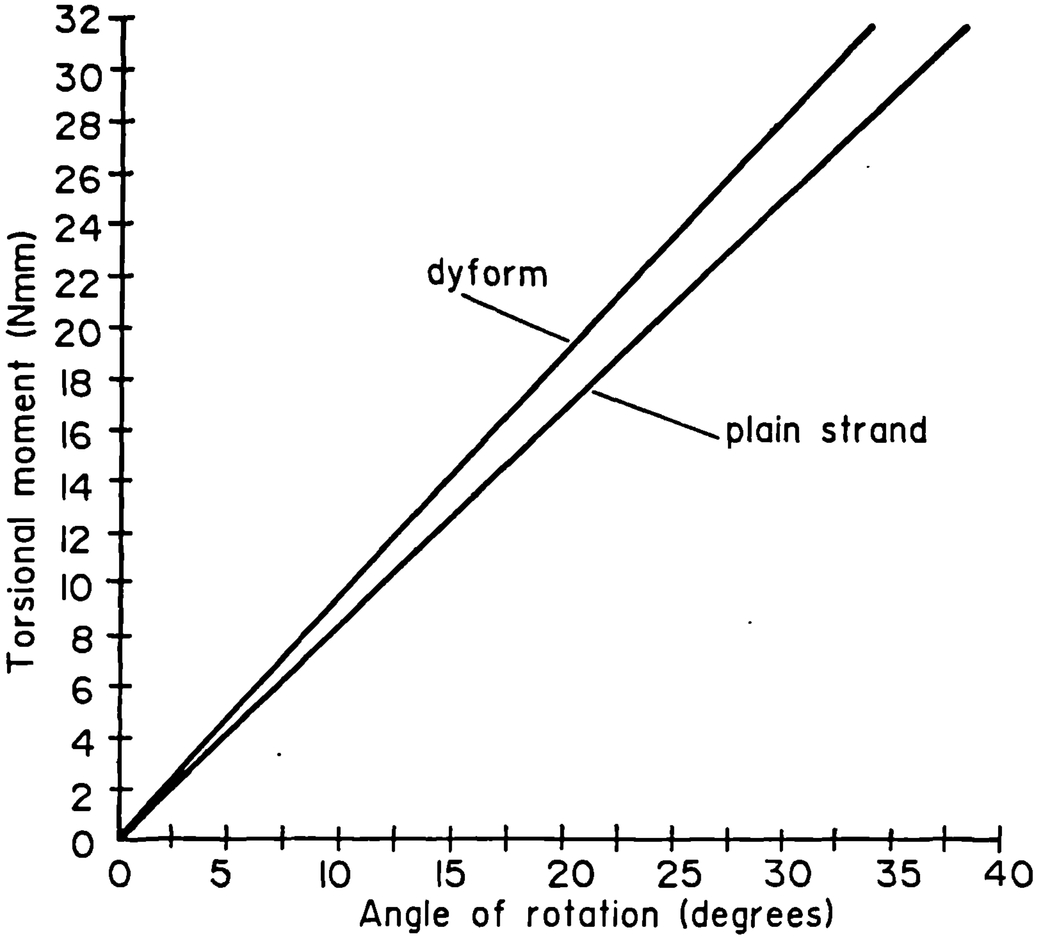

Fig. 2.5 Average moment rotation relationships of plain strand and dyform

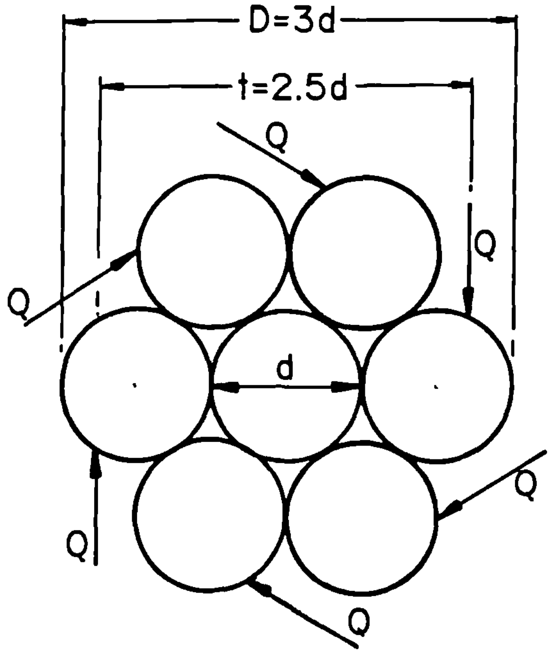

Fig. 2.6 Assumed force distribution on cross section due to untwisting of strand.

k becomes :

$$k = \frac{4.\pi.T}{t.p.\theta} \tag{2.26}$$

where T is the torsional moment

t is the moment arm which approximately equals to 5/6 of the diameter of the strand(average of diametral distance between point of contact of exterior wires and their external diameter.)

p is the pitch of the strand

θ is the angle of rotation of the strand.

Using the results of figure 2.4 on normal strand the spring constant k for 12.9mm normal strand is found to be 27 kg/mm (0.27 KN/mm). Taking a coefficient of friction ν=0.28, and an angle of twist α=11.45, the additional part of bond force that may be generated within the grout by the torsional stiffness of the strand can be determined for different length of slip. The table 2.1 below summarizes the calculated values of that part of pull-out load generated by the torsional stiffness of the strand.

Slip(mm)	1	1.5	2	2.5	3	3.5	4
dP(KN)	0.22	0.33	0.44	0.55	0.66	0.77	0.88

TABLE 2.1 Effect of Torsional Stiffness on Pull-out Load

The tabulated results apply only to the gauge length of 187mm. They can be smaller if the length over which the torsion is applied is longer, this is because the torsional moment is inversely proportional to the length as given by the expression:

$$T = G.I_p \frac{\theta}{l} \qquad (2.27)$$

where T is the torque

G is the shearing modulus of elasticity

I_p is the polar moment of inertia

θ is the angle of torsion (in radians)

l is the free length over which the torsion is applied

CHAPTER 3 PULL-OUT TESTS

3.1 INTRODUCTION:

Among other tests such as the beam test, and the double tension pull-out test, a modification of the standard pull-out test [20] is considered the most appropriate test to represent the practical arrangement of ground anchorage sketched in figure 3.1.

In order to determine a direct relationship between slip and bond force, the magnitude of the slip and the bond stress along the bonded length would have to be known. Usually approximations can be made by assuming, for example, a constant bond stress distribution along the bonded length. However, the assumption is no longer true if the length of embedment is very long. A qualitative variation of bond stress of a plain bar during a pull-out as presented in DD81[2] and redrawn in figure 3.2, indicates that the bond stress is not uniformly distributed from the loaded end to the free end of the specimen. Therefore the ideal would have been to test reinforcement with an infinitesimal small bonded length thus assuring a uniform slip and consequently a uniform bond stress distribution. In practice,of course, a bonded length of finite value had to be adopted. This method was first used by Rehm[6] in an investigation on bond characteristics of plain and deformed bars. This approach is adopted in this test programme in an attempt to obtain a direct bond force-slip relationship. Bonded lengths of 25.4mm,50.8mm, and 76.2mm were used in this investigation

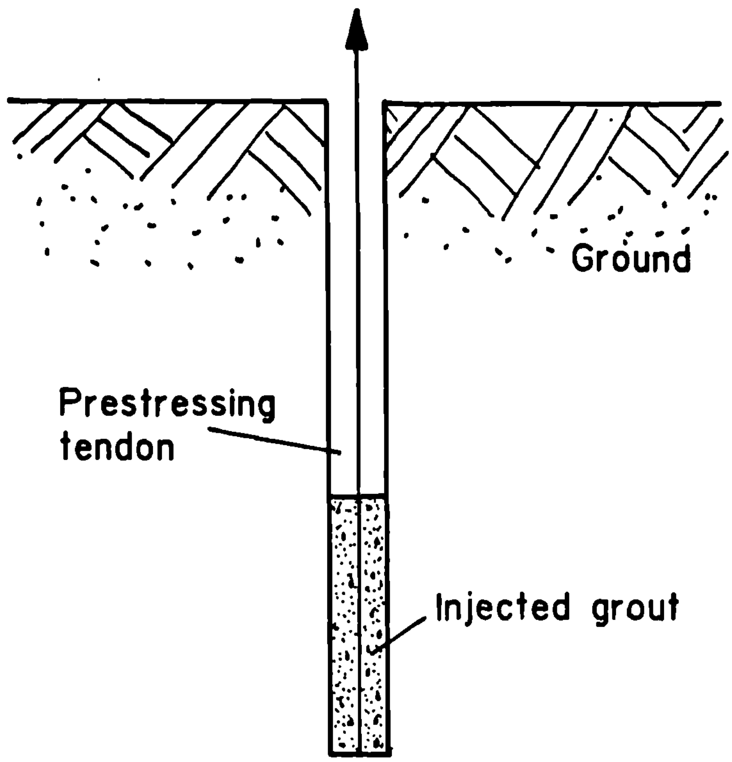

Fig. 3.1 Type of cement grout injection anchorage

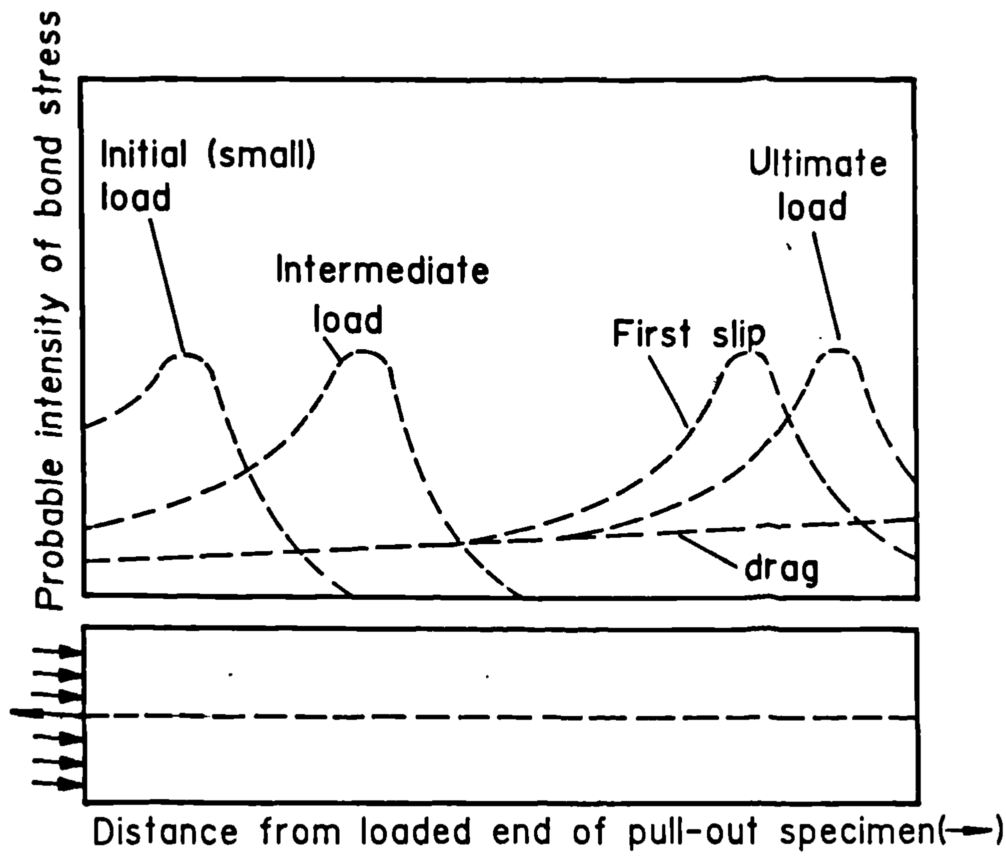

Fig. 3.2 Qualitative variation of bond stress during a pull-out test

3.2 MATERIALS

3.2.1 CEMENT

Ordinary Portland cement was used for the whole this test programme in compliance with BS12[21].

3.2.2 AGGREGATE

Washed river sand with a maximum size of 5mm in accordance to BS882[22].

3.2.3 STEEL

The steel used in this programme consisted of seven-wire strand. Three different types were investigated as shown in Plate 2.

Normal strand shown in Plate 2a is an ordinary strand which was made up by spinning six round wires together in helical form around a straight slightly larger center one.

Dyform is made up similarly to normal strand but is drawn through a die which compresses it making the strand smoother and compact (see Plate 2b).

Indented strand is similar to normal strand but the surface of the exterior wires are indented. The characteristics of the indentations, following BS5896[23], are as follows:

Depth 0.12 $\pm$ 0.05mm

Length 3.5mm

They are spaced at 60° around the outer wire of the strand and at 2mm longitudinally. The parts that separate two indentations from each other longitudinally are very similar to the ribs in deformed bars in that they project from the

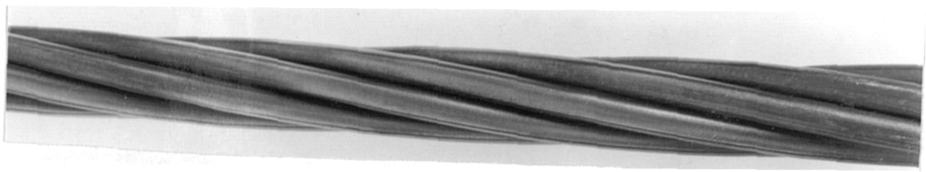

Plate 2a Normal strand

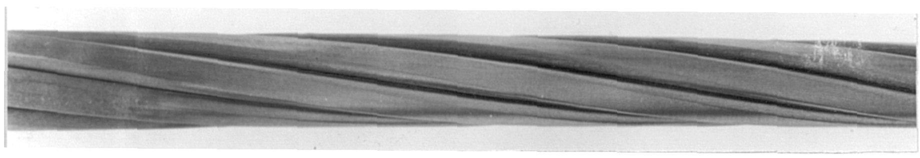

Plate 2b Dyform strand

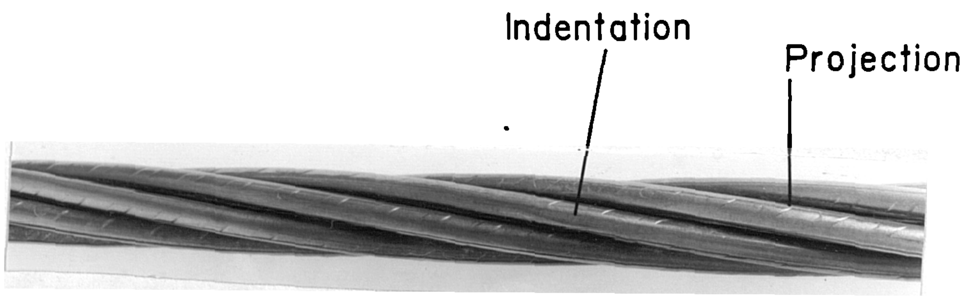

Plate 2c Indented strand

rest of the surface of the strand (see PLATE 2c).

3.2.4 GROUT PROPERTIES

The recommendations for ground anchorages given in DD81, ensuring that cement grout has good bond and shear strength are: (i) the mix should attain an unconfined compressive strength of $40N/mm^2$ minimum at 28 days when the samples are manufactured, cured, and tested in accordance with BS1881 part 111[24] (ii) the water to cement ratio should normally lie in the range of 0.35 to 0.60 (iii) for anchorages installed in low permeability ground e.g rock or clay, the water to cement ratio should not exceed 0.45.

Accordingly, in this test programme the mix proportions were chosen so that the compressive strength reached a minimum value of strength of $38N/mm^2$ within 15 days. They were chosen in such a way that while the amount of sand and cement was kept constant throughout the whole of this study the amount of water/cement ratio of 0.4,0.5 and 0.6 was used to vary the grout strength. Twenty five to twenty six mixes were carried out throughout this investigation and for each mix the number of samples cast are as follows:

i) Twelve pull-out specimens

ii) 3 to 4 cubes for compressive strength.

iii) 2 to 3 cylinder for splitting tensile strength.

The testing of the cubes and cylinders was carried out in accordance to BS1881, part 116[25] and 117[26] respectively.

3.3 MANUFACTURE OF TEST SPECIMEN

The basic pull-out specimen consisted of a 100x100x100mm

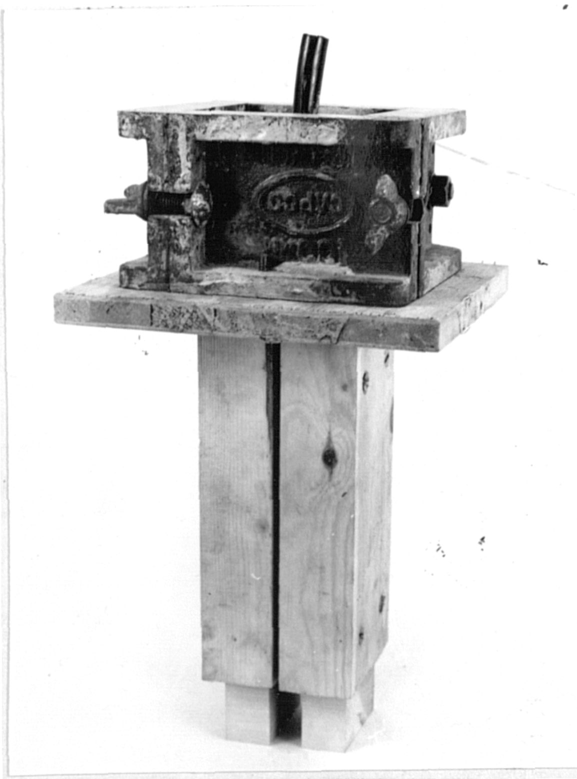

Plate 3a

Mould ready for casting

Plate 3c

Strand with only the bonded length visible grout prism. Figure 2.5 shows a typical specimen split into halves. The strand was positioned concentrically to the specimen. The length over which the steel was actually bonded to the grout was shorter than the length of the grout prism. The rest of the embedded length was, at the early stage of the project, kept from bond by using a transparent plastic sheath. However, it was found that the clear plastic film had an effect on the sliding bond resistance. Therefore this was replaced, for all the tests reported, by a thin-walled P.V.C tubing that was drawn over the steel. In the whole of this test program, the bonded length was located at the midheight of the grout specimen.

In order to produce a flat bottom face of the grout specimen which rests during test on a base plate, a special mould was designed (see Plate 3). The wooden base of the mould has a hole drilled in the centre through which the strand could project. This projecting end was held in a vertical position by a wooden clamp on which the whole mould was supported.

The strand was first cleaned of surface dirt and rust. Then it was carefully washed with trichloroethylene to remove any grease that might have been deposited on the surface while handling the steel. In order to assure a uniform slip of all individual wires during the test, the strand was tack-welded at the loaded end. Two P.V.C tubings with a wall thickness of approximately 1mm were pulled over both ends of the steel so far that only the bonded length was still visible (see Plate 3b). The inner diameter of the P.V.C tubing was chosen so that the tubes could slide along the steel with a minimum of clearance between the tube and the steel. The clearance at the ends near the bonded length was sealed with plasticine. For further precautions the P.V.C tubings were carefully greased with mould oil in order to prevent any bonding of the grout. Accordingly, their extraction from the specimen once the grout had hardened would not cause any disturbance of the bond between the grout and the steel. Consequently their removal before tests ensured that there would be no interference with behaviour after first slip. After casting and vibrating, the specimens were left in their forms for about 24 hours and kept moist by covering them with wet hessian. After 24 hours the cubes were demoulded and stored in tanks at a constant temperature of 20^{o}c in compliance with BS1881 Part111[24], until the fifteenth day (day of testing).

3.4 LOADING ARRANGEMENT

In order to design an experimental test rig which can reflect as close as possible the mode of operation of a ground anchorage, the special rig shown in Plate 4 was designed. It consisted of a main frame (100x100x400mm) resting on a stand on which a square flat base plate was bolted. At the interface between the base plate and the main frame, packing shims were used to provide clearance to prevent friction between the base plate and the 100x100 mm bearing plates which were used to apply lateral pressure on the specimen. Two of the four bearing plates were fitted on two cylindrical heads of two 200 KN hydraulic jacks, used to exert the lateral pressure. The two jacks were rigidly fixed on two adjacent sides of the main frame. The two other plates were also rigidly fixed on the two other adjacent sides of

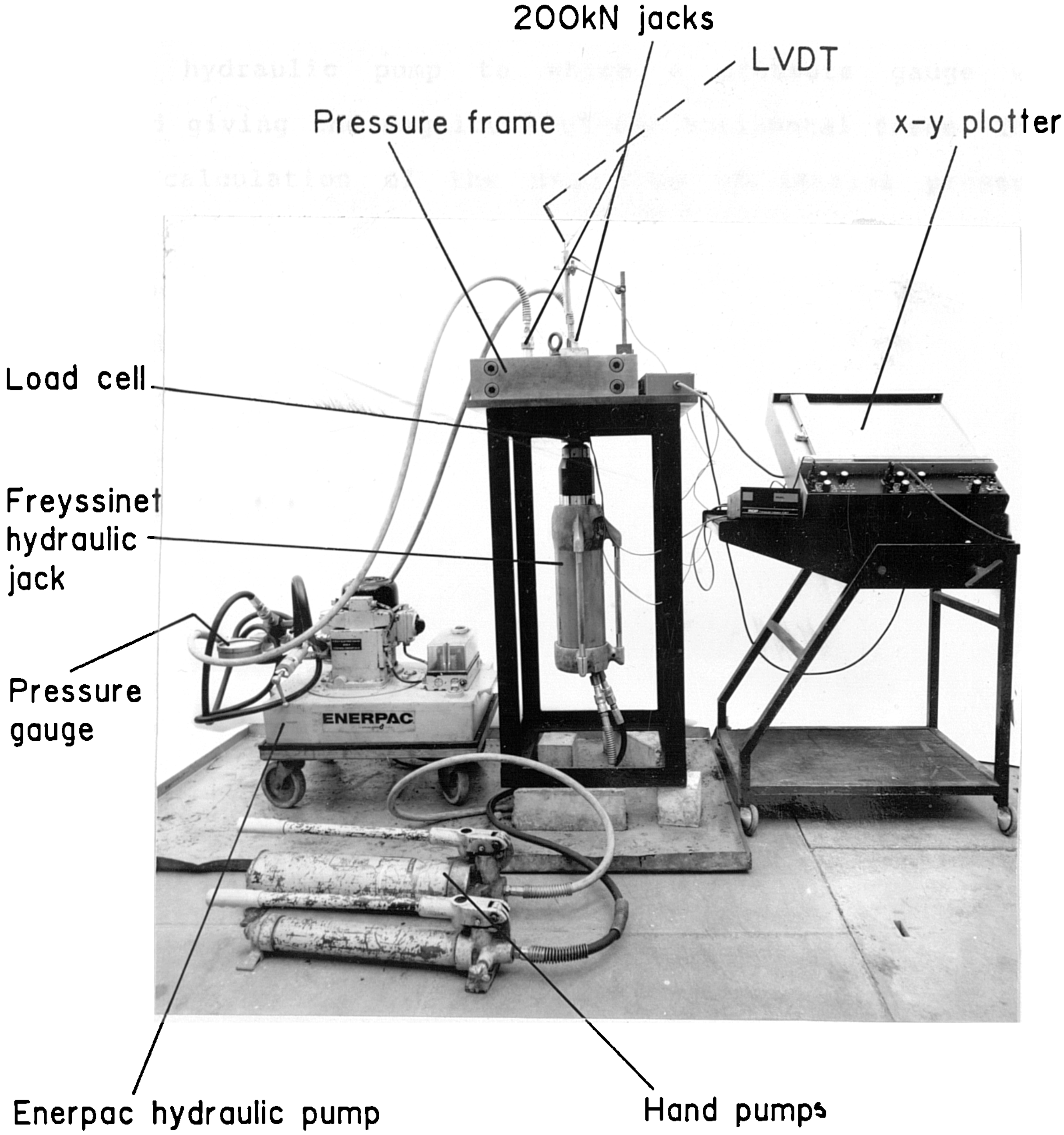

Plate 4 Testing rig

the frame. The bearing plates were 25.4 mm thick and assumed to be undeformable. The jacks were driven by an Enerpac electric hydraulic pump to which a pressure gauge was connected giving the magnitude of the horizontal force. This enables calculation of the magnitude of lateral pressure which is assumed to be uniformly distributed over the surface of the bearing plates. The test procedure for the specimens being subjected to lateral pressure was basically the same for all tests. The Enerpac electric pump was switched on and the control valve connected to it was manipulated until the desired lateral pressure was attained and the valve was then locked at that point. The pressure was applied before the pull-out of the strand started and held constant throughout the test. An exception was made in the test to establish the coefficient of friction described in section 3.5.3. The pull-out load of the strand was induced by a Freyssinet hydraulic jack pressurised by a hand pump. A second pump was used to reverse the action of the pump to enable removal of the specimen. The rate of loading was measured on almost all tests to maintain repeatability and the average rate was 6KN/min. To check the rotation of the frame, that may be encountered during tests due to strand rotation on loading, the displacement of the frame with respect to the base plate was measured using a dial gauge mounted on one corner of the frame. Negligible rotation was observed. The mode of operation of the test rig and its transfer of load mechanism is shown in figures 3.3a and 3.3b. The bottom face of the specimen subjected to lateral pressure is no longer in compression because the specimen does not rest on the base plate but it is held laterally by the applied pressure. A

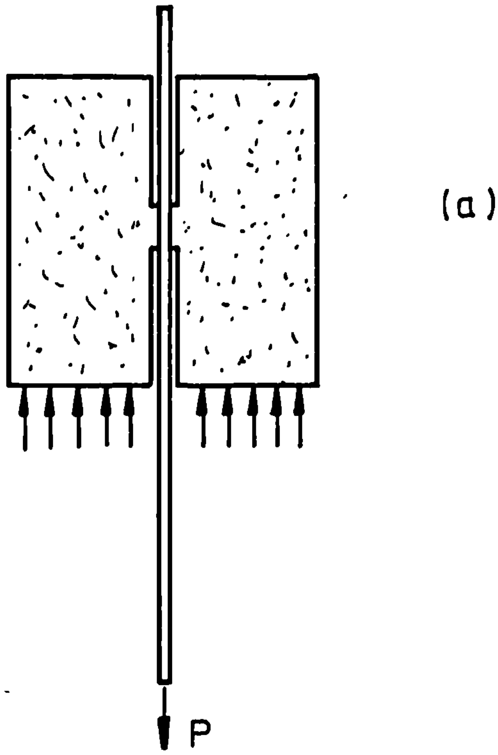

Specimen non subjected to lateral pressure

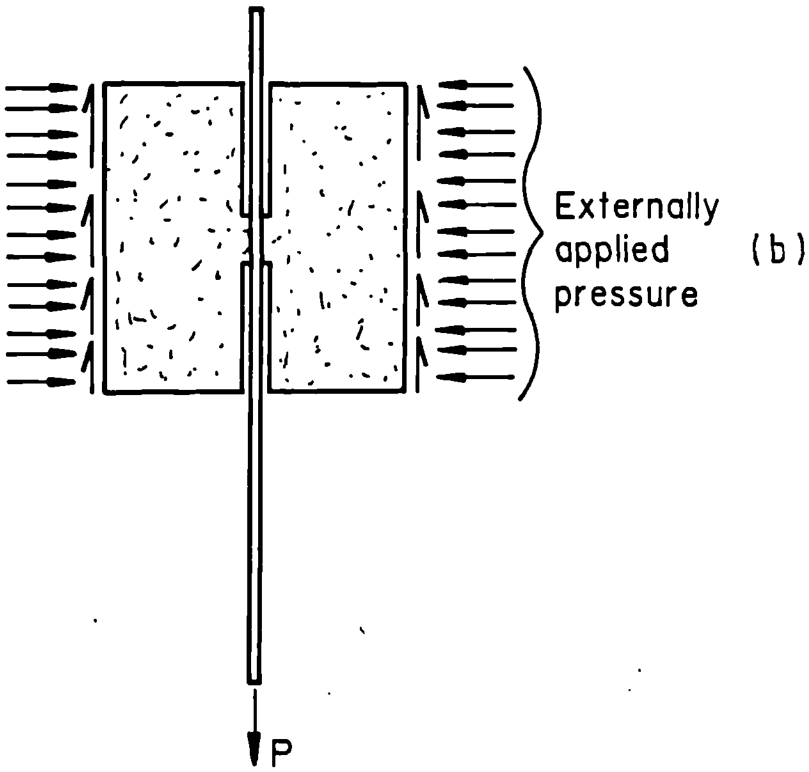

Specimen subjected to lateral pressure

Fig.3.3 Reacted load during pull-out

precalibrated load cell was fitted between the Feyssinet jack and the base plate. The tension in the strand was monitored by the load cell by giving a voltage output via a digital voltmeter. A precalibrated linear voltage displacement transducer (L.V.D.T) mounted at the free end of the strand of the specimen was used to measure the slip of the strand with respect to the adjacent grout. A X-Y plotter was connected to the load cell and the LVDT outputs, to plot the pull-out load vs slip (see Plate 4).

3.5 RESULTS

3.5.1 GROUT PROPERTIES

Three different mix proportions have been investigated in this programme and the properties of each mix are presented in table 3.1.

c:s	w/c	f'_c	f_t	E_c	ν_m
1:1	0.4	57	3.76	21.5	0.17
1:1	0.5	46	3.3	-	-
1:1	0.6	39.5	2.98	-	-

TABLE 3.1 Properties of Grout Mixes

where c:s proportion of cement to sand (1:1).

f'_c is the compressive strength of the grout N/mm^2.

f_t is the tensile splitting strength of the grout N/mm^2

E_c is the modulus of elasticity of the grout N/mm^2

ν_m is the Poisson's ratio of the grout.

3.5.2 SHRINKAGE

Regarding the difficulty in adopting the apparatus described in BS1881: Part5[27], the measurement of shrinkage was carried out using a different simple technique. Instead of using the size of specimen recommended (150mm to 300mm length and a cross section of 75mmx75mm) and seating the specimen on a 6mm stainless steel ball fixed on a frame, a 100x100x100 grout prism was used. The cubes immediately after being demoulded (about 10 hours after casting) were put on a surface table in a room temperature of $20^o c \pm 0.5$. Sensitive linear transducer graduated to 0.001mm was mounted on each cube (some 3 to 4 cubes were made) thus giving any change in length of the specimen during curing. Figure 3.4 shows the average variation in shrinkage with time during a period of 15 days, for grout with w/c = 0.4.

3.5.3 MEASUREMENT OF FRICTION COEFFICIENT

The measurement of friction coefficient between the grout (w/c=0.4) and the normal strand was carried out using two different methods.

A) First Method

This method consisted of sliding a flat piece of steel having the same surface roughness of the strand, on a grout prism. The measurement of the roughness of the the exterior wires of the normal and dyform strand, and the piece of steel was carried out using a Talysurf. A rectilinear recorder was connected to plot the roughness of the materials. The comparison of the graphs obtained showed that the normal strand had the same surface roughness as dyform. Many tests were made to obtain the piece of steel with the required roughness. The sliding of the piece of steel on the grout prism was carried out several times on the same traverse. The initial and the final coefficient of friction was measured. It was found that the coefficient of friction remained pratically constant and equal to 0.25 $\pm$ 0.02

B) Second Method

This method was first used by Stocker & Sozen[10]. It involves the application of step increases in lateral

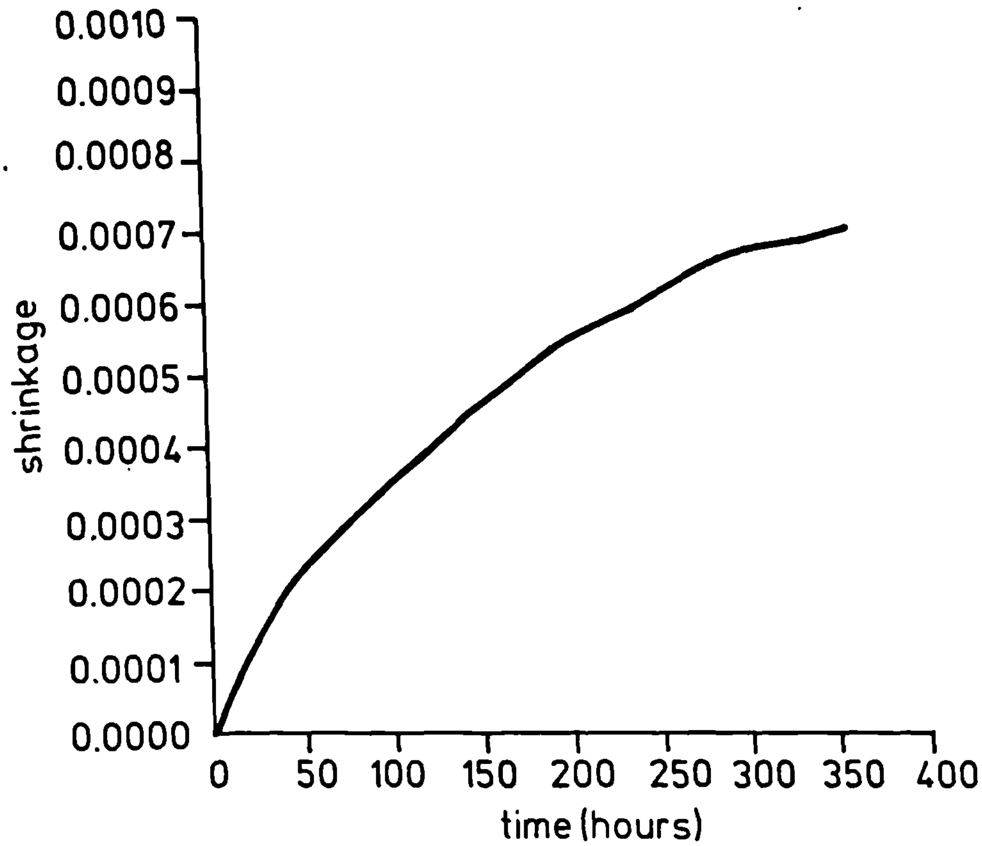

Fig 3·4 Drying shrinkage for a mix of w/c=0 4

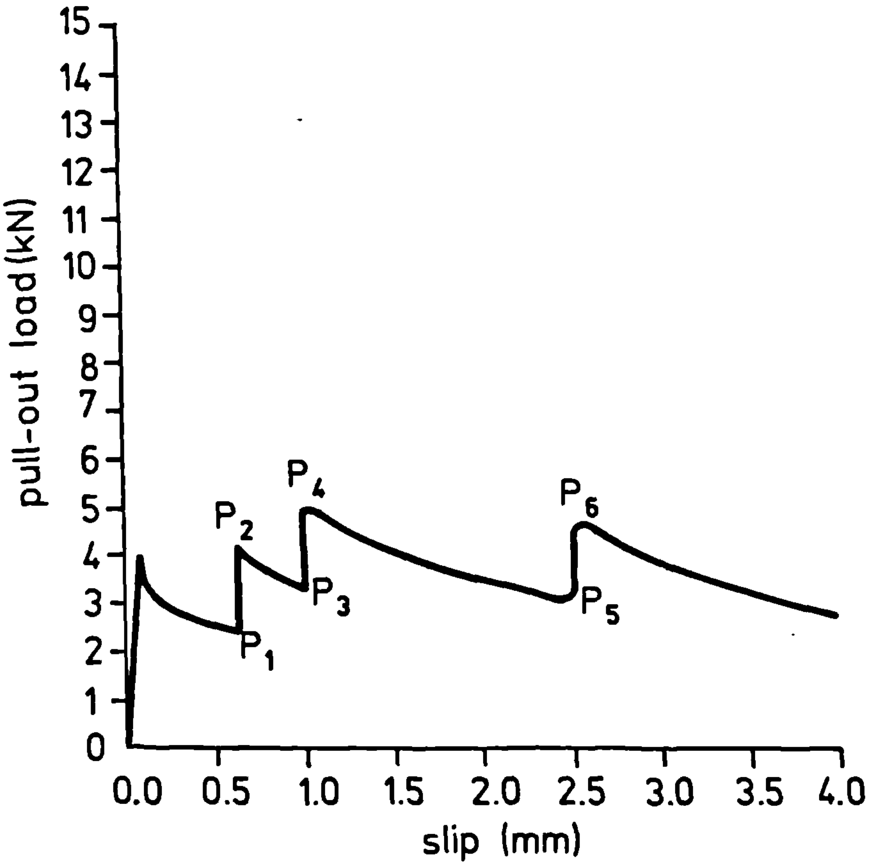

Fig 3·5 Typical pull-out load/slip for specimens with normal strand subjected to lateral pressure (do) increased in steps.

pressure after slip has occured and the measurement of the increase in bond force that results. A typical pull-out load/slip relationship obtained in this way is shown in figure 3.5. The lateral pressure is increased in steps of $1.4N/mm^2$, the first step being applied after an initial slip of 0.7mm. This causes an increase in pull-out load from P_i to P_{i+1} . Neglecting elastic deformation, the increase of lateral pressure on the strand $d\sigma$ equals the external lateral pressure and so the friction coefficient μ is given by:

$$\mu = \frac{P_{i+1}-P_i}{A.d\sigma}$$

where P_{i+1}, P_i = bond force according to figure 3.5

$d\sigma$ = increase of lateral pressure.

A = nominal bonded area.

Tests were conducted on several specimens over a range of slip varying from 0.7mm to 4.0mm. The mean value obtained for μ was 0.28 with a variation of $\pm$ 0.02. The reason for the discrepancy between this value and the value obtained from the first method was due to the fact that in the second method there is a combination of sliding of cement grout on steel and grout on grout at the interstices of the wires.

3.5.4 EFFECT OF LATERAL PRESSURE

The effect of a wide range of lateral pressure onto the pull-out specimens with a w/c=0.4 was studied. Lateral pressure ranging between 0 to $14.78N/mm^2$ (0 to 0.26 the cube strength of the grout) were applied onto the specimens, the levels applied are in table 3.2. For each lateral pressure 6 to 7 specimens were tested, the results being subsequently averaged, and the average pull-out load/slip relationship for each type of strand is plotted in figures 3.6(normal), 3.7(dyform), 3.8(indented).

Series	1.00	2.00	3.00	4.00	5.00	6.00
Lateral pressure (N/mm^2)	0.00	2.96	5.92	8.88	11.84	14.78

TABLE 3.2 Levels of Lateral Pressure

The shape of the pull-out load/slip relationship is unaffected by the magnitude of the lateral pressure. The pull-out load increases rapidly to a maximum bond force after which it falls off. Figures 3.6 to 3.8 also show that common to all the strands is a significant increase in pull-out load with increasing lateral pressure. For comparison purposes representative values of pull-out load have to be selected. A study of the pull-out load/slip curves and published work suggests that two values can be used i.e the maximum pull-out load at failure of the adhesion and the pull-out load obtained at a slip of 0.1mm. The latter value termed the critical bond resistance by Navaratnarajah and Speare[13] is considered to be an appropriate criteria in relation to permissible cracking.

The variation of the maximum bond force and the critical bond resistance of each strand with lateral pressure is shown in figures 3.9 to 3.11, also shown is the fit line obtained using the method of least squares. The graphs show that within the range of lateral pressure considered, the maximum bond force and the critical bond resistance increase linearly with the externally applied pressure. Further tests carried out using grout with a higher w/c ratio and of reduced strength suggests that there is a limit to the linear

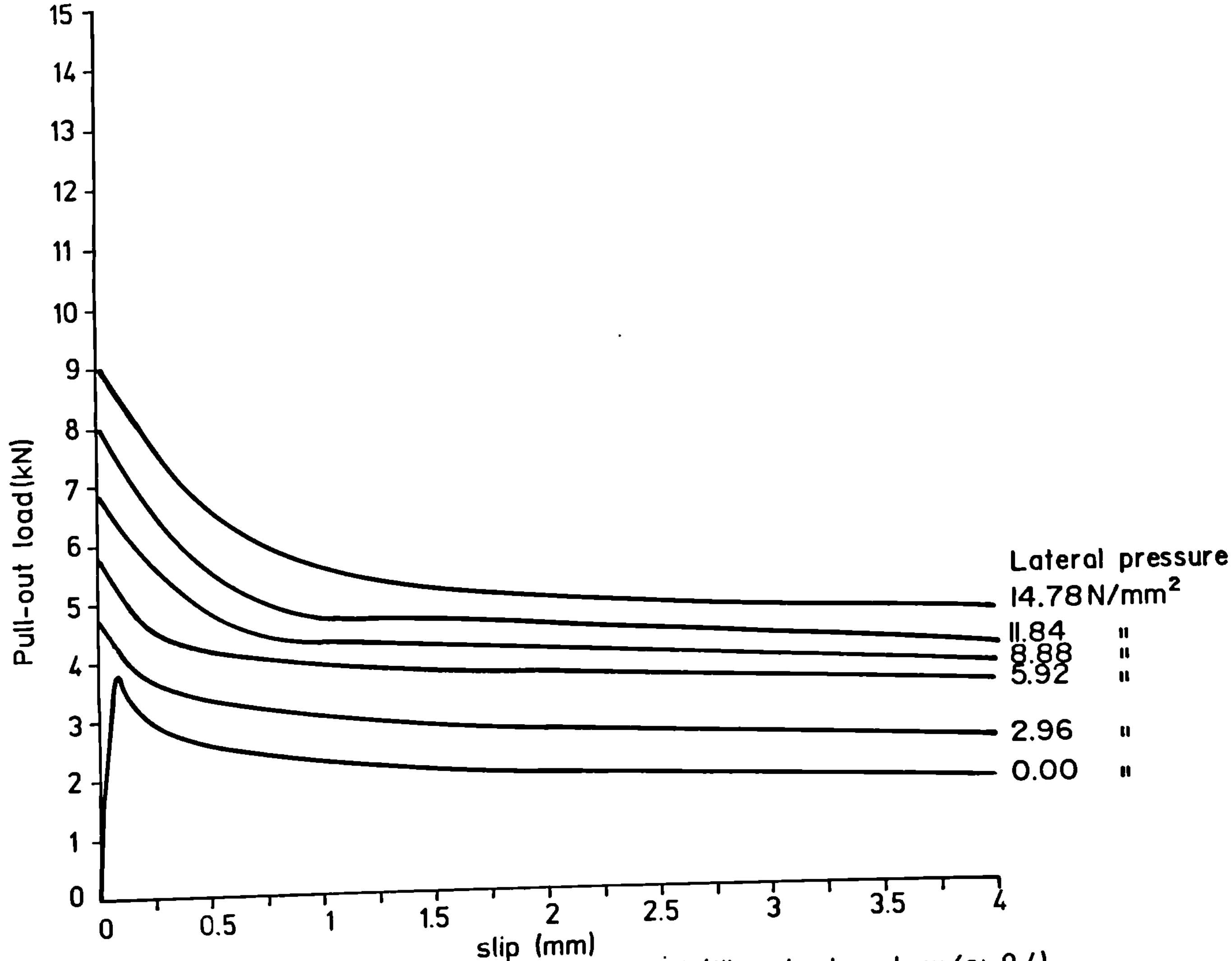

Fig. 3.6 Pull-out load/slip for plain strand (1" embedment, w/c = 0.4)

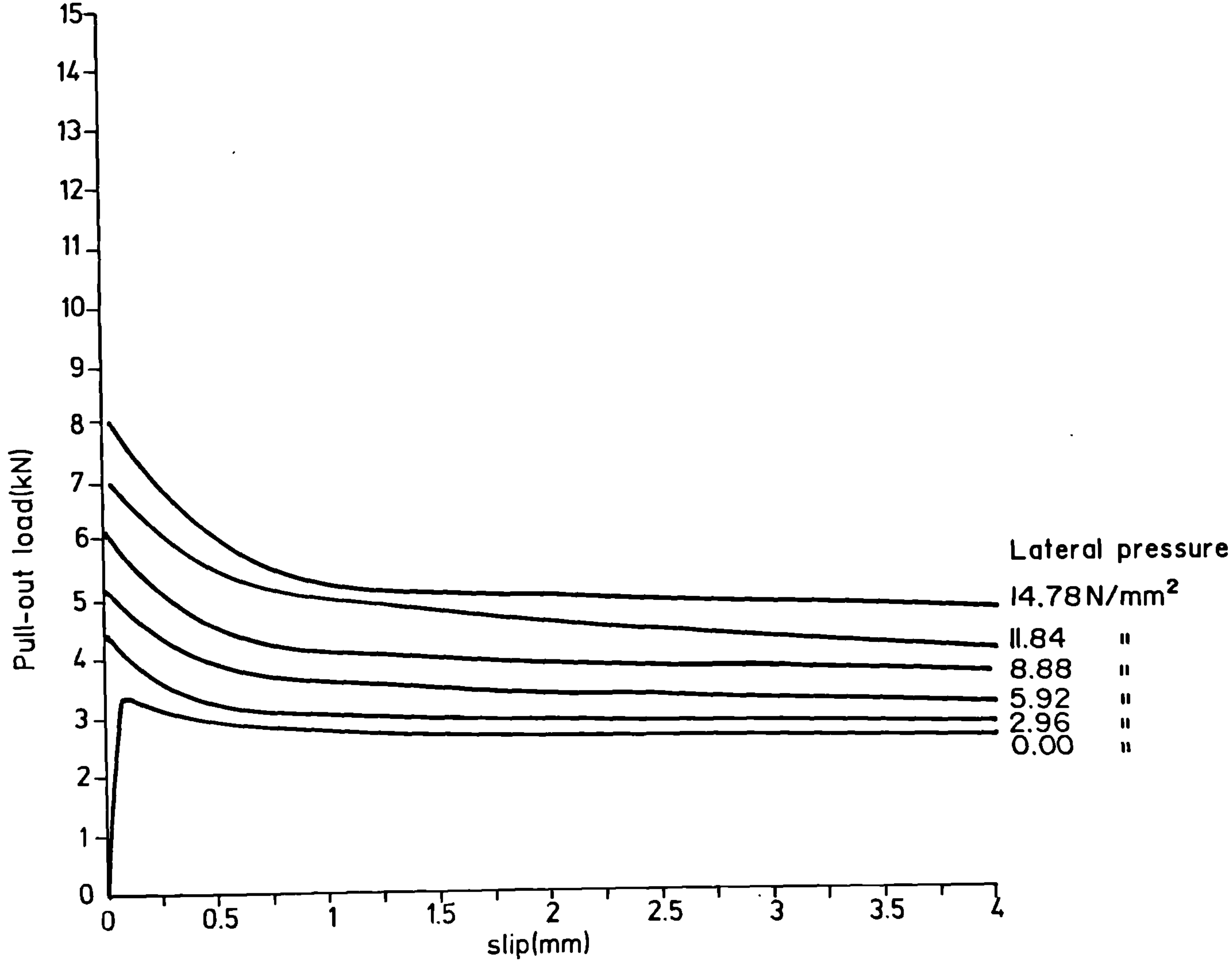

Fig. 3.7 Pull-out load/slip for dyform strand (25.4mm embedment. w/c=0.4)

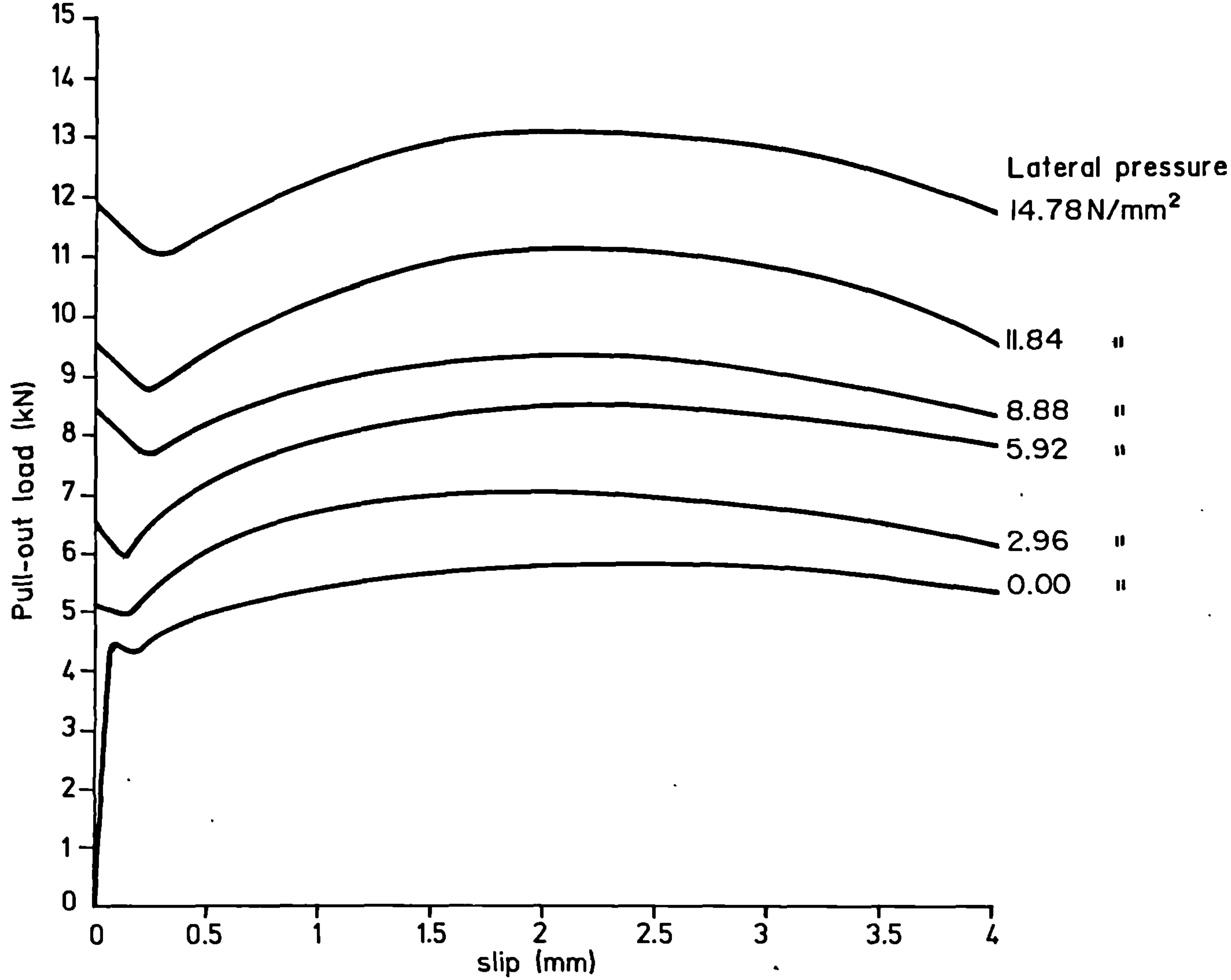

Fig. 3.8 Pull-out load/slip for indented strand (25.4mm embedment, w/c=0.4)

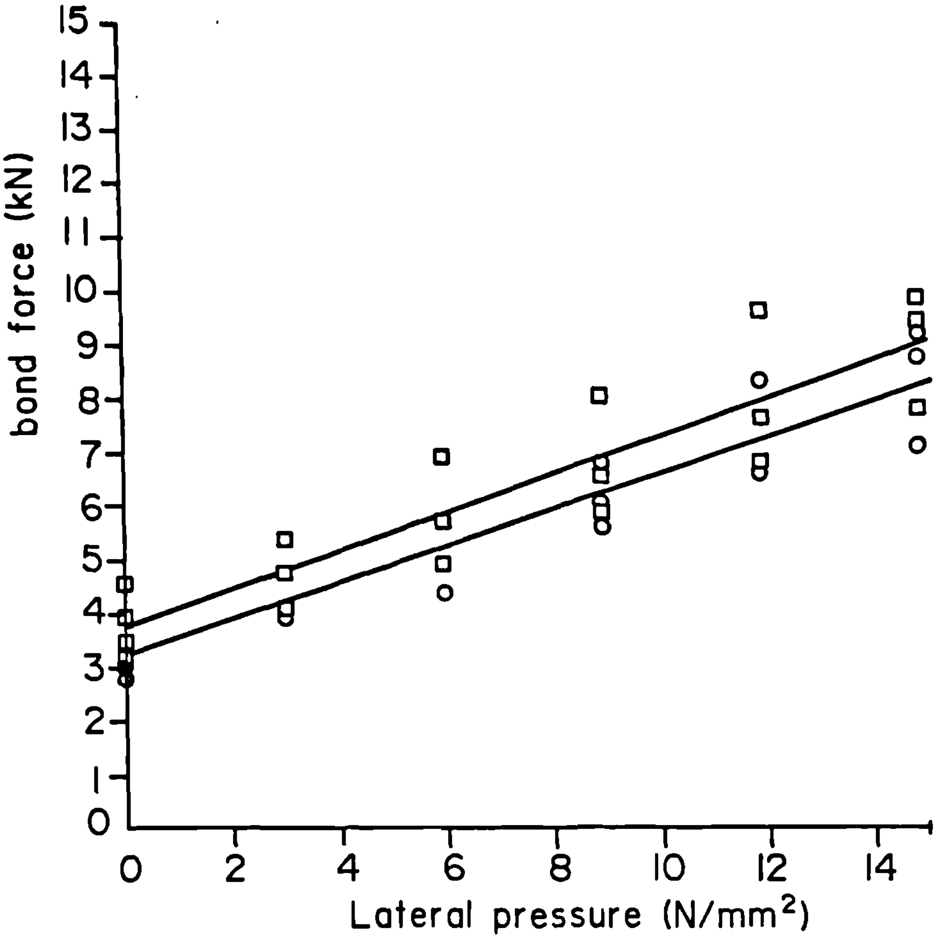

Fig 3.9 Effect of lateral pressure on maximum bond force and critical bond resistance for normal strand.

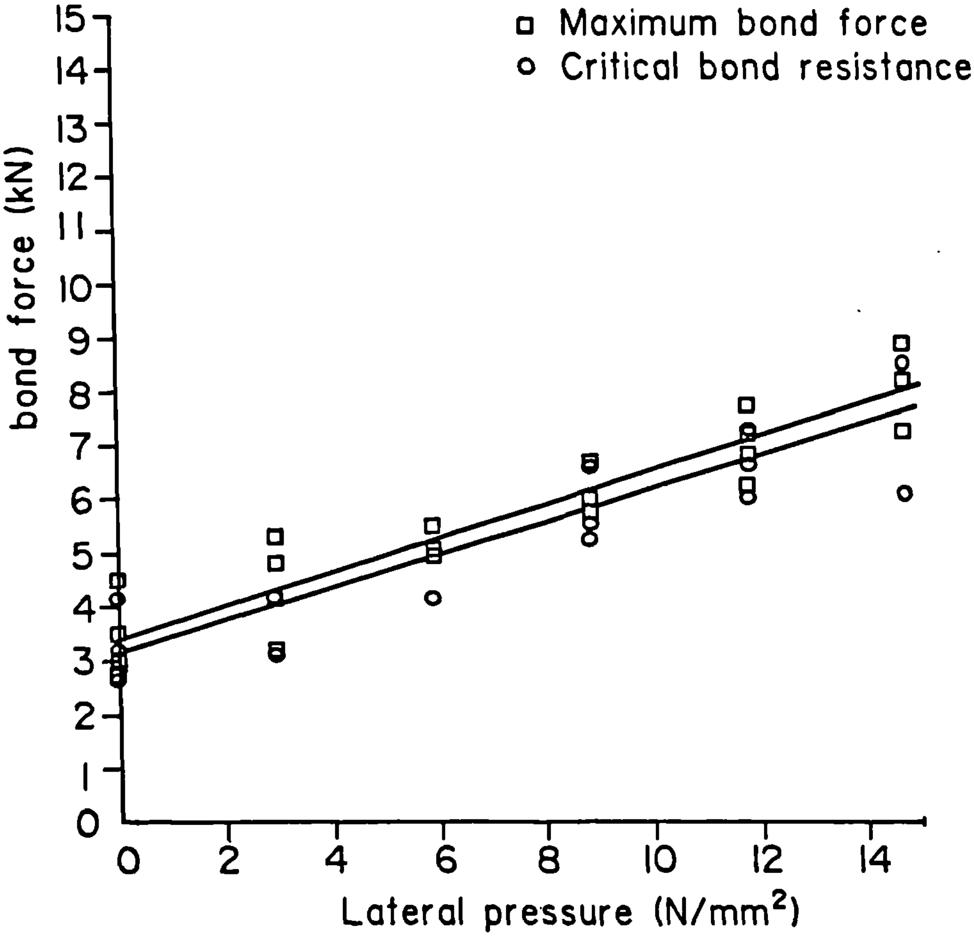

Fig 3.10 Effect of lateral pressure on maximum bond force and critical bond resistance for Dyform.

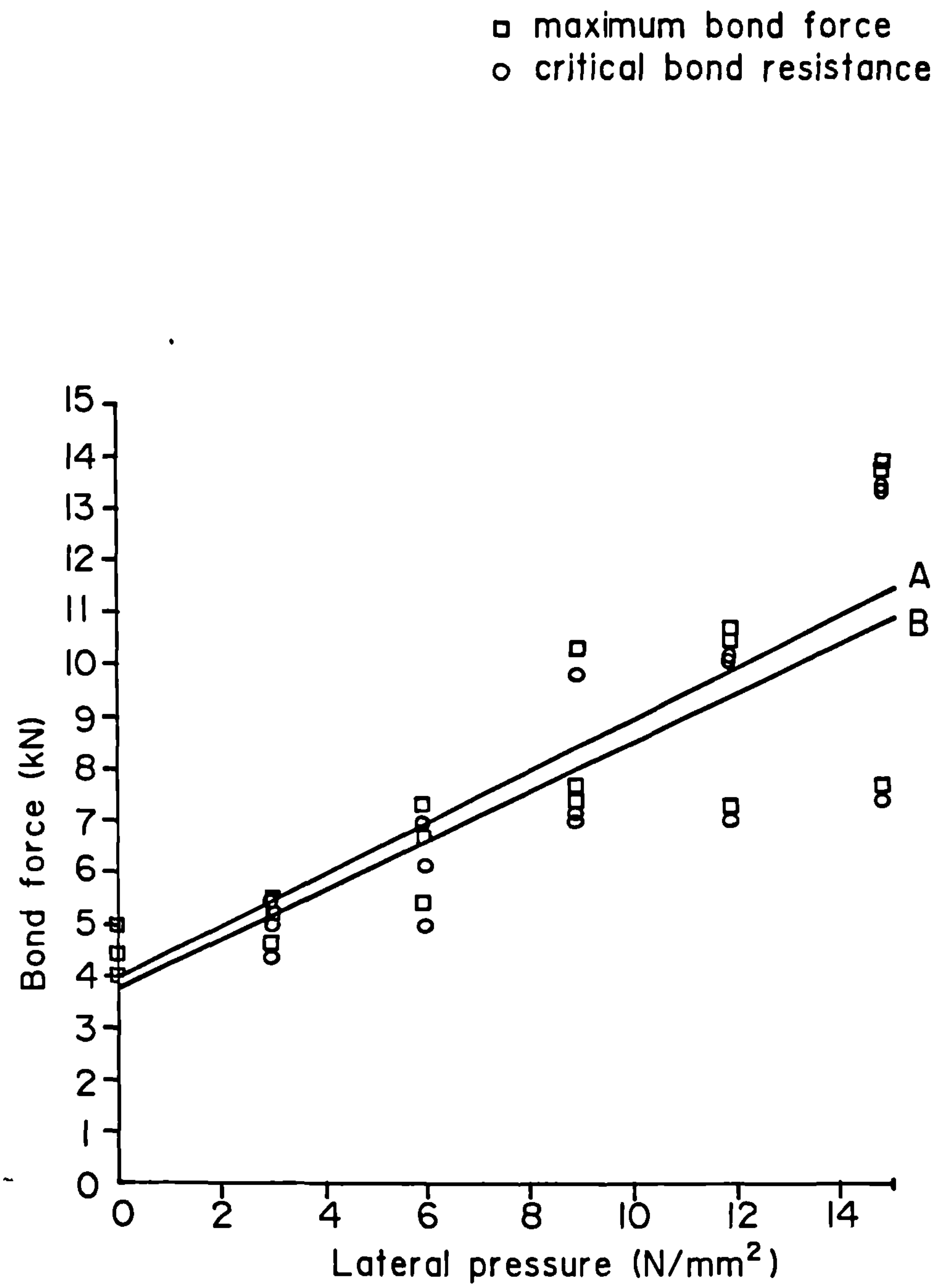

Fig. 3.11 Effect of lateral pressure on maximum bond force and critical bond resistance for indented strand

relation for a lateral pressure somewhere between 0.26 and 0.32 times the cube strength (see section 3.5.8). The rate of increase of bond with lateral pressure is different for each type of strand. The maximum bond force and the critical bond resistance increase as follows:

For normal strand by an average of 0.35KN $\pm$ 0.04 and 0.33KN $\pm$ 0.05 respectively for every 1N/mm^2 increase in lateral pressure.

For dyform strand by an average of 0.32KN $\pm$ 0.04 and 0.30KN $\pm$ 0.07 respectively for the same amount of lateral pressure.

For indented strand by an average of 0.50 $\pm$ 0.27 and 0.47 $\pm$ 0.29 respectively for the same amount of lateral pressure.

3.5.5 EFFECT OF STRAND TYPE

The maximum bond forces and the critical bond resistances produced by the different strands are summarized in table 3.3 and 3.4 respectively.

Comparison of the bond forces obtained at different levels of lateral pressures shows that the maximum bond force of indented strand is, on average, 15 percent with a variation of $\pm$ 0.12 and 31.5 percent higher with a variation of $\pm$ 0.15 than that of normal and dyform strand respectively. Its critical bond resistance is, on average, 27 percent higher with a variation of $\pm$ 0.09 and 34 percent higher with a variation 0.12, than that of normal strand and dyform respectively. The normal strand, in turn, developed, on average, a maximum bond force of 11 percent higher with a variation of $\pm$ 0.03 and a critical bond resistance of 6 percent higher with a variation of$\pm$0.020 than dyform.

3.5.6 EFFECT OF EMBEDMENT LENGTH

In addition to the tests made earlier on normal strand with 25.4mm bonded length, two other lengths 50.8mm and 76.2mm were tested in an investigation of the effect of embedment on bond. The tests series comprised either 5 to 6 cubes. The average pull-out load/slip relationship are plotted in figure 3.6, 3.12, 3.13. The maximum pull-out load and the critical bond resistance developed by each test series of a given length of embedment is presented in tables 3.5 and 3.6.

As expected the pull-out load increases as the length of embedment increases. This is due to the increase in the surface area of contact. However, doubling the length of embedment does not double the bond force e.g increasing the length of embedment by a factor of 2 and 3 the average maximum bond force increased by a factor of 1.67 with a variation of $\pm$ 0.11 and 2.36 with a variation of $\pm$ 0.26 respectively and the critical bond resistance by a factor of 1.77 with a variation of $\pm$ 0.08 and 2.57 with a variation of $\pm$ 0.23. The variation of the maximum bond stress (maximum bond force per unit area) and the critical bond stress with embedment length is plotted in figure 3.14 and 3.15 respectively.

3.5.7 EFFECT OF GROUT STRENGTH

Three different mix proportions for the grout were used to study the influence of grout strength on bond. The mix proportions, as reported earlier, were chosen so that while the amount of sand and cement remained constant for all

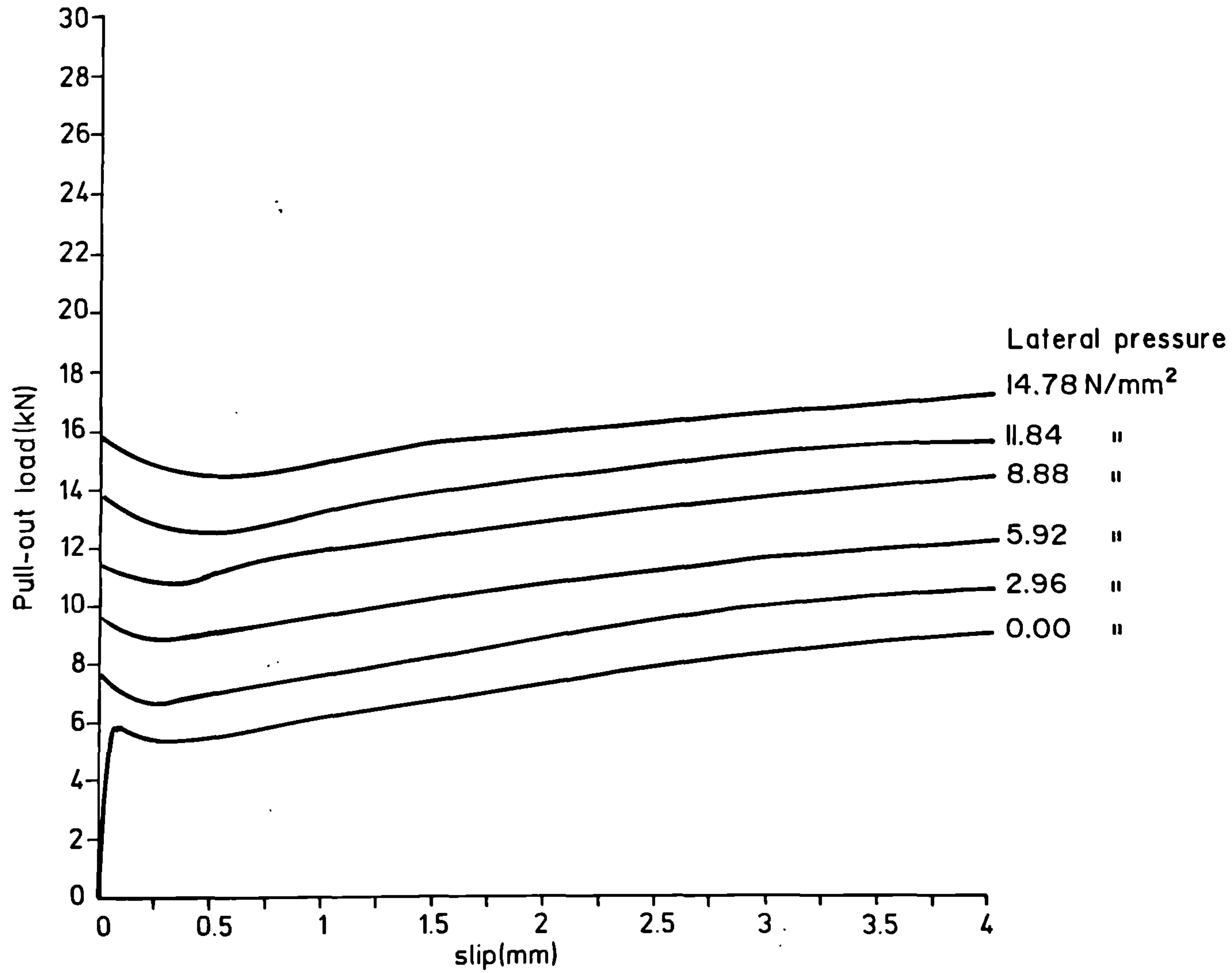

Fig. 3.12 Pull-out load/slip for plain strand (50.8mm embedment w/c=0.4)

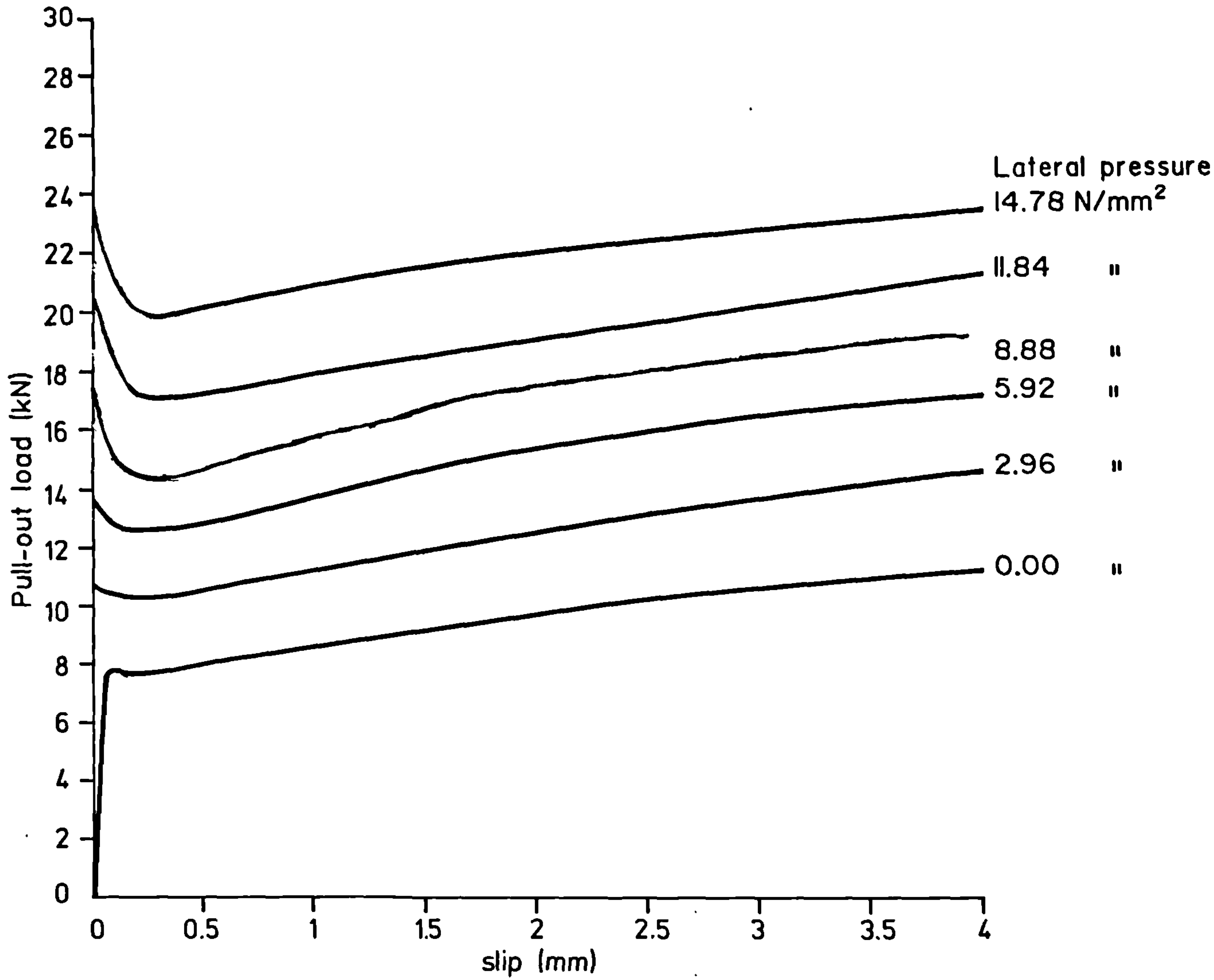

Fig. 3.13 Pull-out load/slip for plain strand(76.2mm embedment, w/c=0.4)

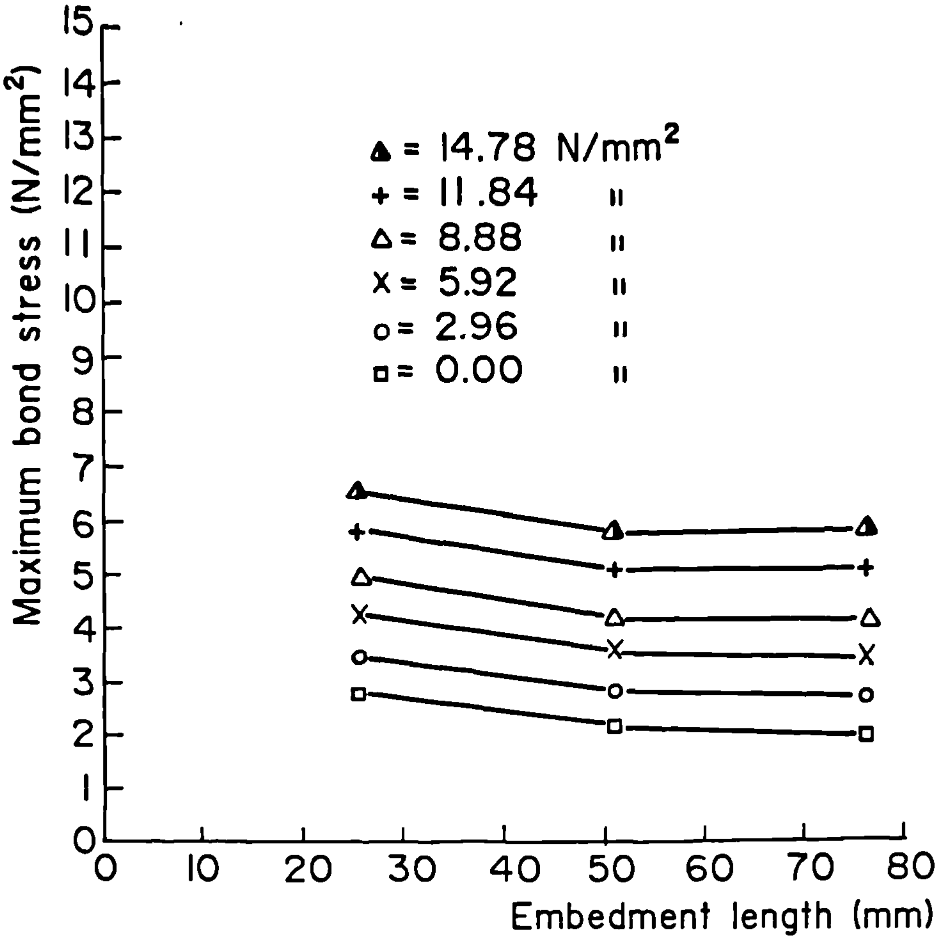

Fig. 3.14 Variation of maximum bond stress with embedment length (normal strand)

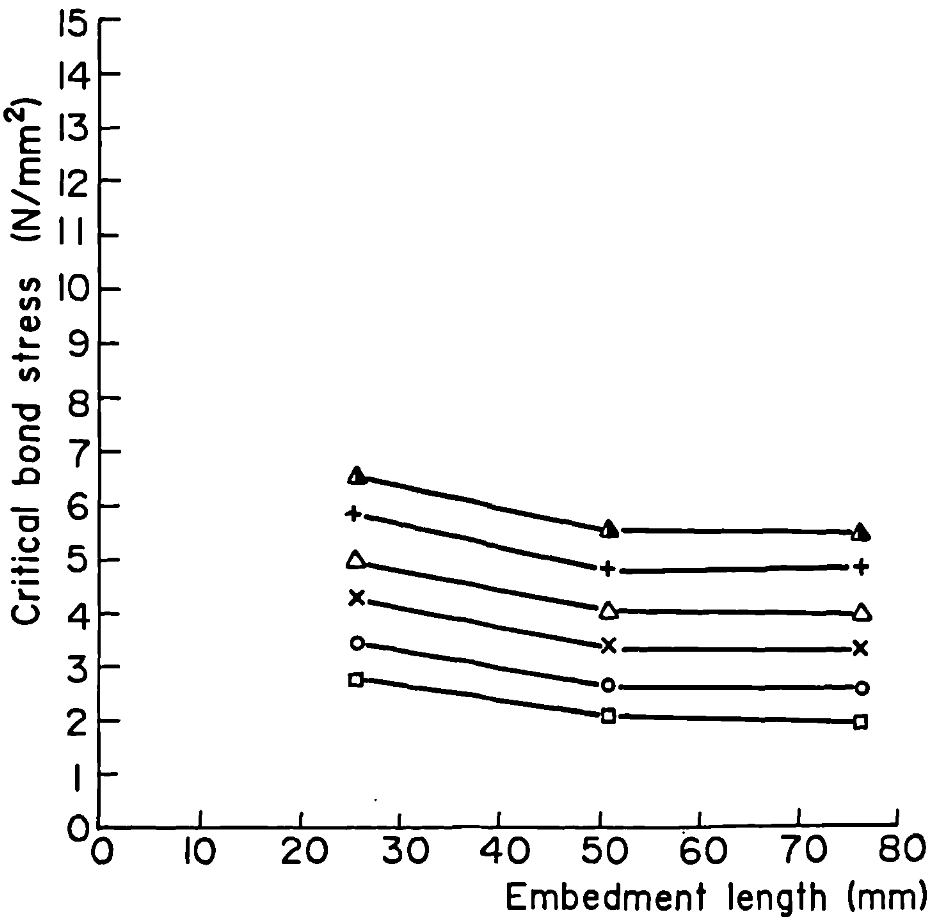

Fig. 3.15 Variation of critical bond stress with embedment length (normal strand)

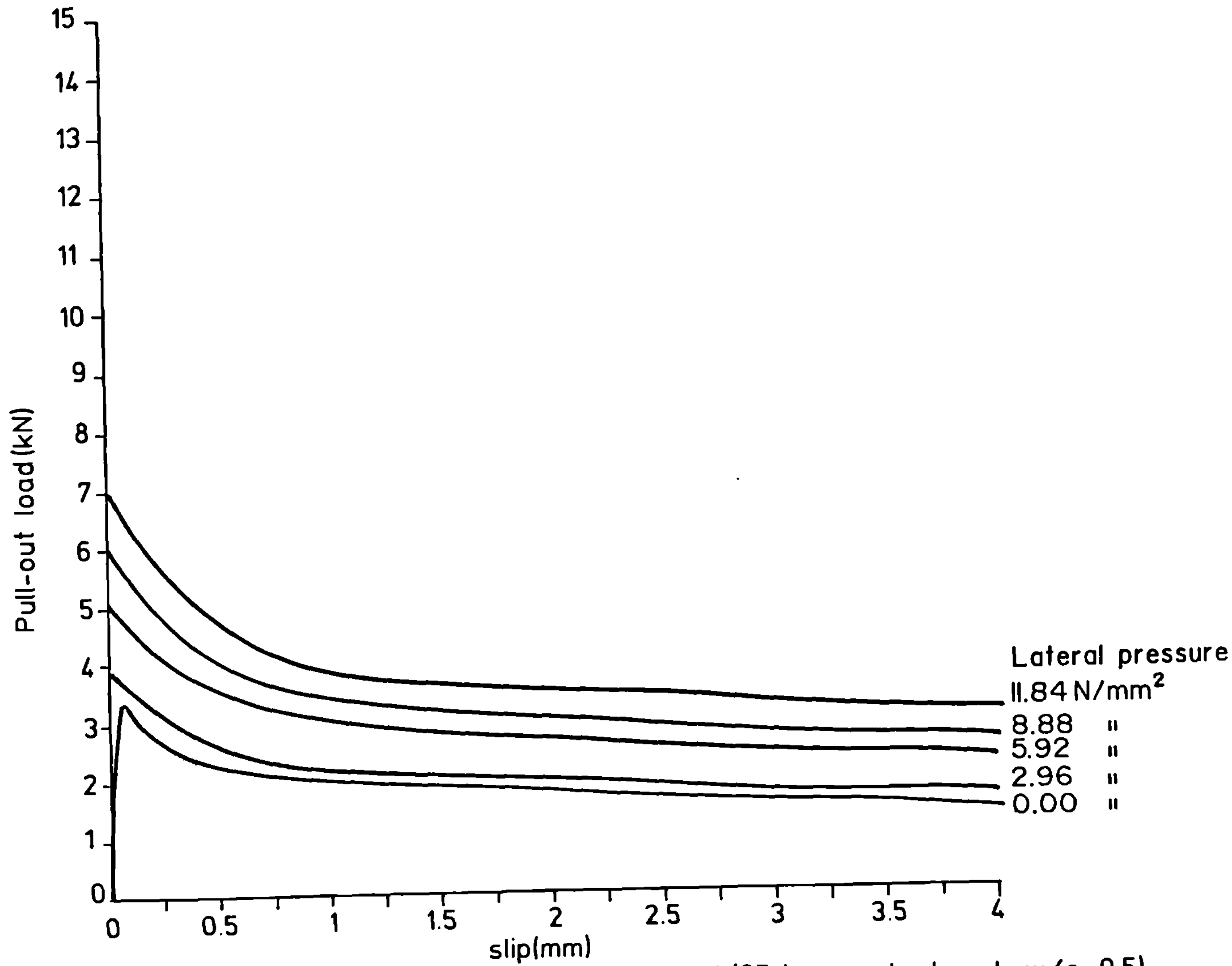

Fig. 3.16 Pull-out load/slip for plain strand (25.4mm embedment, w/c=0.5)

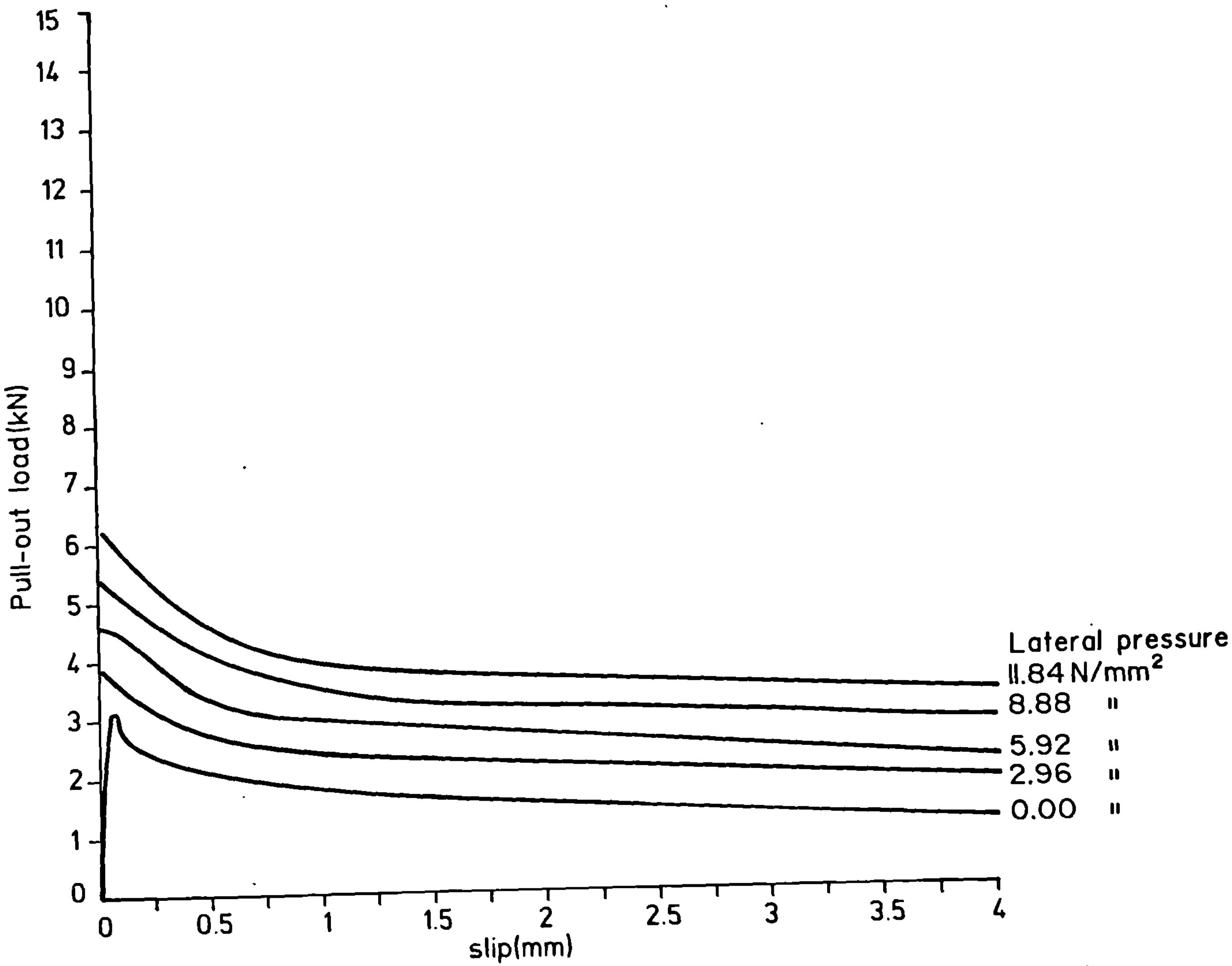

Fig. 3.17 Pull-out load/slip for plain strand (25.4mm embedment, w/c=0.6)

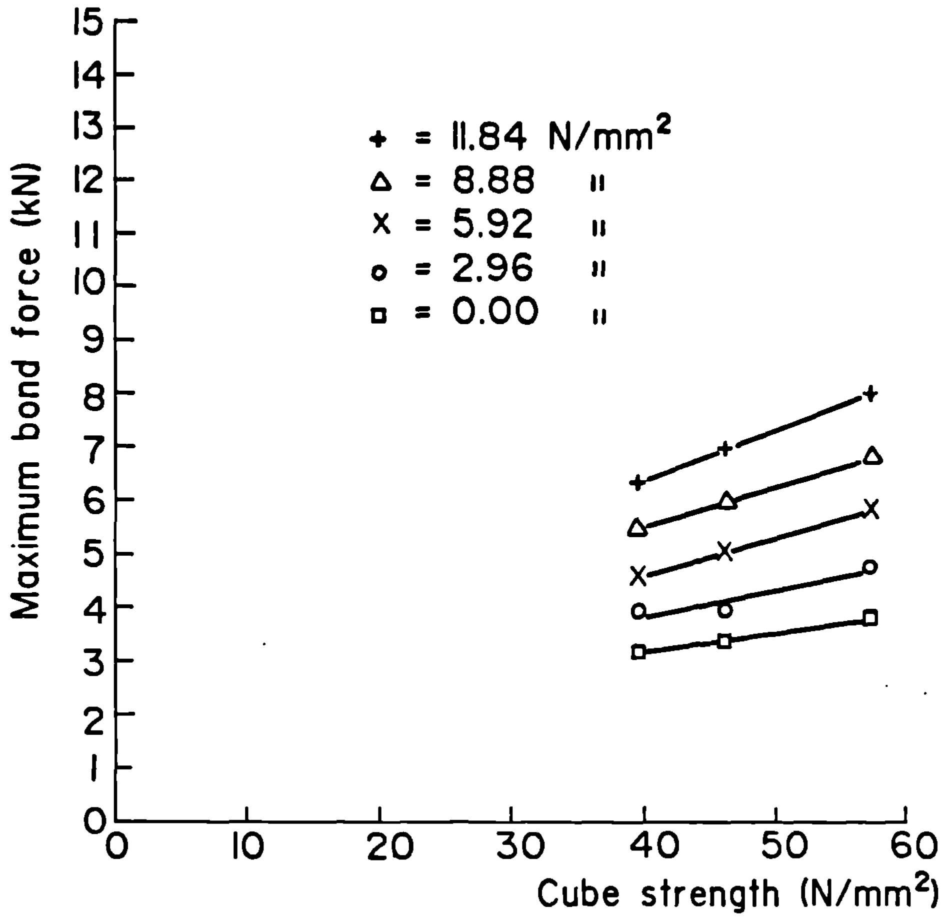

Fig 3·18 Variation of maximum bond force with cube strength

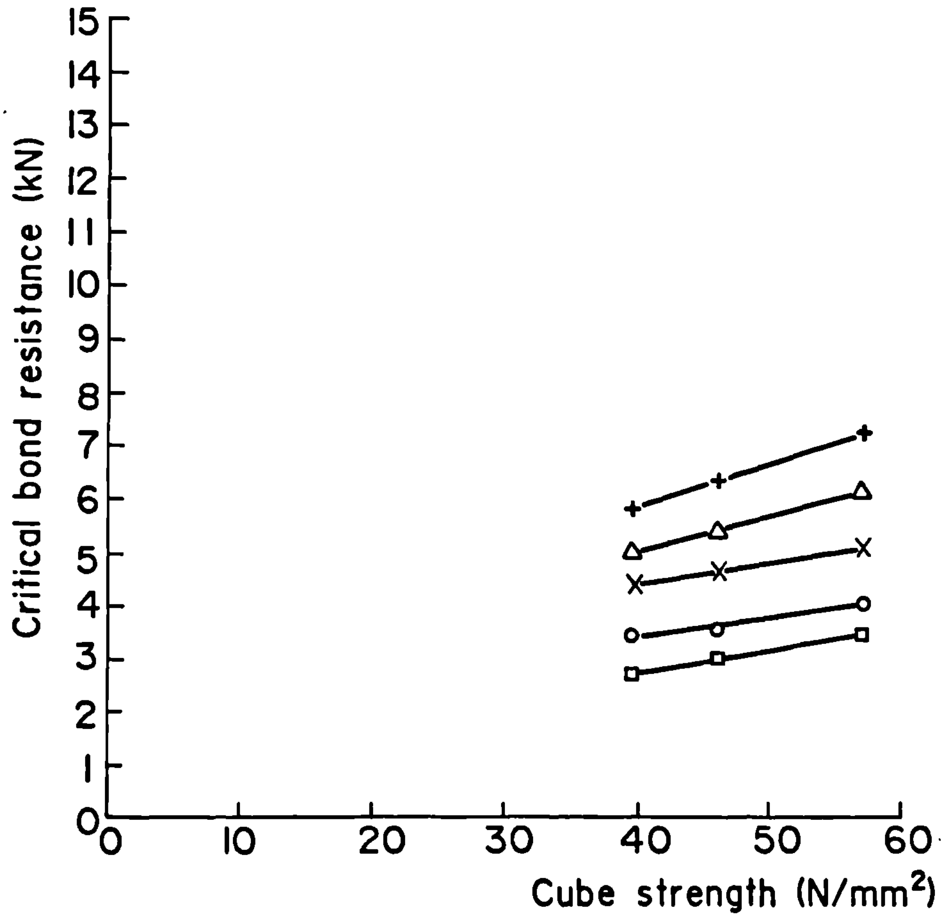

Fig 3·19 Variation of critical bond resistance with cube strength.

3 mixes the amount of water/cement ratio is different. The tests were made on normal strand with an embedment length of 25.4mm and this performed similarly to the previous tests. Each test comprised an average of 4 to 5 cubes.

The average bond force-slip relationships are presented in figure 3.6, 3.16,and 3.17. The maximum bond forces and the critical bond resistances of each mix are summarized in table 3.7 and 3.8.

The grout strength, as affected by the water to cement ratio, appears to have a definite effect on the bond force throughout the whole series of lateral pressures. The effect of cube strength on the maximum bond force and the critical bond resistance is shown in figures 3.18, 3.19. The rate at which the maximum bond force and the critical bond resistance increased with the compressive strength (ranging from 39.5 to 57 N/mm^2) is, in average, 0.07KN increase for each N/mm^2 increase increase in cube strength.

3.5.8 MODE OF FAILURE

The specimens of normal strand and the dyform with 25.4mm embedment length all failed in a similar manner. For a lateral pressure from 0 to about 0.30 of the cube strength, the pull-out load increased linearly with the applied pressure and the bond force-slip curves were identical whatever the pressure was. The pull-out load started increasing sharply until the maximum bond force was reached and the adhesion had failed, then a sudden drop in load took place. The strand pulled out without damage to the grout block leaving smooth polished surfaces in the grout which, in turn, left some particles lodging between the wires (there

Plate 5 Failure of a specimen with 50.8mm embedment

block leaving smooth polished surfaces in the grout which, in turn, left some particles lodging between the wires (there was some evidence of grout paste adhering to the strand).

Specimens of normal strand with 50.8mm and 76.2mm embedment, however, failed differently from those with 25.4mm embedment. After failure of the adhesion and at a slip of about 0.25mm the pull-out load started increasing presumably because of the imperfect shape of the strand. Under a lateral pressure of over 0.26 of the cube strength and at a slip of about 3mm, some specimens broke. The failure occured by cracking of the grout near the middle of the specimens in a plane perpendicular to the direction of the pull-out force (see Plate 5). The failure is attributed to a combination of the higher compressive stresses and longitudinal tensile stresses that may be generated along the embedded length while the strand is pulled out.

The mode of failure of indented strand with 25.4mm embedment is different from the above. After failure of the adhesion and at a slip of 0.2mm the bond force started increasing again, presumably because of bearing action of the projections on the surface of the indented strand against the surrounding grout. Under very high bearing stresses the grout lodging in front of the projections crushes which causes the resistance to motion to diminish and consequently the pull-out load to decrease. No splitting nor bursting occured. Clear imprints of the projections at the grout interface were observed.

For some of the specimens with a w/c ratio of 0.5 and 0.6 and a 25.4mm embedment length the lateral pressure reached values greater than 0.3 times the cube strength (0.32

in section 3.5.4 i.e under a lateral pressure of $14.78 N/mm^2$ the maximum bond force remained nearly the same as that of the specimens under a lateral pressure of $11.84 N/mm^2$ (see figure 3.20 for w/c ratio of 0.5). The second phenomenon was the large drop in the pull-out load following the failure of the adhesion i.e after failure of the adhesion the pull-out under a lateral pressure of $14.78 N/mm^2$ dropped to a lower level than that of the specimens under a lateral pressure of $11.84 N/mm^2$ (see figure 3.21).

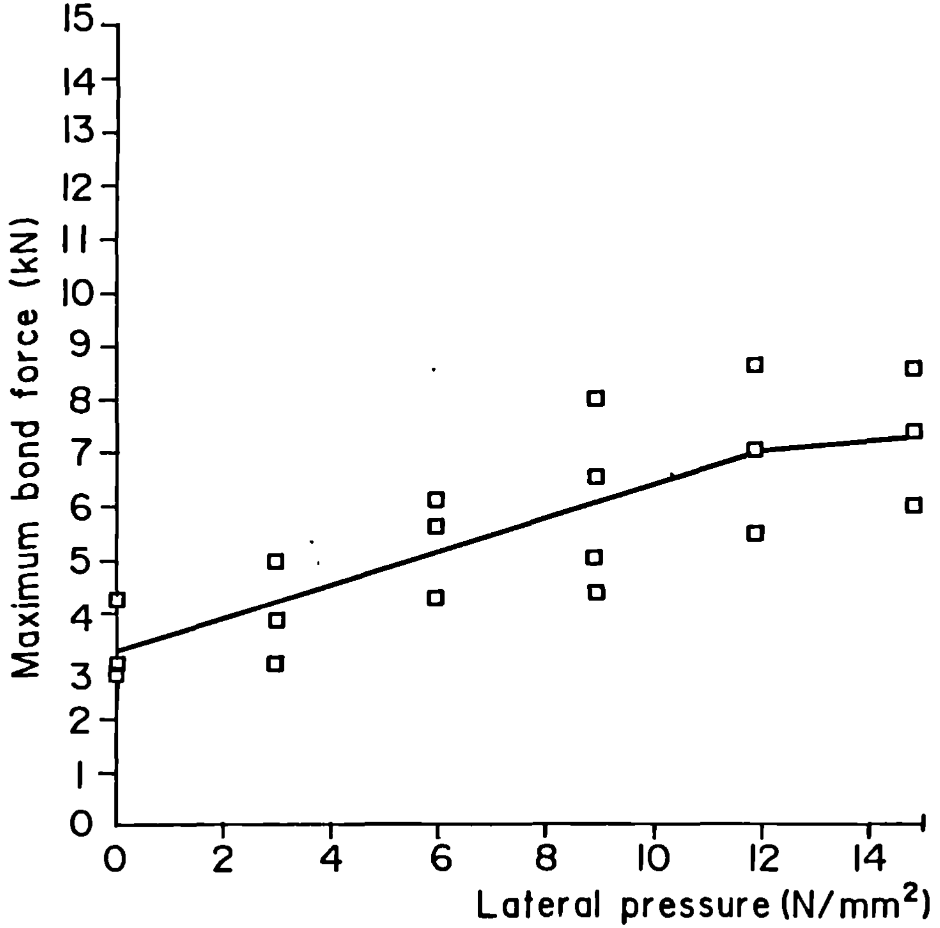

Fig. 3.20 Variation of the maximum bond force with lateral pressure (ranging from 0 to 0.32 times the cube strength) for w/c ratio of 0.5

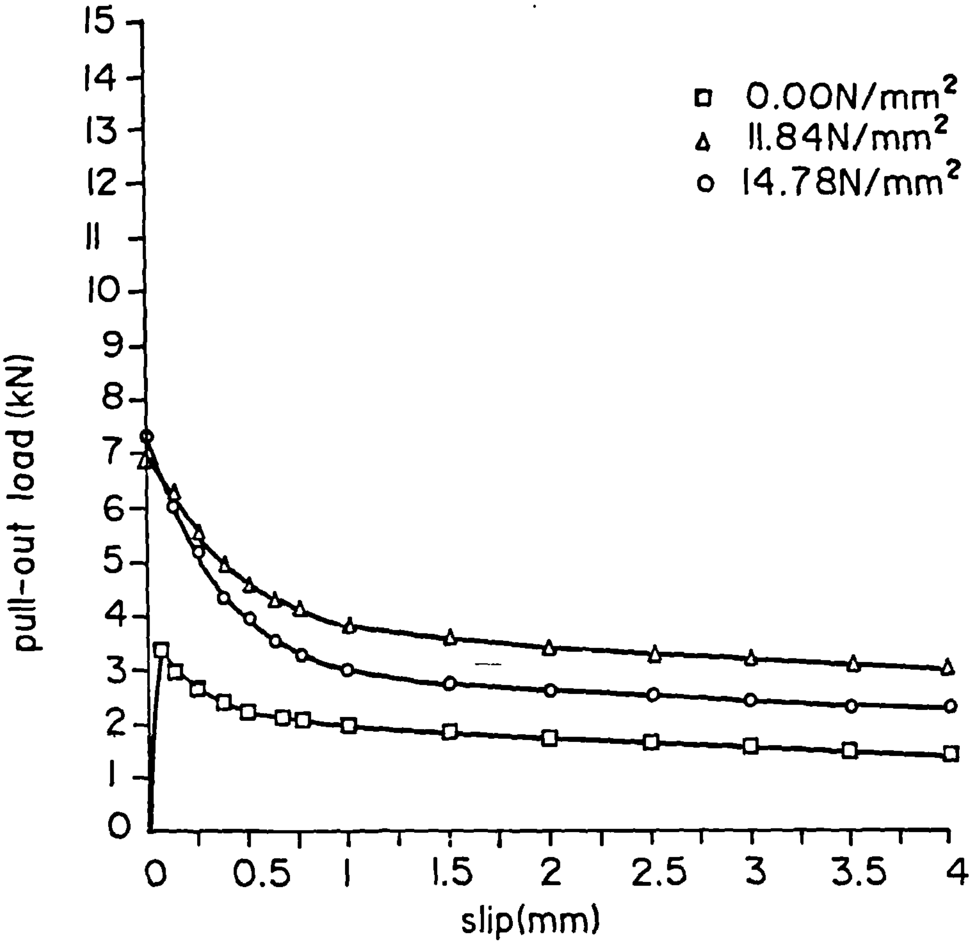

Fig 3.21 Pull-out load/slip for normal strand of w/c=0.5
(Lateral pressure up to 0.30 times the cube strength)

Max.Bond Force (KN)	Lateral Pressure(N/mm^2)					
	0	2.96	5.92	8.88	11.84	14.78
Normal	3.80	4.73	5.83	6.78	7.98	8.99
Dyform	3.37	4.41	5.20	6.18	7.04	8.12
Indented	4.46	5.12	6.46	8.46	9.50	11.80

TABLE 3.3 Maximum Bond Forces

Critical Bond Resistance KN	Lateral Pressure (N/mm^2)					
	0	2.96	5.92	8.88	11.84	14.78
Normal	3.43	4.03	5.06	6.12	7.18	8.33
Dyform	3.20	3.89	4.86	5.80	6.73	7.70
Indented	4.36	4.96	5.98	7.95	9.04	11.37

TABLE 3.4 Critical Bond Resistance

Max.Bond Force (KN)	Lateral Pressure(N/mm^2)					
	0	2.96	5.96	8.88	11.84	14.78
25.4mm	3.80	4.73	5.83	6.78	7.98	8.99
50.8mm	5.87	7.68	9.66	11.38	13.88	15.79
76.2mm	7.84	10.68	13.50	16.38	20.30	23.30

TABLE 3.5 Maximum Bond Force

Critical Bond Resistance KN	Lateral Pressure(N/mm^2)					
	0	2.96	5.92	8.88	11.84	14.78
25.4mm	3.43	4.03	5.06	6.12	7.18	8.33
50.8mm	5.66	7.16	9.11	11.02	13.00	15.15
76.2mm	7.75	10.35	13.20	16.00	19.50	22.29

TABLE 3.6 Critical Bond Resistance

Max.Bond Force KN	Lateral Pressure(N/mm^2)					
	0.00	2.96	5.92	8.88	11.84	14.78
W/C=0.4	3.80	4.73	5.83	6.78	7.98	8.99
W/C=0.5	3.38	3.95	4.95	5.98	6.98	7.26
W/C=0.6	3.16	3.90	4.60	5.47	6.30	6.42

TABLE 3.7 Maximum Bond Forces

Critical Bond Resistance (KN)	Lateral Pressure (N/mm^2)					
	0.00	2.96	5.92	8.88	11.84	14.78
W/C=0.4	3.43	4.03	5.06	6.12	7.18	8.33
W/C=0.5	3.00	3.52	4.58	5.34	6.28	5.99
W/C=0.6	2.66	3.43	4.36	4.97	5.75	5.42

TABLE 3.8 Critical Bond resistance

CHAPTER 4 DISCUSSION

4.1 LATERAL PRESSURE

Before the failure of the adhesion, all the specimens subjected to zero lateral pressure exhibit a small slip. This is attributed to the way the vertical pull-out load is reacted. As shown in figures 3.3a and 3.3b, the bottom face of the specimens is resting on the base plate. The contact area between this face and the plate is determined by the rough surface of the specimens and that of the plate. So that when the pull-out load is initially applied particles of the specimen in contact with the plate crush and movement of the specimen relative to the frame is recorded by the transducer, in addition to slip of the strand with respect to the adjacent grout. Specimens subjected to lateral pressure do not exhibit this initial slip as the vertical force is reacted by the vertical bearing plates in these load cases. The abrupt change in pull-out load after the first slip of the strand takes place, as observed in all of the pull-out load/slip graphs, suggests that the interlocking structure has failed and static friction has been overcome at that point. The bond developed from then on is either a matter of sliding friction and/or mechanical interlock. In the following discussion in which the results obtained experimentally are compared to those derived theoretically, only the maximum bond force is considered. This is because the load developed at 0.1mm slip involves many unknown parameters such as the real area of contact and the true

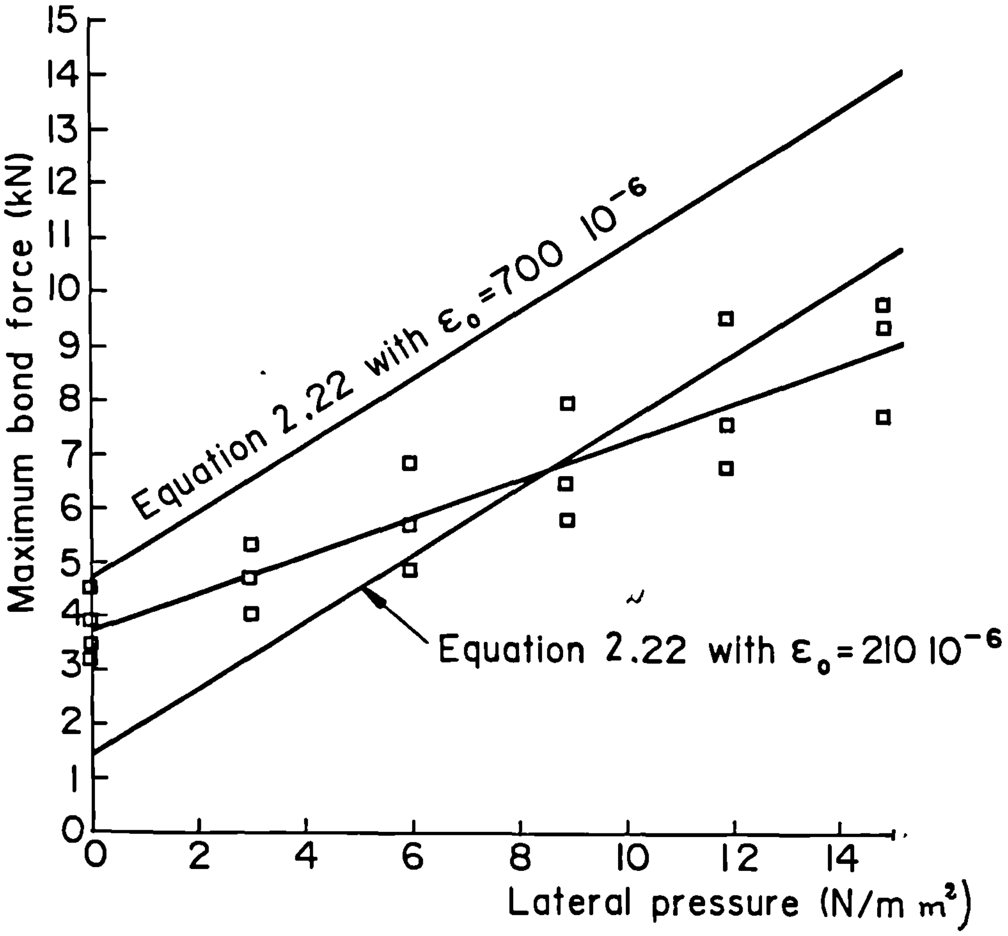

Fig 4·1 Effect of pressure on maximum bond force for normal strand.

contact pressure.

Table 4.1 presents the properties of the grout and the strand obtained experimentally and subsequently used to calculate the bond forces. The upper value of shrinkage is that obtained from the test described in section 3.2. The lower value of shrinkage is the irreversible part of shrinkage (0.3 x drying shrinkage) that Neville[16] suggests is the value to use when the specimens are cured under water.

Figure 4.1 provides a comparison of the experimentally obtained maximum bond forces for normal strand with values calculated using equation 2.22 for the various lateral pressures. Two sets of theoretical values are given corresponding to the assumptions.

i) drying shrinkage 700×10^{-6} ii) irreversible shrinkage of 210×10^{-6}.

Properties	steel	grout
Poisson'ratio	0.30	0.17
Young's modulus	$207 KN/MM^2$	$21.5 KN/MM^2$
Radius(mm)	6.45	43.55
Drying shrinkage Irreversible shrinkage		700.10^{-6} 210×10^{-6}
Coef.of friction	0.28	

Table 4.1 Properties of the materials.

It can be seen from figure 4.1 that the predicted rate at which the maximum bond force increases with lateral pressure, is much greater than that measured experimentally. This could be due to an overestimate of the true contact pressure acting at the grout-strand interface resulting from the externally applied pressure. The results derived from the elastic approach indicate that the internal pressure is twice as great as the stress applied externally to the grout prism (see equation 2-22). It must be noted, however, that an elastic solution makes the following assumptions:

1) The materials in contact are homogeneous and linearly elastic.

2) The moduli of elasticity and Poisson ratios must be known.

3) A perfect contact is made between the steel and the grout.

4) A uniform stress is assumed along the bonded length.

The magnitude of the contact stress is very sensitive to the quality of the material to material contact between steel and grout. Under externally applied pressure the grout around the strand may become ineslatic. It is likely that air pores get trapped between the two materials as a consequence of bleeding, settlement, and vibration in the course of the specimens preparation. This reduces the area of true contact and stiffness of the grout near the strand. According to Pinchin[18] the hardness of cement paste increases with the distance from the wire surface (see figure 4.2). He found that the region at the paste/steel interface was a region of increased porosity. Any reduction of the stiffness of the surrounding grout would result in a decrease in contact pressure. To confirm this statement an argument similar to that put forward by Stocker and Sozen[10] is used.

Consider, for instance, a test specimen which contains a layer of grout with an arbitrary thickness of roughly 3mm and a reduced modulus of elasticity around the steel (see figure 4.3). Using the theoretical analysis of concentric cylinders of different materials subjected to external pressure, a revised expression of the contact pressure can be calculated as follows:

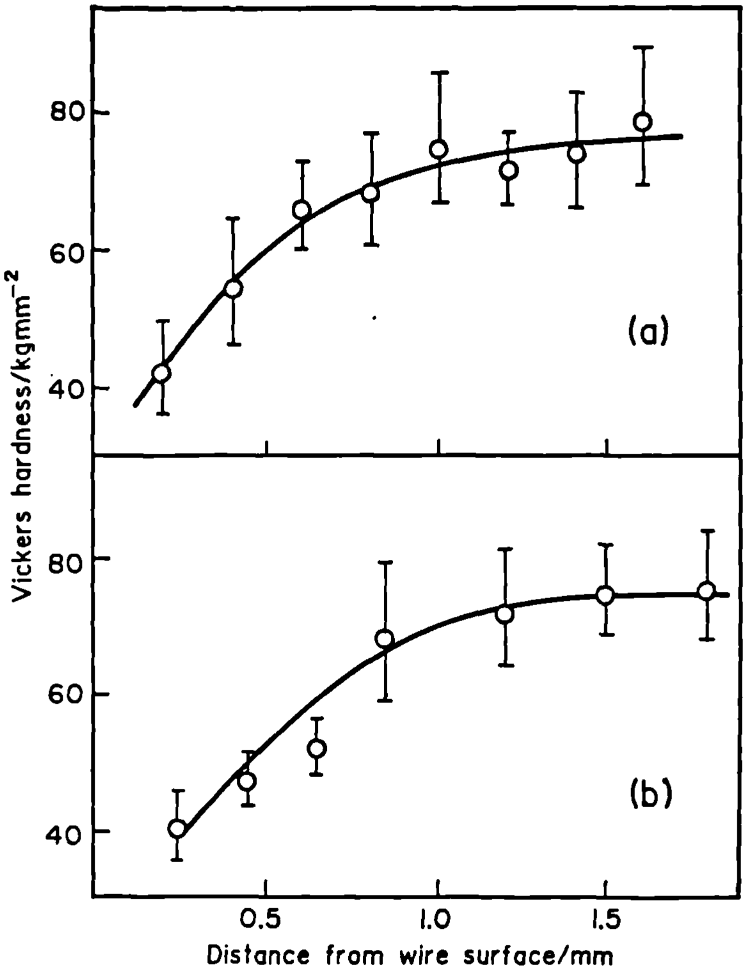

Fig. 4.2 Vickers hardness/Kgmm ^{2} of cement paste as a function of distance from the wire surface/mm.
4 weeks cure (a) water cured (b) sealed
(From Ph.D thesis of D.J.Pinchin)

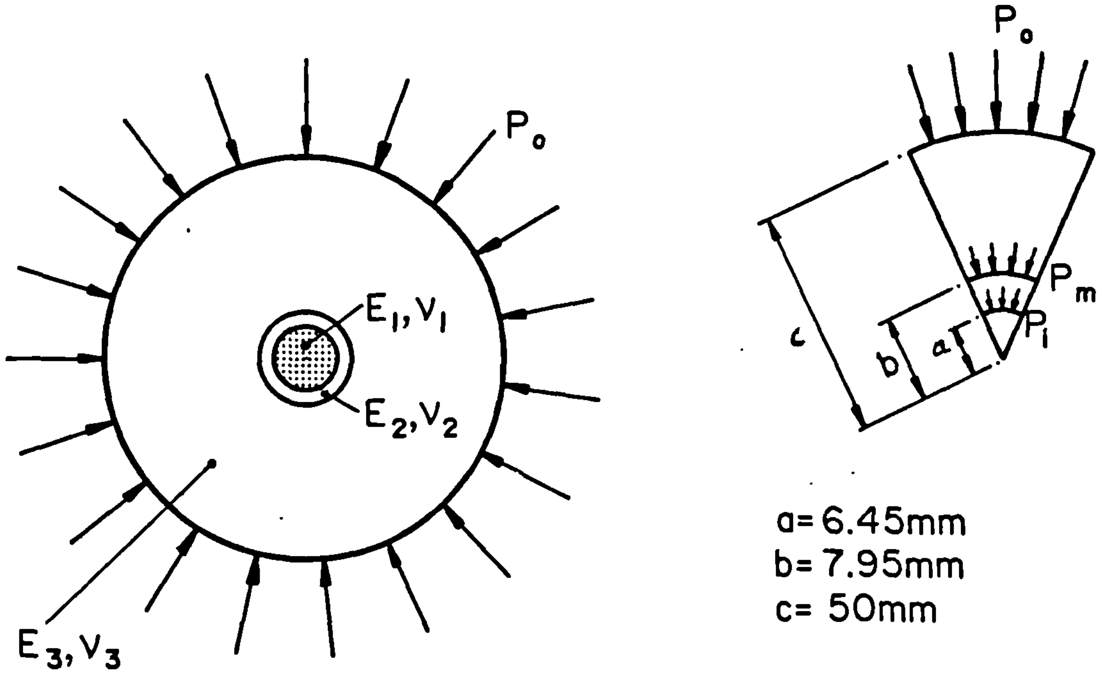

Fig. 4.3 Concentric cylinders of different materials subjected to external pressure.

$$p_i = \frac{4.m.n.b^2.c^2.(b^2 - a^2).p_0}{\left\{(b^2-a^2)(1-\nu_1)+ m\left[b^2(1+\nu_2)+a^2(1-\nu_2)\right]\right\}\left\{ n.(b^2-a^2)\left[c^2(1+\nu_3)+b^2(1-\nu_3)\right]+ (c^2-b^2)\left[a^2(1+\nu_2)+b^2(1-\nu_2)\right]\right\}- 4.m.a^2.b^2.(c^2-b^2)} \quad ......(4.1)$$

where E_1, E_2, and E_3 are moduli of elasticity of the different cylinders shown in figure 4.3, ν_1,ν_2,ν_3 are Poisson's ratio , and a,b,c are radi of the corresponding cylinder, $m=E_1/E_2$ and $n=E_2/E_3$.

The variation of p_i/p_0 with E_2/E_3 is plotted in figure 4.4. It can be seen that the contact pressure decreases as $n=E_2/E_3$ decreases (the stiffness of the grout near the strand reduces).

The above discussion shows that the contact stress is highly sensitive to a change in the conditions of contact. The trend indicates that the actual value of the internal pressure derived from the elastic approach is too high. Because of the uncertainties of the assumptions about the elastic behaviour at the interface between the two materials, it was decided to take the internal pressure equal to the externally applied pressure in the analysis of the test data. Consequently if the internal pressure p_i of equation (2-18) equals the external pressure p_0 then $F_1 = A.p_0$ and by substituing F_1 into equation (2-19a) and by following the same calculations we get a new expression for the pull-out load P_1 as:

$$P_1 = \frac{A_s.E_s}{\nu_s}(K.p_0+\varepsilon_0)\left[1 - \exp\left(- \frac{L.C.\mu.\nu_s}{A_s.E_s.K.\cos\alpha(1-\mu\tan\alpha)}\right)\right] \quad ....(4.2)$$

with all the variables keeping the same meaning as in

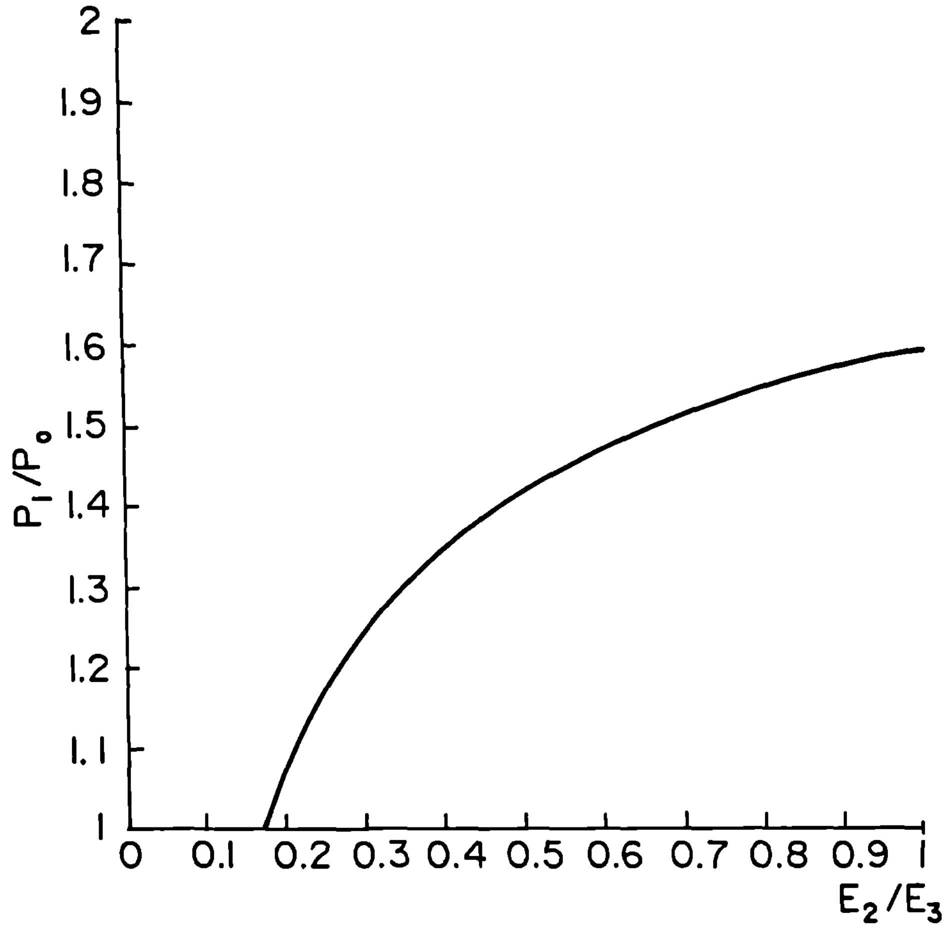

Fig 4.4 Variation of the internal pressure acting at the grout/strand interface with the module of elasticity of the grout near the strand

equation (2-22)

The results derived from this equation are compared with the experimental results obtained from the specimens of normal strand and dyform (see figures 4.5,4.6). The effect on the maximum bond force of an increase in lateral pressure is predicted quite well, considering the difficulty in measuring an absolute shrinkage for the grout and an absolute value of contact stress. The upper and lower bound lines of figures 4.5 and 4.6 reflect the variation to be expected in the initial shrinkage value ε_0 of the grout (as defined above). These are dependent on the method of curing and the composition of the mix.

The behaviour of indented strand is not in accord with the prediction of the frictional elasticity approach (see Table 3.3). The number of indentations were not carefully counted during the specimens preparation and it is possible that the inconsistency in the rate of increase in bond force with the lateral pressure is due to the variation between specimens. Although there is considerable scatter, the indented strand considerably improved the bond.

The tests on the weaker grout demonstrated that there is an upper limit on the magnitude of lateral pressure for which the linear relationship between bond force and lateral pressure is valid. The results (see figure 3.21) show that this limit lies between 0.26 and 0.32 times the cube strength. Above this value there is little change in bond with increase in lateral pressure. This suggests that the resistance of the grout surrounding the steel has reached a maximum value and that under higher lateral pressure, plastic deformations occur. As the theory assumes elastic behaviour

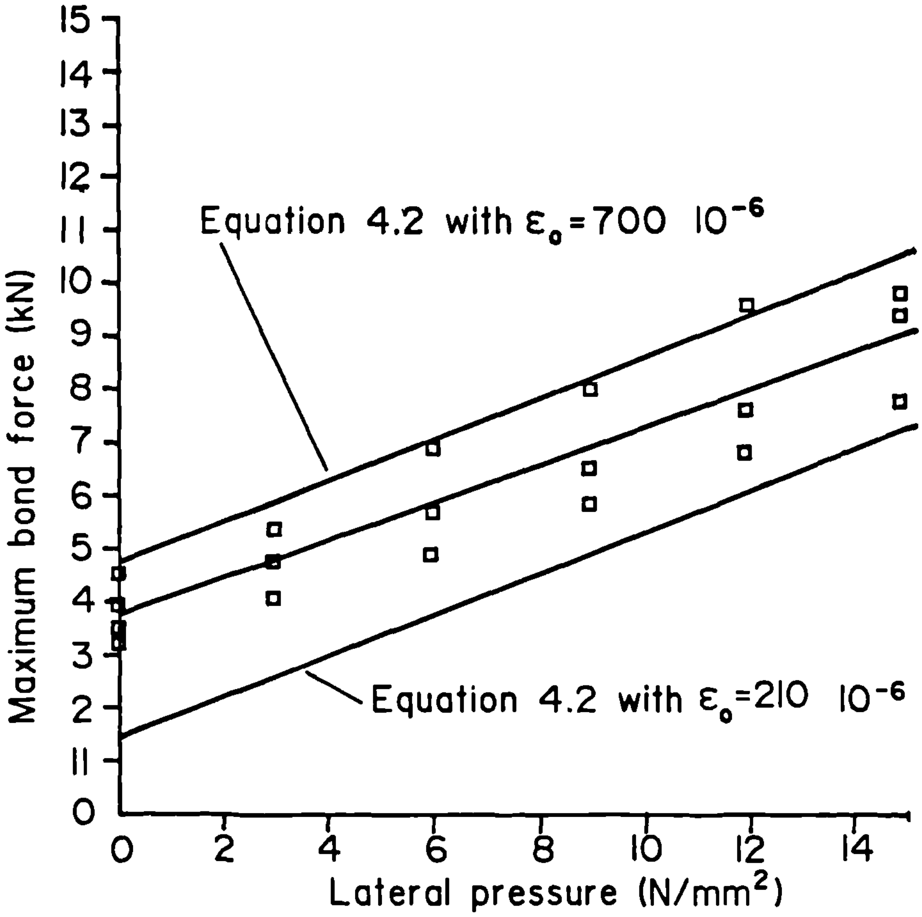

Fig 4·5 Effect of lateral pressure on maximum bond force for normal strand. (25.4 mm embedment)

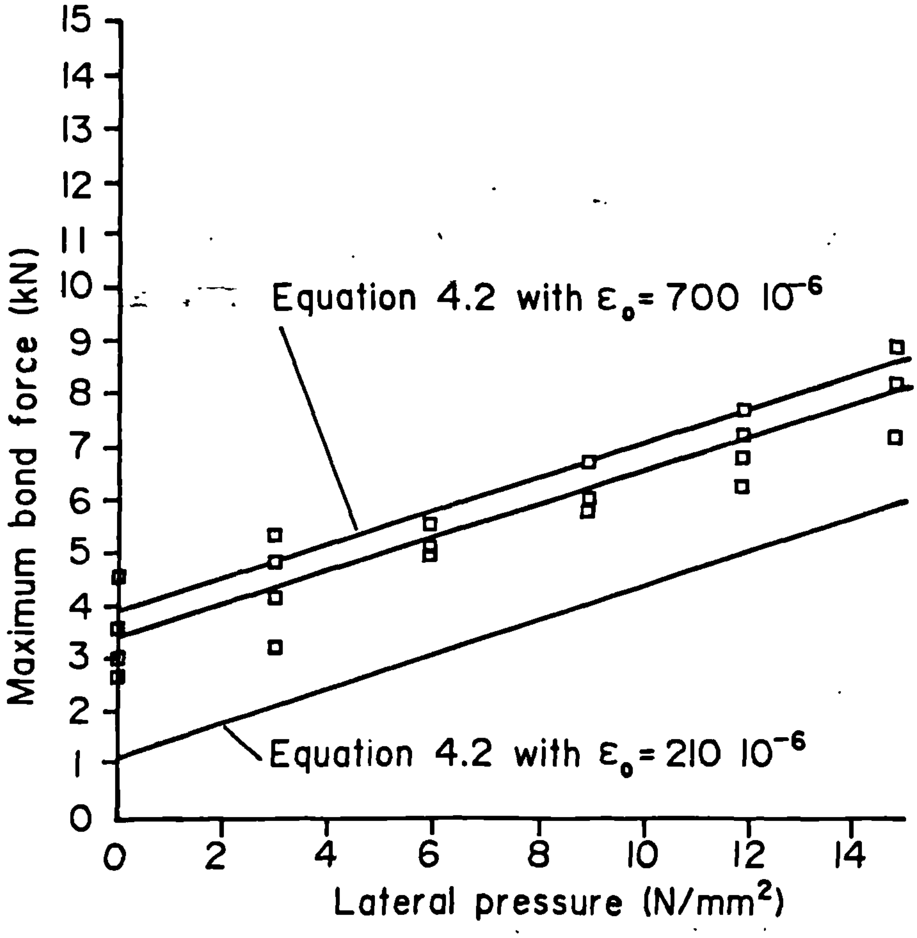

Fig 4·6 Effect of lateral pressure on maximum bond force for Dyform strand. (25.4 mm embedment) this point also defines the limit of application of equation 4.2.

4.2 STRAND TYPE

The maximum bond force developed by normal strand, irrespective of lateral pressure, is 11 percent higher than that of dyform. This can be attributed to the more deformed surface geometry of normal strand when compared to the smooth surface of dyform. Using equation 4.2 it can be shown theoretically that, even allowing for the difference in cross section area $100mm^2$ for normal strand and $110mm^2$ for dyform, the difference in the angle of twist between the two strands (11.45^o for normal and 8.45^o for dyform) results in an increase in bond for normal strand of 21 percent.

Despite the difference in shape and in bond forces between the normal strand and dyform their pull-out load/slip relationships are very similar. After critical bond resistance has developed the curves of pull-out load/slip relationship of both strands decrease as slip increases with the rate of decrease reducing.

The indented strand, however, developed higher bond forces and a different pull-out load/slip characterestic. The maximum bond developed by the indented strand was 15 percent, with a variation of $\pm$ 12 percent higher than the normal strand. This is attributed to the presence of the projections existing on the surface of the wires of the indented strand. These projections provide an additional physical key between strand and grout which has to be overcome. After maximum bond force is reached there is a slight drop in pull-out load. This drop marks the transition between one bond mechanism to another. This point is discussed further in section 4.5. After the critical bond resistance has developed, the pull-out load increases to a maximum at a slip of about 2.5mm.

4.3 EMBEDMENT LENGTH

The variation in bond stress with embedment length as predicted theoretically is shown in figure 4.7 (assuming a shrinkage of 700×10^{-6}). This is obtained by dividing the maximum bond force, calculated using equation (4.2), by the bonded area. A comparison of the predicted variation with that obtained experimentally for a lateral pressure of $2.96 N/mm^2$ is shown in figure 4.8. This indicates that even allowing for the overestimate of bond stress by theory for embedment length of 25.4mm the values of bond stress obtained experimentally decrease more rapidly than predicted for an increase in embedment length from 25.4mm to 50.8mm. This can be explained on the basis that the bond stress is not constant along the bonded length but varies as shown in figure 3.2. Following the DD81[2] proposed diagram for variation of bond stress along a bonded length (see figure 3.2) the results obtained in this present investigation may be explained on the basis of the following discussion. At small bonded length, as no substantial diferential slip between the loaded end and the free end will be encountered, the bond stress may be considered as uniformly distributed along the bonded length (see figure 4.9a). However for a larger embedment, the variation in slip along the bonded length becomes an important factor and the error in assuming a constant bond stress distribution along the bonded length

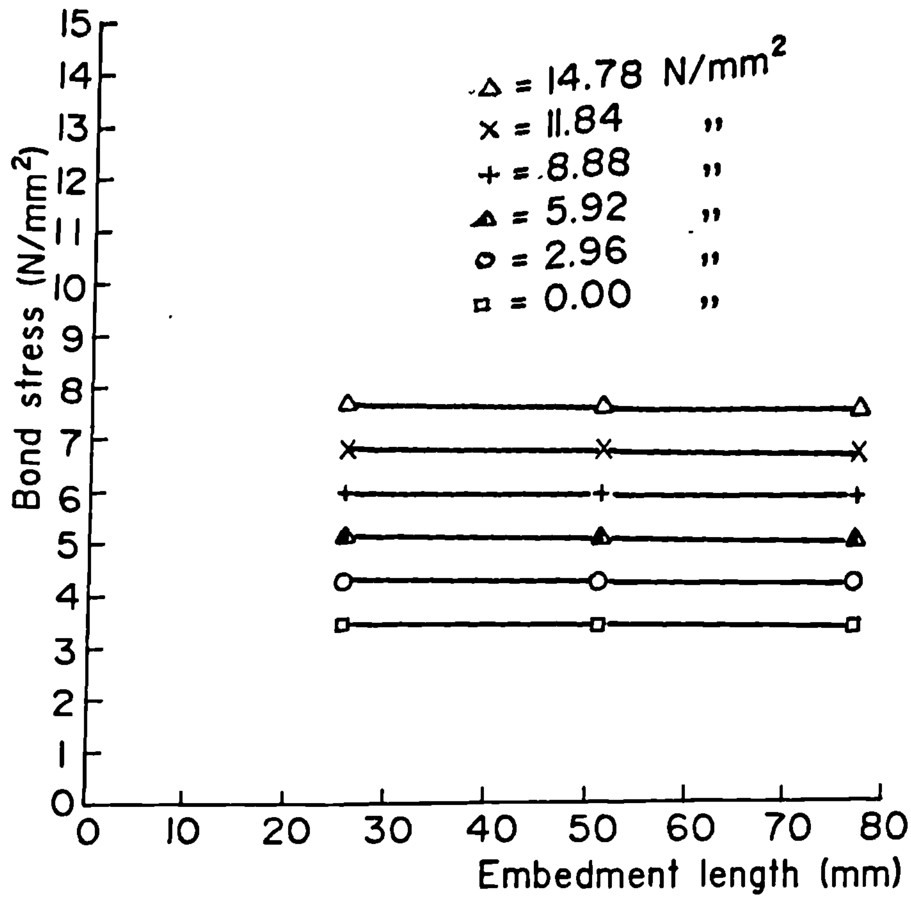

Fig 4·7 Variation of bond stress with embedment length for normal strand predicted theoretically

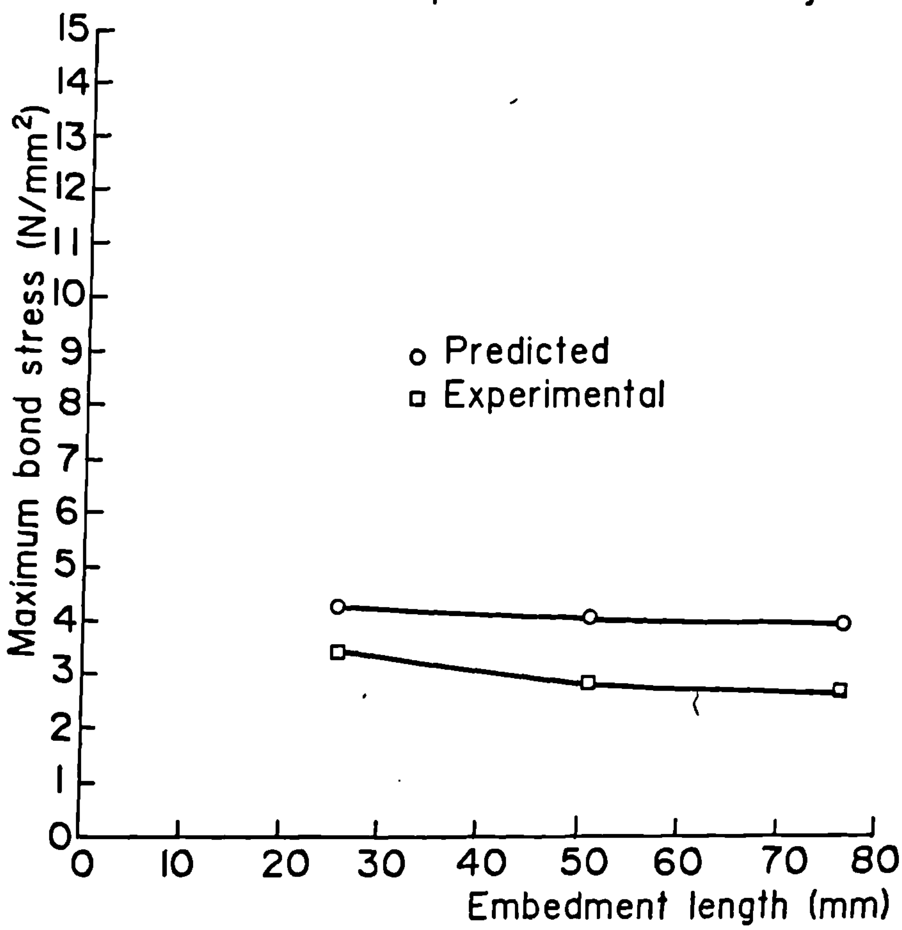

Fig 4·8 Comparison of the predicted variation in bond stress with that obtained experimentally (normal strand).

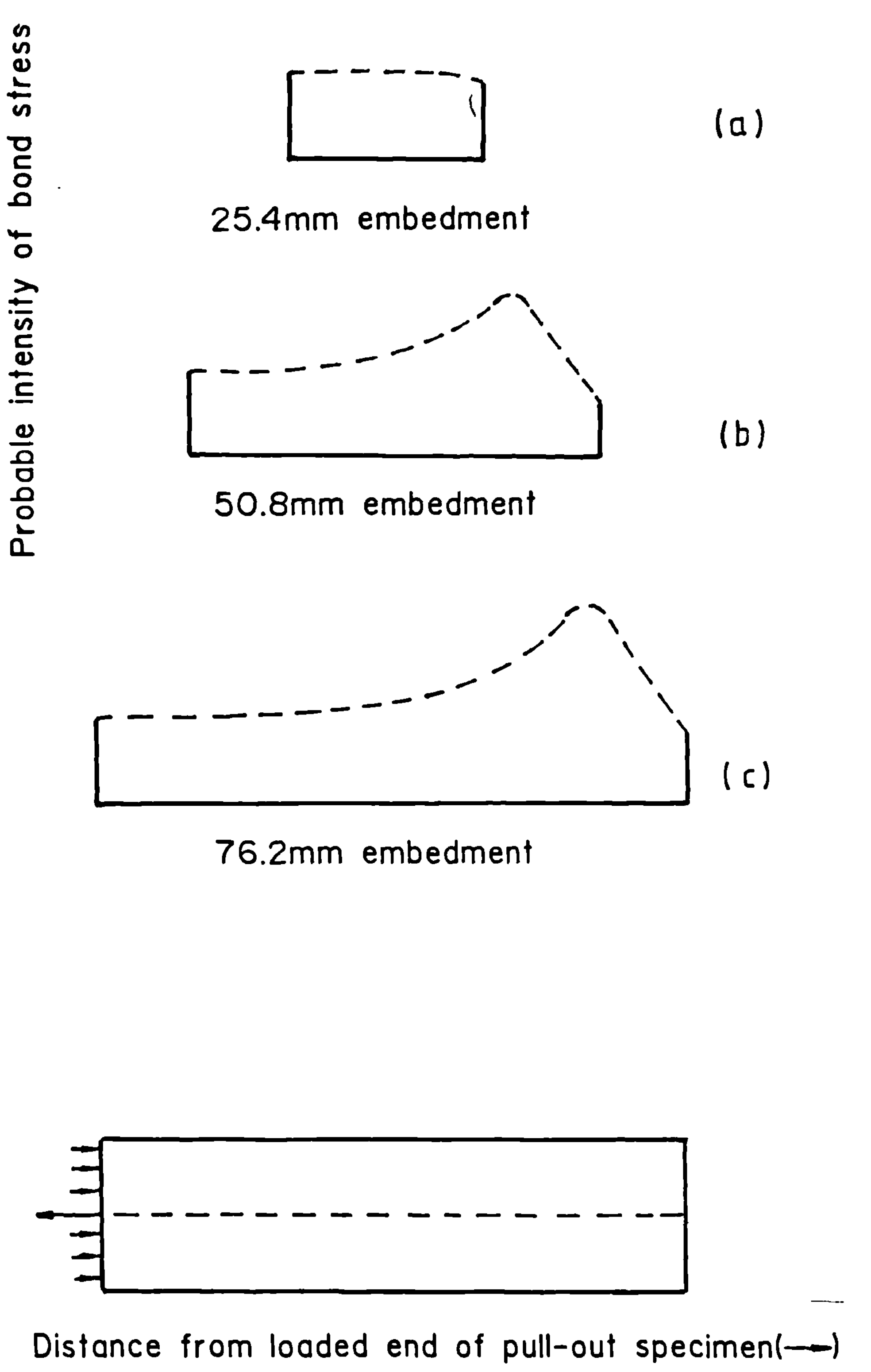

Fig.4.9 Qualitative variation of bond stress during the pull-out test for different embedments (at first slip)

may be significant. The distribution in bond stress along a larger embedment may be assumed to be in the form shown in figure 3.2. Since the maximum bond stress levels off as the length of embedment increases from 50.8mm to 76.2mm, it may be concluded that the stress distribution for a 50.8mm embedment and for a 76.2mm embedment is in the form shown in figure 4.9b and 4.9c. The integration of the bond stress over the surface would lead to the calculation of the corresponding pull-out load. The theoretical value predicts the maximum value whereas the experimental results given are for average values.

4.4 GROUT STRENGTH

The results obtained experimentally show that for the particular mixes investigated and for lateral pressures up to 0.26 times the cube strength, the maximum bond force increases linearly with the cube strength. An average rate of increase of 0.07KN in bond force for each N/mm^2 increase in cube strength. The improvement in maximum bond force with the cube strength may be a result of the improvement of the other properties of the grout such as stiffness, shrinkage, Poisson's ratio, and friction which are related to the compressive strength. Theoretically, using equation 4.2, it can be shown that the modulus of elasticity and the coefficient of friction has important effects on the maximum bond force and on the rate at which this increases with the lateral pressure. Figure 4.10 presents the variation of the bond force with the lateral pressure for different moduli of elasticity and 4.11 shows the variation of the bond force with the lateral pressure for different coefficients of

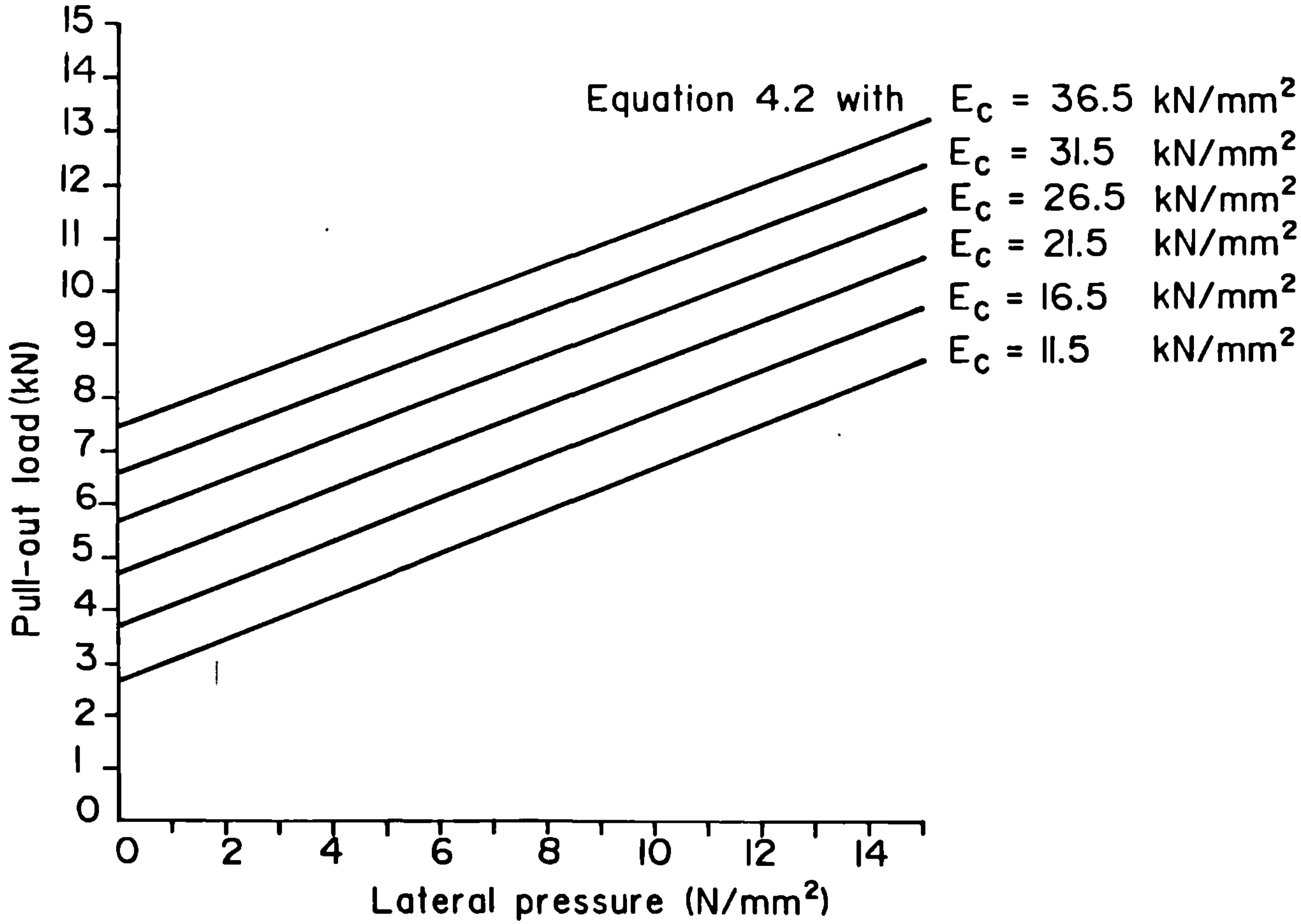

Fig.4.10 Effect of Young's modulus of grout on pull-out load for normal strand

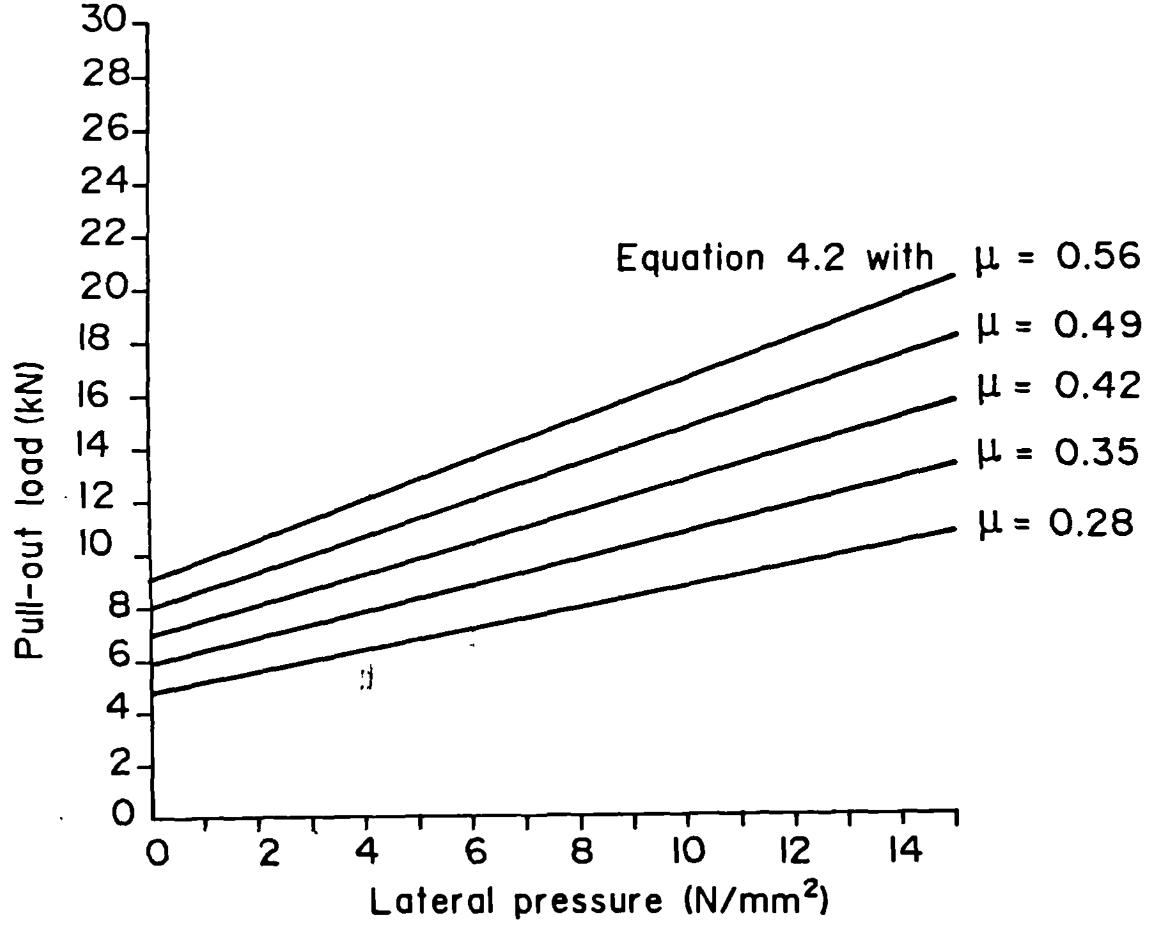

Fig. 4.11 Effect of friction coefficient on pull-out load for normal strand

friction. Apart from the modulus of elasticity which is related to the compressive strength, there is little information on how friction, shrinkage, and Poisson's ratio are related to the compressive strength. As the measurement of the grout properties was conducted only on the mix of water/cement ratio of 0.4 no general conclusion can be drawn on the effectiveness of the compressive strength on bond.

4.5 BOND CHARACTERISTICS AFTER MAXIMUM BOND FORCE

Up to a slip of about 0.2mm the pull-out load/slip relationship of all the specimens investigated in this test programme shared a similar characteristic. Commom to all the variables investigated, is an increase in pull-out load with negligible slip until the maximum bond force is reached and the adhesion fails. There is then a drop in bond force until a slip of 0.2mm is reached. Divergences in the behaviour of the pull-out load/slip relationship are observed as slip increases above 0.2mm.

The curves of specimens of normal strand and dyform with 25.4mm embedment show that the pull-out load continues to decrease, with the rate of decrease reducing with slip. This decrease in pull-out load is not due to a decrease in the coefficient of friction, which showed little change with slip (see section 3.5.3), but may be explained on the basis of the two following phenomena:

a) Compaction of the cement paste at the interface through displacement. According to Serada et al[28] cement paste may be compacted by pressure without obvious desintegration of the particles at the interface. They reported that fibre-matrix contact pressure, particularly at asperity contacts during pull-out will cause local compaction or reduction of the porosity in the cement near the wire. This consequently, will result in a decreased fibre-matrix contact pressure and a frictional stress transfer. This compaction phenomenon was later confirmed by Pinchin[18] during his investigation. He found that the magnitude of compaction is dependent upon the laterally applied pressure during pull-out. Accordingly, this can explain the fact that, the greater the lateral pressure the larger was the decrease in pull-out load as shown in figure 3.6 to 3.8.

b) Change in structure arrangement of the particles at the interface through displacement. Grout (or concrete), in general is a porous material with voids that range from micro to macro size. It is assumed, therefore, that shearing of the interlocking keys results in the formation of loose wear particles. Through displacement of the contact surfaces, the wear particles are transported and deposited in pores that are opened by the shear failure. This phenomenon can be compared to the behaviour of loosely packed sand subjected to shear deformation caused by a lateral displacement. The sand grains in the shearing zone rearrange themselves in a more compact manner which results in a reduction of volume and consequently to a loss of contact stress that will, necessarily, cause the shearing load to decrease.

The curves of indented strand, after a slip of 0.2mm has taken place, show that the pull-out load begins to increase as slip increases. This increase is due to the action of the projections in transmitting strand forces into the grout comparable to the action of the ribs in deformed bars[6]. Through displacement, the projections bear against the surrounding grout producing very high bearing (compressive) stresses. According to Rehm[6], these stresses can be up to 10 times greater than the compressive strength of the specimen. The bearing action will, consequently, lead to an increase in pull-out load. However, stresses generated under the bearing action can lead to circumferential tensile stresses which can cause radial cracking immediately around the strand and also splitting of the specimen if the cover of the steel is not sufficient[9]. This phenomenon has not been observed in this investigation but under very high stresses with increasing slip, the grout under the indentations crushes, which leads to a decreased pull-out load (see figure 3.8). The difference between the relative movement at the interface of each type of strand can be illustrated diagramatically in figure 4.12. The slight drop in pull-out load of indented strand following the failure of the adhesion may be called a "pause" or "transition" between one bond mechanism (adhesion) to another(mechanical interlock).

Increasing the length of embedment not only affects the magnitude of the pull-out load but also the overall pull-out load/slip relationhip. Figure 3.12 and 3.13 show that at a slip of nearly 0.3mm the pull-out load starts to increase. This suggests that a new source of bond has been activated within the strand-grout interface, as slip increases. If the coefficient of sliding friction remains constant, any change in the friction force is therefore assumed to be caused by a change in contact stress between the grout and the strand. Since strand has some torsional stiffness the manner in which it slides through the grout, either by winding itself like a screw or untwisting itself

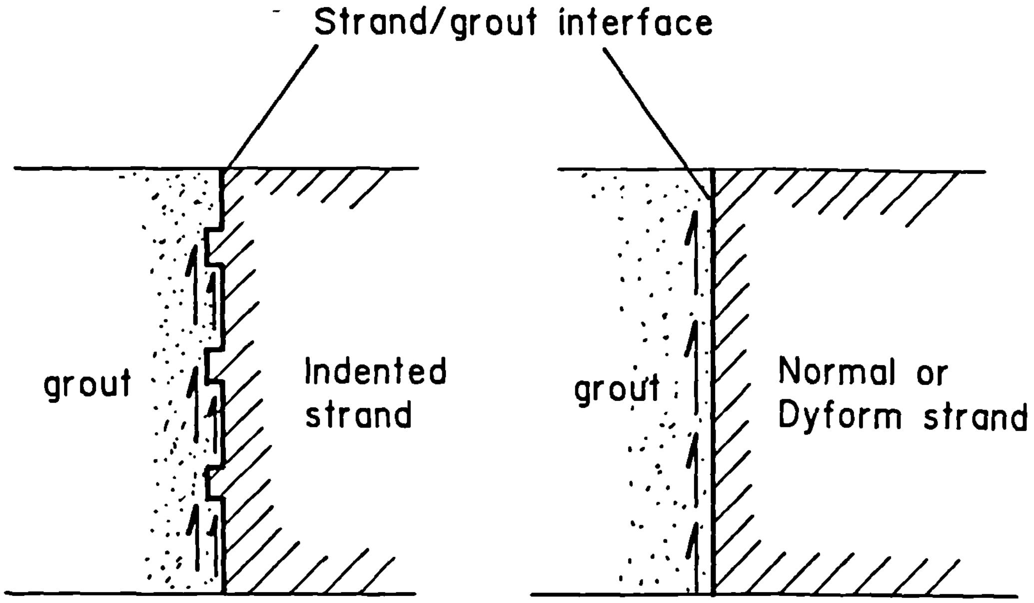

(a) Idealized indented model (b) Idealized normal and Dyform mode

Fig 4.12 Relative movement at strand/grout interface depending on the test setup, may affect the magnitude of the contact stress between the two materials. To investigate this possibility two different cases of sliding have been carried out.

1) Specimens were tested without the lateral pressure frame so that the grout specimens could rotate on the base plate while the strand was pulled out.

2) Specimens were tested with the lateral pressure frame. The specimens, as was the case for the whole of this investigation, were inserted in the apparatus so that no rotation or rather a negligible rotation was allowed while the strand was pulled out.

Since the strand in case (1) can rotate, no rotational moment will be induced into the grout. In case (2), however, the strand is forced to untwist itself through the presumed rigid grout embedment. Therefore a torsional moment is generated within the grout. Three lengths of embedment (25.4mm, 50.8mm and 76.2mm) of normal strand were tested using both test setups and the results obtained are plotted in figures 4.13 to 4.15. It can be seen from the two set of curves that while the pull-out load/slip relationship of 25.4mm embedment remained unaffected, that of 50.8mm and 76.2mm embedment was slightly affected by the test setup. This suggests that the torsional stiffness of the strand is very small to cause a significant effect on bond. Theoretically using the result obtained on a 187mm gauge length it can be shown by multiplying the values of table 2.1 by the ratio of the gauge length over the twist length, that the torsional stiffness has a small effect on bon. But this is not to such a degree as to generate an increase in

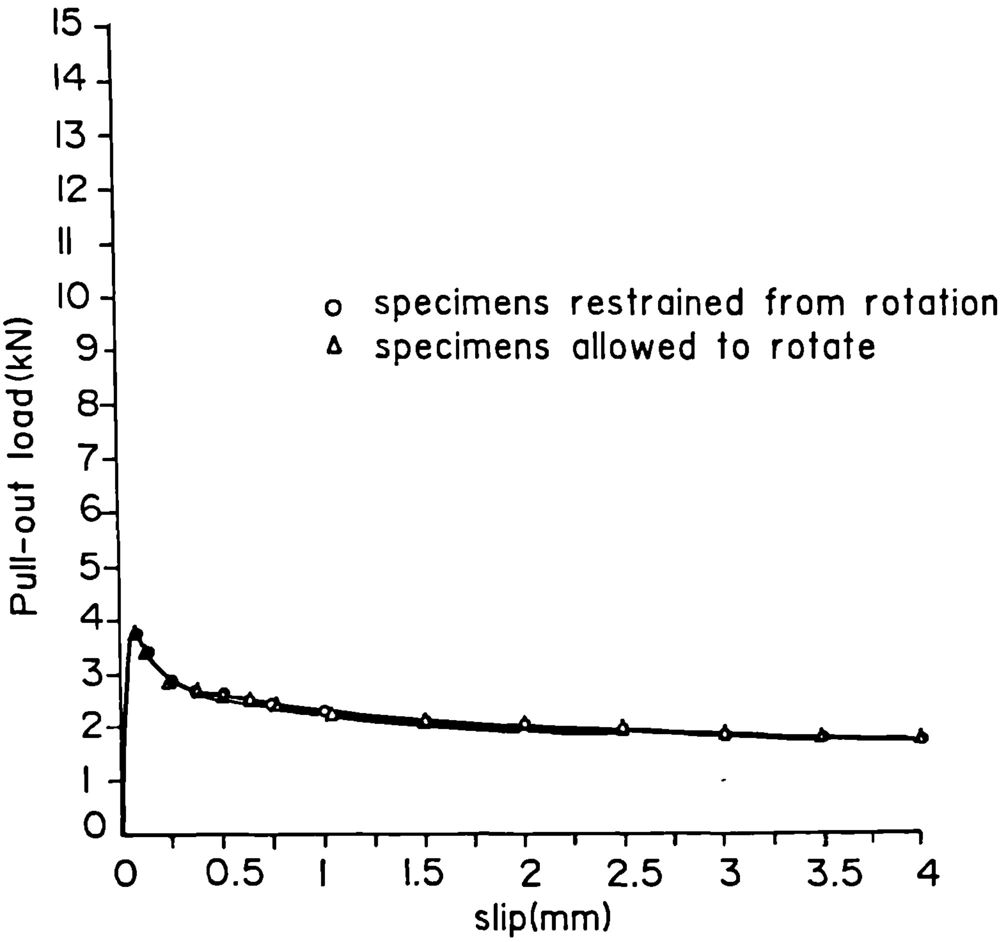

Fig 4.13 Pull-out load/slip for normal strand (25.4mm embedment)

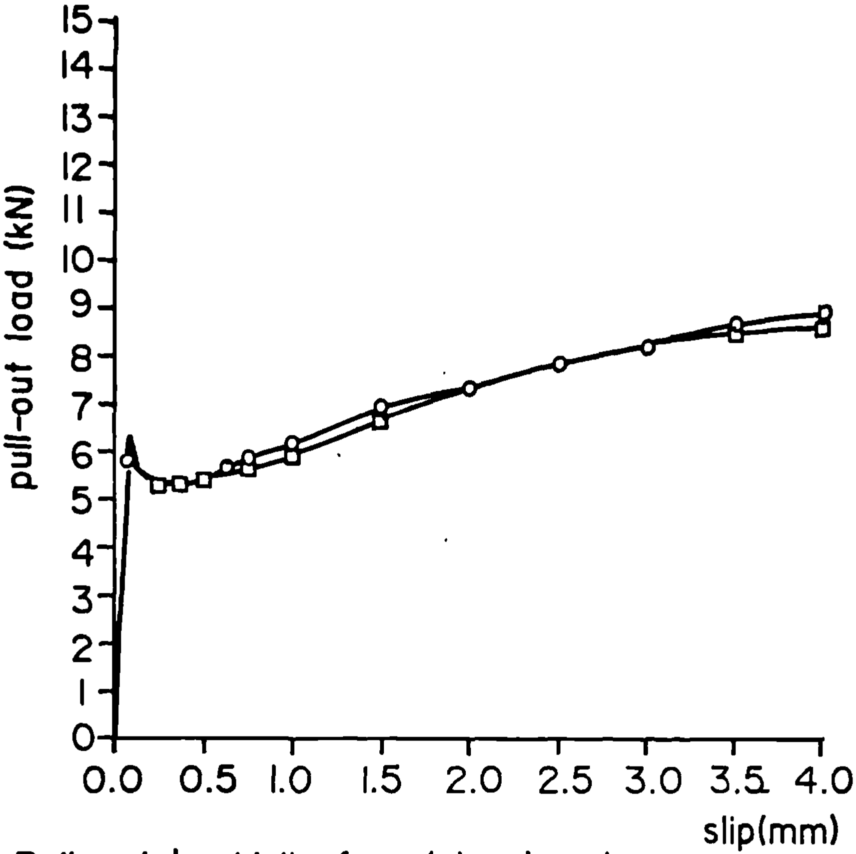

Fig.4.14 Pull-out load/slip for plain strand (50.8mm embedment)

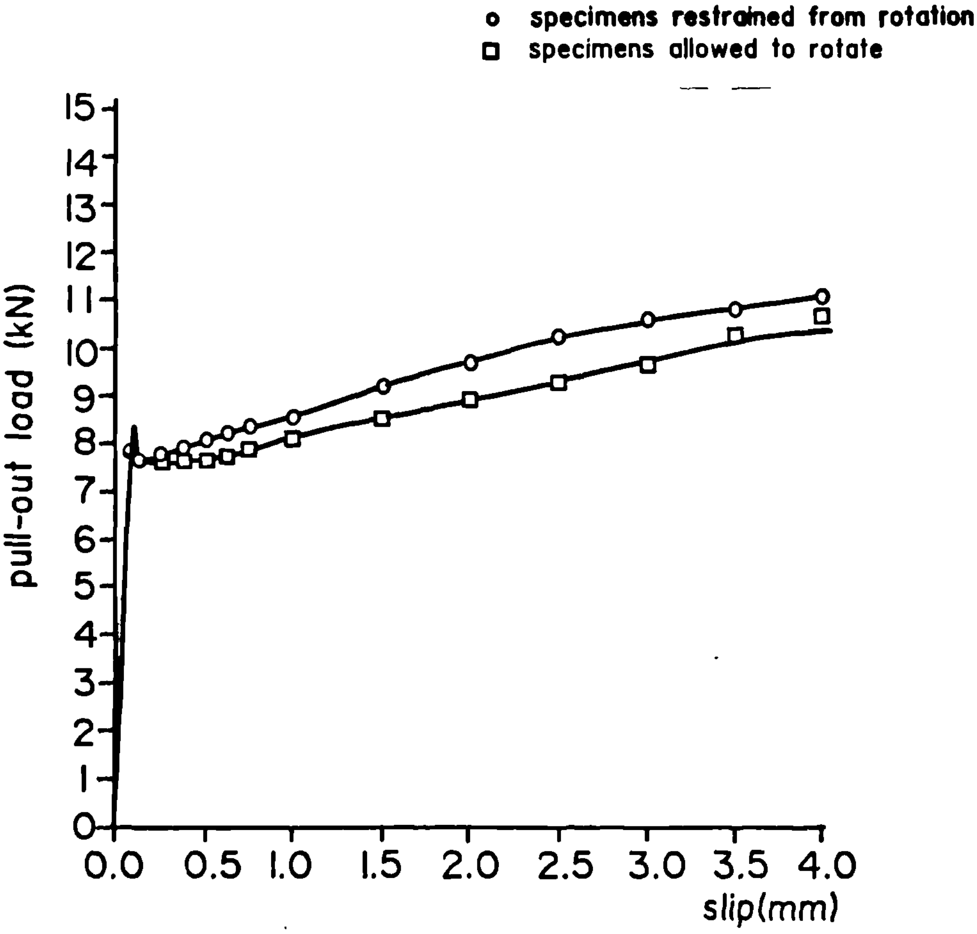

Fig. 4.15 Pull-out load/slip for plain strand (76.2mm embedment)

pull-out load of the magnitude of 3.15KN $\pm$ 1.46 observed experimentally. Table 4.3 presents the values of that part of pull-out load caused by the torsional stiffness obtained theoretically .

Torsional Stiffness(KN)	Slip(mm)						
	1.00	1.50	2.00	2.50	3.00	3.50	4.00
50.8mm	0.12	0.17	0.23	0.28	0.34	0.39	0.46
76.2mm	0.12	0.17	0.23	0.28	0.34	0.39	0.4

Table 4.3 Estimated Torsional Effect

It may be concluded, therefore, from the theoretical as well as from the experimental investigation that the increase in pull-out load with slip for specimens of long embedment length (50.8mm, 76.2mm) cannot be explained in terms of torsional stiffness only. Therefore the source of bond that activated within the interface can also be attributed to the imperfect shape of the strand referred to it as "lack of fit" by Stocker and Sozen[10]. According to the report on prestressing strand made by FIP[29]: "Anchorage and Application of Prestensioned 7 Wire-Strands." the varying shape of the strand along its axis is a result of:

1) The greater diameter of the central wire (2% greater than the exterior wires.)

2) Difference in the twist angle of the exterior wires.

3) Difference in the shape of the single wire.

Stocker and Sozen[10] showed that the cross sections of a piece of strand located at a distance of 25.4mm from one another were different.

If the angle of twist, the pitch, or the diameter varies along the strand axis, the strand would tend to wedge as soon as it starts slipping through the presumably rigid concrete embedment. This is because of a certain lack of fit between the cross sections of the strand displaced through slip and the stationary grout channel. Theoretically using equation 8 it can be shown that an increase of the diameter of the strand by $3.2.10^{-3}$mm would suffice to generate a contact stress of the magnitude of about 8.8N/mm^2, which would develop a pull-out load of about 3.45KN (of the magnitude observed in the tests). For short embedment length (25.4mm) the above phenomenon does not occur i.e either the shape of the strand remains constant over this length or the contact area is not sufficient to resist to any stresses that may be caused while the strand is pulled through and therefore the grout over that bonded region crushes. Practically it is extremely difficult to measure any change in diameter of the magnitude mentioned above.

CHAPTER 5 COMPARISON WITH OTHER WORK

5.1 STRAND/GROUT BOND

As mentioned earlier in chapter 1 there is scanty data available on the bond developed between strand and grout. DD81[2] recommends that the ultimate bond stress (assumed uniform over the tendon bond length) should not exceed $2.0N/mm^2$ for clean strand embedded in a grout of $30N/mm^2$ compressive strength. A study of the results obtained with this investigation (see figure 3.14) shows that for the case of zero lateral pressure and a long embedment length, a maximum bond stress of $1.9N/mm^2$ is obtained for normal prestressing strand embedded in a grout of $57N/mm^2$ compressive strength. Note, however, that this value is based upon the true contact perimeter of $4.\Pi.\Phi/3$ (see Appendix). Based upon the nominal strand of $\Pi.\Phi$, the maximum bond stress rises to $2.5N/mm^2$. This value is further increased (by up a to factor of 3 for longer embedment) by the addition of lateral pressure of $14.78N/mm^2$.

There is little other information in the technical literature on strand/grout bond. Investigations into the bond of strand/concrete and bar/concrete systems have been made principally by Stocker and Sozen[10], Robins and Standish[14], Navaratnarajah and Speare[13], and Untrauer and Henry[12].

5.2 STRAND/CONCRETE BOND

A comparison of the test results obtained with those of Stocker and Sozen[10] is given in figure 5.1. The results are for the maximum bond force for 25.4mm embedment with

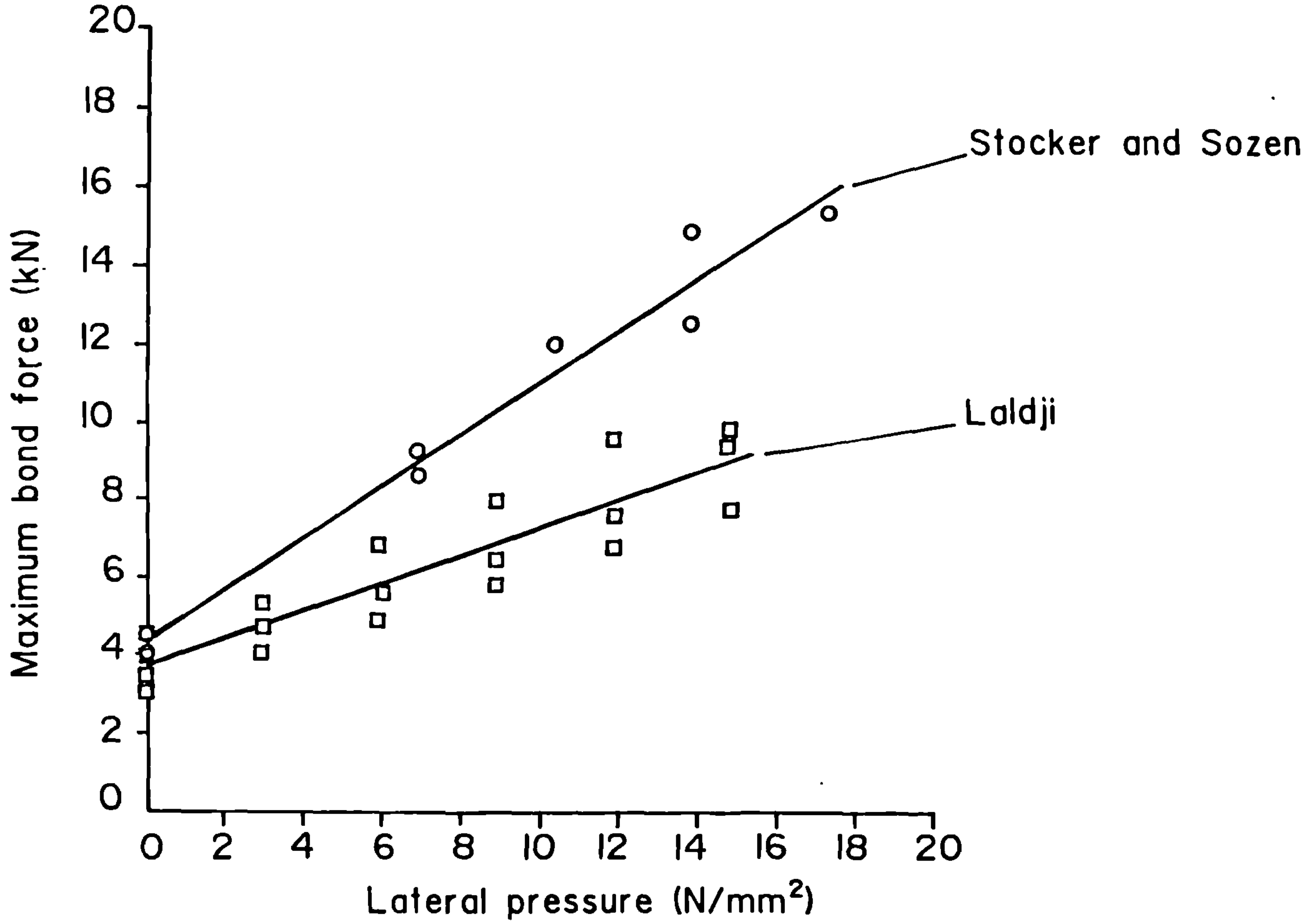

Fig. 5.1 Comparison of the tests results obtained by Stocker and Sozen with those obtained by Laldji

7/16" strand (see figure 1.2) and with 12.9mm normal strand and so a difference in contact area of 16% must be allowed. There is little difference between the compressive strength of the concrete (59.8N/mm^2) and that of the grout (57N/mm^2). There is a good agreement between the two lines of best fit at zero lateral pressure but they diverge as lateral pressure increases. The agreement at zero lateral pressure may be a fortuitous combination of higher shrinkage combined with the lower friction obtained for grout specimens. There appears to be a better friction grip in the case of the concrete surround even though the compresssive strength are similar and the coefficient of friction obtained by Stocker and Sozen[10] (0.3) is fairly close to that obtained by the writer (0.28). Other explanations for the divergence at higher lateral pressures are the differences in the modulus of elasticity (27.6N/mm^2 for concrete and 21.5N/mm^2 for grout), Poisson's ratio (0.13 for concrete and 0.17 for grout), and the type of loading (hydrostatic lateral pressure employed).

Stocker and Sozen[10] proposed an equation by which the bond for a multi-wire strand may be predicted from the test results on a single wire, but did not establish an equivalent equation to (4.2) with which the bond can be calculated using the fundamental properties of the materials. The limit of application of this equation is stated as lateral pressure of 0.36 times cylinder strength equivalent to approximately 0.29 the cube strength. Above this value, and when only a small load was applied to the strand, the specimens failed in a similar fashion as observed in this present investigation.

5.3 PLAIN BAR/CONCRETE BOND

Robins and Standish[14] have carried out tests on bond between plain bar and lightweight concrete using an embedment length of 100mm. There is considerable scatter for the pull-out loads obtained at zero lateral pressure for both 8mm and 12mm round bars with average values of ultimate bond stress varying from 1.84 to $3.04N/mm^2$. At first sight this is surprising in view of the lower compressive strength of lightweight concrete ($33.3N/mm^2$) and the additional resistance provided by the helical twist in the strand. Using the theoretical approach derived in this investigation, it can be shown that the twist angle has an effect of increasing the pull-out load (see figure 5.2) by 1.08 for angle α equal to 11.45^o. However the frictional coefficient obtained by Robins and Standish for concrete/bar of 0.5 is considerably higher than the value of 0.28 for grout/strand and greater shrinkage appears to have taken place with concrete specimens ($1000x10^{-6}$ compared to $700x10^{-6}$), possibly due to the greater age at test. Using equation (4.2) these effects would increase the value of maximum bond stress obtained by the author from $1.9N/mm^2$ to 1.9x0.93x0.66x1.72x1.03x0.99x1.43= $2.95N/mm^2$, where the factors correspond to changes in angle of twist, Young's modulus of matrix, coefficient of friction, Poisson's ratio of matrix, Young's modulus of steel, and strain due to shrinkage. This compares well with the value obtained by Robins and Standish on lightweight concrete with 12mm diameter bar.

A valid comparison of the effect of lateral pressure in the two cases is not possible as Robins and Standish[14]

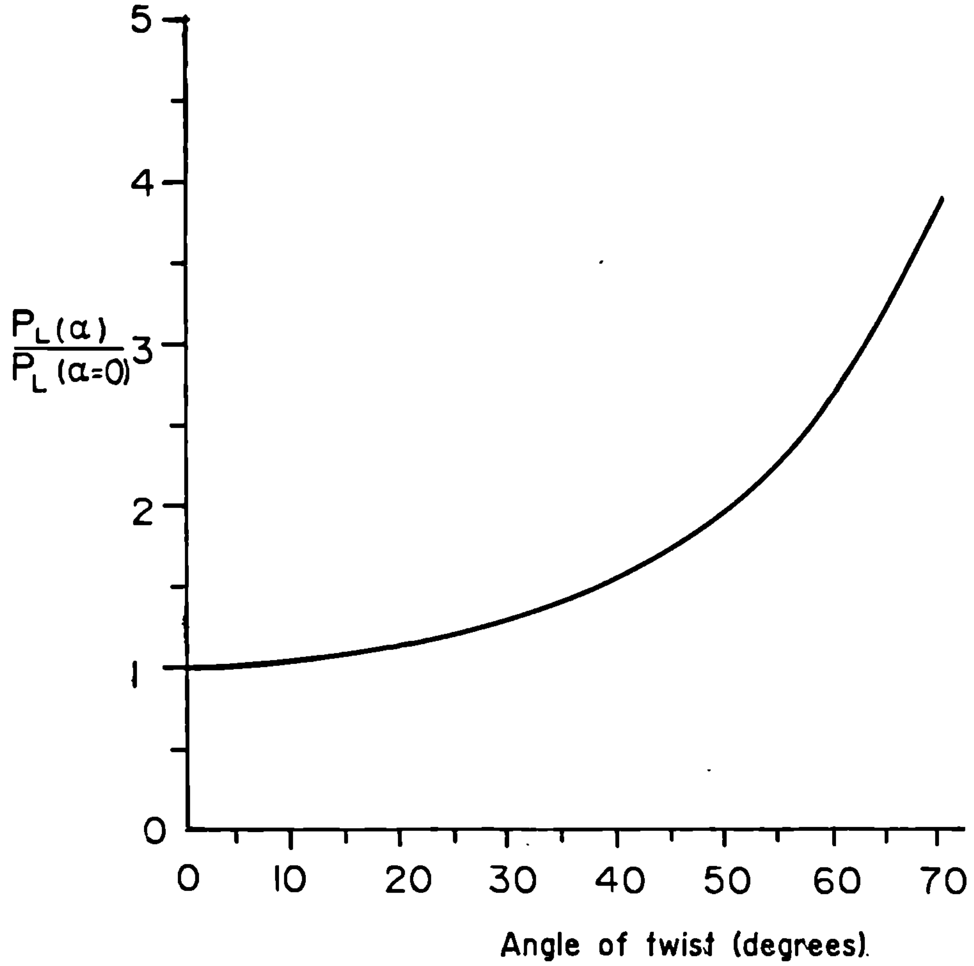

Fig 5.2 Effect of strand twist angle on pull-out load

only applied lateral pressure to one set of opposite faces and used different materials. Consider for instance the effect of lateral pressure of 14.78N/mm^2: under this pressure Robins and Standish[14] find that the bond stress has increased by a factor of 1.9 compared to a factor of 3 that is obtained in this investigation. If however, the difference in the mechanical properties of the materials is taken into account, the increase in maximum bond stress obtained in this investigation becomes 4.9. This implies that the bond stress developed under hydrostatic pressure is greater than twice that developed under a lateral pressure applied on two parallel faces. This is understandable since in the case of a lateral pressure applied on two sides , tensile stresses can be generated on the other sides which will cause a loss in contact pressure. The theoretical equations developed in both investigations (Robins and Standish, and the author) are similar in form, for an angle α equal to zero, equation 4.2 reduces to that derived by Robins and Standish[14] except for the lateral strain term due to the externally applied pressure. The equation established in this investigation can be applied for both round bar and multi-wire strand provided that the lateral pressure is applied on four sides of the specimens.

Robins and Standish[14] did not find an upper limit for the linear bond/lateral pressure response of plain bars, although they applied lateral pressures up to 0.84 times the cube strength.

5.4 DEFORMED BAR/CONCRETE BOND

Depending on the type *of deformation projecting from* the surface of the bar, the bond of deformed bars in concrete is relatively more complex when compared to that of plain bars. Navaratnarajah and Speare[13] have carried out an investigation on bond between concrete and different types of deformed bars (hybar, torbar, square twisted) using 25mm diameter bar with an embedment of 100mm. The average ultimate bond stress with no lateral pressure obtained for specimens with bottom cast bars of 50mm cover varied with the type of bar. Torbar developed an ultimate bond stress of $4.93 N/mm^2$, hybar $4.10 N/mm^2$, and square twisted $3.12 N/mm^2$ and this is for a compressive strength of $35 N/mm^2$. An exact comparison between these results and those obtained in this investigation is not possible because of the unknown mechanical properties of the materials used by Navaratnarajah and Speare[13]. However since twisted bars used by Navaratnarajah and Speare[13] are of BS4461[30] type 1 (pitch not greater than 14 times the diameter) i.e angle of twist not greater than 12.6^o which is comparable to that of normal strand used by the author, it is considered of interest to evaluate the range of the maximum bond stress of normal strand relative to the ultimate bond stress of twisted bar. The ultimate bond stress of twisted bar (bottom location) of $3.12 N/mm^2$ is higher than that of normal strand of 50.8mm embedment ($2.14 N/mm^2$). However, the ultimate bond stress (top location), was $2.18 N/mm^2$ which is significantly closer. The maximum bond stress of indented strand is 56 percent greater than normal strand. This compares with the equivalent factor for torbar and hybar relative to square twisted of 58 percent and 32 percent respectively.

The experimental results obtained by Navaratnarajah and Speare[13] for square twisted 25mm bar, 50 mm cover, bottom location and subjected to lateral pressure are compared with the results of this present investigation in figure 5.3. The comparison is restricted to the range of lateral pressure less than 0.3 times the cube strength. It can be seen that the rate at which the best fit straight line for the increase in bond stress increases with the lateral pressure obtained in this investigation, (0.25), is higher than that obtained by Navaratnarajah and Speare[13], (0.19). This can be attributed to the differences in loading system (type of pressure), and may also be the result of differences in the materials investigated.

Untrauer and Henry[12] also investigated the bond between concrete and deformed bars. The ultimate bond stress for specimen of compressive strength of 47.7N/mm^2 was found to vary from 7.9N/mm^2 to 9.17N/mm^2 for zero lateral pressure depending onwhether the specimens are tested wet or dry. It is remarkable that these values are significantly higher than those obtained by others on bar or strand. Since little information was given on the mechanical properties of the materials used a comparison appears to be impossible.

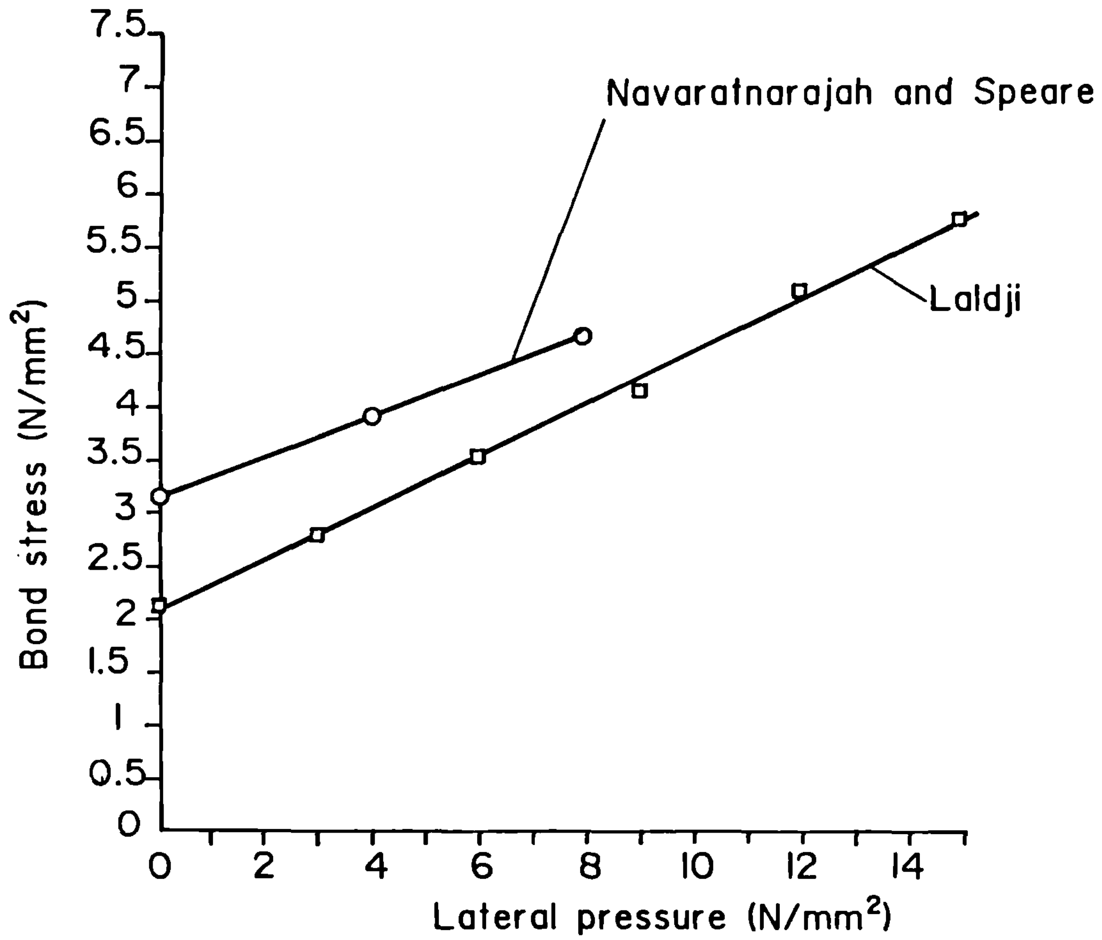

Fig 5.3 Comparison of the tests results obtained by Navaratnarajah and Speare with those obtained by Laldji

CHAPTER 6 CONCLUSIONS

1) For the case of zero lateral pressure and a long embedment length a maximum bond stress of $1.9N/mm^2$ is obtained for normal prestressing strand embedded in a grout of $57N/mm^2$ compressive strength. This value is less than that recommended by DD81 but is based upon the true contact area.

2) The effect of biaxial lateral pressure up to 0.26 compressive strength is to linearly increase the maximum bond stress as follows:

Normal strand $0.26N/mm^2 \pm 0.04$ per $1N/mm^2$ increase in lateral pressure.

Dyform strand $0.24N/mm^2 \pm 0.04$ per $1N/mm^2$ increase in lateral pressure.

Indented strand $0.47N/mm^2 \pm 0.22$ per $1N/mm^2$ increase in lateral pressure.

The shape of the bond force-slip curve is unaffected by the magnitude of lateral pressure up to 0.26 compressive strength.

3) For biaxial lateral pressures between 0.26 and 0.37 compressive strength, there is a levelling off of maximum bond force. The form of the bond force/slip curve also changes.

4) The maximum bond stress for the case of zero lateral pressure and 25mm embedment length obtained for the different types of strand are as follows:

normal $2.77N/mm^2$.

dyform $2.49N/mm^2$.

indented $3.35N/mm^2$.

5) The increase in bond due to added length of embedment is not linear. An increase in embedment length of a factor of 2 increases the maximum bond force on average by a factor of 1.67 and an increase in embedment length of a factor of 3 gives a corresponding increase factor of 2.36, irrespective of lateral pressure. The maximum bond stress tends towards a constant value beyond an embedment length of 50mm.

6) In general, for the longer embedment lengths the pull-out force, after a slight drop, increases above the initial maximum bond force. With normal and dyform strand and 25.4mm embedment the pull-out force continues to decrease after maximum value. With indented strand no such decrease occurs.

7) The maximum bond force increases linearly with the grout strength with an average rate of increase of 0.07KN in bond force for each $1N/mm^2$ increase in cube strength. This relationship applies to cases of lateral pressure up to 0.26 compressive strength.

8) An equation has been developed (4.2) which predicts the maximum bond force fairly accurately provided values of shrinkage, friction, helix angle, and elastic material constants are known. Approximate values for the grout/strand specimens investigated are as follows:

Shrinkage (drying)	700×10^{-6}.
Friction coefficient	0.28
Young's modulus of grout	$21.5KN/mm^2$.
Poisson's ratio of grout	0.17
Young's modulus of steel	$207.8KN/mm^2$.

Poisson's ratio of steel 0.3

9) Comparison of the predictions using equation 4.2 with the results obtained by other investigators shows good correlation for the case of zero lateral pressure. Differences between the predicted values and those obtained by others with lateral pressure applied occured due primarly to the differences in system of loading.

10) A study of the bond characteristics after maximum bond force has been reached shows a significant increase in bond resistance for the longer embedment lengths. It has been shown by experimental and theoretical work that this cannot be attributed to the torsional stiffness of the strand. It is considered to be the result of "lack of fit" of the strand in the grout channel when slip takes place.

APPENDIX

CIRCUMFERENCE AND CROSS SECTION OF SEVEN-WIRE STRAND

Consider that all the wires of the strand have a same diameter size d (see figure A). The angle α of figure A, shown separately in figure B, is equal to 30^o i.e each wire has an arch contained within an angle of 240^o or a circumference of $\pi.d.2/3$, in contact with the grout. Therefore for seven-wire strand as there are 6 outer wires the total circumference of the strand in contact with the grout is $\pi.d.4$ and as $\Phi=3.d$, where is the nominal diameter of the strand, this leads to $\pi.\Phi.4/3$.

Each wire has a cross section of $\pi.d^2/4 = \pi.(\Phi/3)^2/4$ and as there are 7 wires this leads to a cross sectional area of the strand of $7.\pi.(\Phi/3)^2/4$.

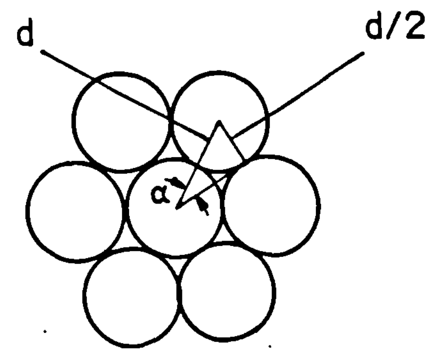

Fig. A

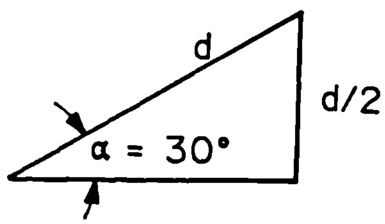

Fig. B

REFERENCES

1 The Institution of Civil Engineers Proceedings — "Design and Construction". Part 1, Volume 82, June 1987,pp 587-635

2 Draft for Development (DD81) — "Recommendations for Ground Anchorages.",British Standard Institution, 1982

3 Martin,H. — "Bond of Reinforcement in reinforced Concrete.", RADEX-RUNDSCHAU, No.2,April 1967,PP486-509.

4 Abrams,D.A — "Tests of Bond Between Concrete and Steel", Bulletin 71,Engineering Experiment Station, University of Illinois,1913.

5 Alexander,K.M. — "The Mechanism of Shear Failure at the Steel-Cement Interface." Int.Conf. on Solid Mechanics and Engineering in Civil Engineering, Univ.of Southamptom,april 1969, pp 317-326.

6 Rehm,G. — "The Basic Principles of the Bond between Steel and Concrete.", Cement and Concrete Association, Translation No134.

7 Lutz,L.A.,Gergely,P. and, and Winter,G. — "The Mechanics of Bond and Slip of Deformed reinforcing Bars in Concrete." Structural Engineering Report No.324, Cornell University, August 1966.

8 Menzel,A.C. "Some Factors Influencing Results of Pull-out Tests." ACI,Proceedings,Vol No43,December 1946,pp 381-400.

9 Tepfers,R. "Cracking of Concrete Cover along Anchored Deformed Reinforcing Bars.",Magazine of Concrete Research,Vol.31,No106,March 1979,pp3-12.

10 Stocker,M.F.; and Sozen,M.A "Bond Characteristics of Prestressing Strand." Part IV of Investigation of Prestressed reinforced Concrete For Highway Bridges,University of Illinois, 1969.

11 Shaffu,N.G. "Bond and Transmission Length of Strand in Pre-tensioned prestressed Concrete". M.Phil thesis, University Leicester, December 1983.

12 Untrauer,R.E and Henry,R.L. "Influence of Normal Pressure on Bond Strength.", Journaf of ACI, Proceedings, vol.62,No5, May 1965,pp577-585.

13 Navaratnarajah,V., and Speare,P.R.S "An Experimental Study of the Effects of Lateral Pressure on the Transfer Bond of Reinforcing Bars with variable Cover.", Proc.Instn.Civ.Engrs, Part 2, Vol.81,dec.1986,pp 697-715.

14 Robins,P.J,and Standish,I.G. "The Effect of Lateral Pressure on the Bond of Round Reinforcing Bars in Concrete.", Inter. Journal of Adhesion and Adhesives,April 1982,pp129-133.

15 Gilkey,H.J et al — "The Bond between Concrete and Steel." ACI.Proceedings, Vol.35,September 1938,pp1-20.

16 Neville,A.M. — "Properties of Concrete.",Second Edition (Pitman Publishing Ltd,1973)

17 Takaku,A.,and Arridge,R.G.C. — "The Effect of Interfacial Radial and Shear Stress on Fibre Pull-out in Composite Materials.", J.Phys(D), Appl.Phys No6,1973, pp2038-2047.

18 Pinchin,D.J. — "The Cement-Steel Interface: Friction and Adhesion.",PhD Dissertation, University of Cambridge, April.1977.

19 Timoshenko,S. — "Strength of Materials.",Part II, Third Edition,D.Van Nostrand Company,Inc,1956.

20 BS1881 Part 201 — "Testing Concrete: Guide to the use of non-destructive of test for hardened Concrete", 1986

21 BS12 — "Ordinary and Rapid-Hardening Portland Cement.", 1978

22 BS882 — "Aggregates from Natural Sources for Concrete.", 1983.

23 BS5896 — "High Tensile Steel Wire and Strand for the Prestressing of Concrete." 1980.

24 BS1881, part111 — "Testing Concrete: Method of normal curing of test Specimens.", 1983.

25 BS1881, part116 — "Method of Determination of Compressive Strength of Concrete Cubes.", 1983.

26 BS1881, part117 "Method for Determination of Tensile Splitting Strength.", 1983.

27 BS1881, part5 "Method of Testing hardened Concrete for other than Strength.", 1970

28 Serada,P.J et al "Effect of Sorbed Water on some Mechanical Properties of Hydrated Portland Cement Pastes and Compacts." Highway Research Board, Symp.on Structures,vol 90, 1966, pp 58-73.

29 FIP: Report on Prestressing Steel "Anchorage and Application of Pretensioned 7-wire Strands.", Part2,June1978.

30 BS4449 "Hot Rolled Steel Bars for the Reinforcement of Concrete.", 1978.